Cape Peninsula
University of Technology

ENERGY MANAGEMENT OF A BATTERY ENERGY STORAGE SYSTEM FOR RENEWABLE ENERGY DC MICRO-GRID

by

CHRISTIAN NDEKE BIPONGO

Thesis submitted in partial fulfilment of the requirements for the degree

Master of Engineering in Energy

In the Faculty of Engineering and the Built Environment

At the Cape Peninsula University of Technology

Supervisor: Dr Marco Adonis

Bellville
August 2021

CPUT copyright information

DECLARATION

I, Christian NDEKE BIPONGO, declare that the contents of this thesis represent my own unaided work, and that the dissertation has not previously been submitted for academic examination towards any qualification. Furthermore, it represents my own opinions and not necessarily those of the Cape Peninsula University of Technology.

Signed

15 November 2021

Date

ABSTRACT

This research presents a regime for energy management of a battery energy storage system in a renewable DC micro-grid. The increase in world electricity demand is one of the principal drives to the exhaustion of fossil fuels and expanded greenhouse gas emissions. To solve these problems, several countries have adopted actions for large deployment renewable energy sources, which includes wind energy, solar power, biomass power, tidal and hydropower. These sources are considered as significant in delivering clean energy and reducing greenhouse gas emissions for sustainable improvement. These renewable energy sources are often connected to the conventional power system through the distribution network near consumer loads, thus no extensive transmission system is needed. In such a case, these are referred to as distributed generation systems.

Distributed generation can impact negatively the performance of the distribution network as the distribution network will no longer operate with a unidirectional power flow pattern. Some of the known issues are known to affect voltage quality, protection equipment settings, desensitised relays, augmented fault currents, increased maintenance of equipment used, and even a landing portions of the distribution network. To address these issues, micro-grids are used as a platform to integrate distributed generation systems, as they provide significant benefits to end-users and to the distribution network. The utilization of energy storage systems is necessary in renewable micro-grids as they can ensure the reliability of the supplied power. Battery energy storage systems are the types of energy storage widely utilized in renewable micro-grids. Comparatively to Li-ion battery, most of the technologies present some issues (the relation between the charge / discharge rate on their operating conditions, unbalance SoC conditions), which can impact on the battery lifetime as well as the average of energy stored in the battery. In case of battery bank, the deep discharge or the premature charge of battery can lead to a reduced lifetime of the storage system.

The problem of this research was the lack of a proper battery management system in a renewable DC micro-grid. The DC micro-grid and energy management system algorithm was implemented and developed using MATLAB/Simulink software, which used a physical modelling approach. The aim of this research was to develop a battery management system algorithm to control the charging / discharging of a battery bank and to keep its state of charge (SoC) in the admissible limits to avoid the deep charging / discharging of the battery within a DC micro-grid. Moreover, in a micro-grid, given that several power sources are connected, an energy management system needs to be implemented to ensure their proper operation. The objectives of this research were to develop DC micro-grid component models to be used in

the simulation model; to design and develop function block logic to be used for the simulation using State-Flow logical programming environment in MATLAB/Simulink software; to develop a control system schemes for the DC micro-grid; to develop an energy management system (EMS) algorithm for the DC micro-grid and to develop a battery management system (BMS) algorithm and to design and develop a simulation of a DC micro-grid with battery energy storage using MATLAB/Simulink software.

The results of the scenarios of the developed energy management system (EMS) algorithm have successfully shown that this developed algorithm will be able to ensure the reliability, the resiliency, the robustness and the proper operation of the battery systems in micro-grids. The principal advantage of this developed algorithm will be that it will ensure the proper relation between the charge / discharge rate of battery energy storage systems on their operating conditions and will allow to keep its SoC in the admissible limits according to the input power conditions from the EMS flow chart, to avoid the deep charge / discharge of the battery bank, which in return will significantly impact on their lifespan and on the reliability in a DC micro-grid. The results demonstrated that the battery bank was able to handle the load demands for different scenarios studied. Moreover, the developed software model presents another advantage, which enables the users to access and to change any control parameter within the DC micro-grid.

In addition, this developed algorithm will provide a low overall cost and degradation impact on the battery. The SoC of the battery operation will directly affect its achievable lifetime positively and the battery degradation costs will significantly decrease. This algorithm offered a proper operation of the entire developed DC micro-grid system, which could result in reduced battery degradation and improve battery life as well as the energy stored in the battery. The results have shown that the initial investment cost will comparatively be lower and will decrease the economic analyse in terms of LCOE.

ACKNOWLEDGEMENTS

I am most grateful to Almighty God for the grace he has given to me to successfully complete my research work and to the Management of the Cape Peninsula University of Technology for creating a safe and conducive learning environment.

I am grateful to my supervisor – Dr Marco Adonis, for his guidance, immeasurable support, meticulous reviews and endless encouragement over the course of this journey. Your constant supervision has made this thesis a success.

I would like to express my gratitude to Dr Doudou Luta for his constructive criticism and invaluable suggestion throughout this work.

I am thankful to the Cape Peninsula University of Technology Postgraduate Office for funding my studies.

Finally, a hearty appreciation goes to all my sublime family and friends for their support, patience and encouragement through all this time. Without them, I don't know if I could have made it. I am also thankful to who through their several inputs, have made this a dream come true.

DEDICATION

I dedicate this thesis to my father Magellan Ndeke Bipongo and my mother Lydie Kambungu your teachings and unconditional love has moulded me to who I am today. To my lovely sisters Benitha, Rhema, Hervine, Dynamique and Dieudo, my uncle Andre Ndeke and his wife Sarah Pilato, your affection made my life in Cape Town focused.

TABLE OF CONTENTS

DECLARATION ii

ABSTRACT iii

ACKNOWLEDGEMENTS v

DEDICATION vi

TABLE OF CONTENTS vii

LIST OF FIGURES xiii

LIST OF TABLES xv

ABBREVIATIONS xvii

CHAPTER 1: INTRODUCTION 1

1.1. Backgrounds 1

1.1.1. Micro-Grids 1

1.1.2. Energy Storage Systems 1

1.1.3. Energy Management Systems 2

1.2. Statement of the Research Problem 3

1.3. Motivation for Research 3

1.4. Aims and Objectives of the Research 4

1.5. Methodologies 4

1.6. Research Questions 4

1.7. Significance of the Research 5

1.8. Plan of Development 5

CHAPTER 2: LITERATURE REVIEW ON MICRO-GRIDS 6

2.2.1. The Divergence between a Traditional Power Grid and a Micro-Grid 8

2.2.2. Some Benefits of a Micro-Grid 9

2.2.3. Types of Micro-Grid 10

2.2.3.1. The DC Micro-Grid 10

2.2.3.2. The AC Micro-Grid 11

2.2.3.3. The Hybrid Micro-Grid 12

2.2.4. Micro-Grid Architecture 13
2.3. Distributed Generation Systems 14
2.3.1. Solar Power System 15
2.3.2. Photovoltaic System Presentation 16
2.3.2.1. Maximum Power Point Tracking Charge Controllers 16
2.3.2.2. Algorithms for Maximum Power Point Tracking 17
2.3.2.3. Photovoltaic Cell System Operation 17
2.3.2.4. Photovoltaic Module System 18
2.3.2.5. Photovoltaic Array System 19
2.3.2.6. Solar cell efficiency 19
2.3.3. Wind Energy Power System 20
2.3.3.1. Wind Turbine Characteristics 21
2.3.3.2. Power Electronics Converters for Wind Turbines 22
1. Diode rectifier based converter 22
2. Back to back converter 23
2.3.3.3. Voltage Source Converter and Current Source Converter Wind Turbine 23
2.3.4. Geothermal Power 24
2.3.5. Hydropower 25
2.3.6. Biomass Power 27
2.3.7. Micro-Turbines 28
2.3.8. Diesel Generators 29
CHAPTER 3: BACK GROUND ON ENERGY STORAGE SYSTEMS 30
3.1. Energy storage Systems 30
3.1.1. Flywheel 30
3.1.2. Fuel Cell 31
3.1.3. Super-capacitors 32
3.1.4. Secondary batteries 33
3.1.4.1. Lead Acid Battery 34

3.1.4.2. Nickel-Based Battery 34
3.1.4.3. NaS Battery 35
3.1.4.4. Lithium-ion Battery 35
3.1.4.5. Metal-air Battery 36
3.1.4.6. Redox Flow Battery 36
3.1.5. Battery Energy Storage System Control 37
3.1.5.1. Basic Operation Modes of the Distributed Battery Energy Storage Systems 37
3.6. Power electronics converters for batteries 37
3.6.1. Non-Isolated Converters 37
3.6.1.1. Buck converter 37
3.6.1.2. Boost converter 39
3.6.1.3. Buck boost converter 40
3.6.1.4. Cuk converter 41
3.6.1.5. DC-to-DC Bidirectional converter 41
3.6.2. Isolated Converters 42
3.6.2.1. Forward converter 42
3.6.2.2. Fly back converter 43
3.6.2.3. Push-pull converter 43
3.6.2.4. Half bridge converter 44
3.7. Power electronics converters control 44
3.7.1. Primary Control 45
3.7.1.1. Inner loop 45
A. AC to DC converter 45
B. DC to DC converter 45
3.7.1.2. Droop control 46
3.7.2. Secondary control 46
3.7.3. Tertiary control 47
CHAPTER 4: SYSTEM DESCRIPTION AND MODELLING 48

4.1. Introduction 48
4.2. System Description 48
4.2.1. Load Profile of the System 48
4.2.2. Operation of the Designed and Developed System 50
4.3. Mathematical Modelling of Main Components of the Developed DC micro-grid System 50
4.3.1. Modelling of Solar Power 51
4.3.1.1. Photovoltaic module modelling 52
4.3.1.2. Photovoltaic System Design 54
4.3.2. Modelling of Wind Power 55
4.3.3. Modelling of the Battery 57
4.3.4. Modelling and Design of Power Converter 59
4.3.4.1. Design of Converters 61
A. Buck-Boost Converter Parameters 61
A.1. Determination of Inductor Value 61
A.2. Determination of Capacitor Value 63
B. Boost Converter Parameters 63
4.4. Developed Energy Management System Control for Battery Energy Storage system 64
CHAPTER 5: RESULTS AND DISCUSSION OF THE DEVELOPED MODEL 68
5.1. Introduction 68
5.2. Description of Simulation Model for the Developed DC micro-grid 68
5.3. Simulation Results of the Developed PV Array Model for the DC micro-grid 70
5.3.1. Simulation Results of the PV Array Model for the DC micro-grid 70
5.4. Simulation Results of the Developed Wind Power Model for the DC micro-grid 72
5.4.1. Simulation Results of the Wind Power Model for the DC micro-grid 73
5.5. Simulation Results of the Developed Biomass Power Model for the DC micro-grid 76
5.5.1. Simulation Results of the Biomass Power Model for the DC micro-grid 76

5.6. Simulation Results of the Developed Battery System Model for the DC micro-grid 79
5.6.1. Simulation Results of the Battery System Model for the DC micro-grid 80
5.7. Simulation Results of the Load demands for the Developed DC micro-grid 82
5.8. Description of the simulation of the developed energy management system 83
5.9. Simulation Results of the DC MG Using the Developed Energy Management System 85
5.10. Conclusion..... 100
CHAPTER 6: CONCLUSION AND RECOMMENDATIONS 105
6.1. Conclusion 105
6.2. Recommendations and Future Works..... 106
6.3. Publication..... 106
REFERENCES..... 107
APPENDIX 121

LIST OF FIGURES

Figure 2.1: A typical of micro-grid 7
Figure 2.2: the comparison between conventional and micro-grids 9
Figure 2.3: Classification of the micro-grid based power type 10
Figure 2.4: DC micro-grid with AC and DC loads 11
Figure 2.5: AC micro-grid with AC and DC loads 12
Figure 2.6: Conventional Hybrid micro-grid 13
Figure 2.7: Micro-grid architecture 14
Figure 2.8: Distributed Generation Technologies 15
Figure 2.9: Block diagram of a concentrated solar power system 16
Figure 2.10: Photovoltaic cell operation 18
Figure 2.11: Photovoltaic module system 19
Figure 2.12: Photovoltaic array system 19
Figure 2.13: Vertical Axis versus Horizontal axis turbine 20
Figure 2.14: Diode rectifier based converter 22
Figure 2.15: Back to back converter based wind turbine generator system 23
Figure 2.16: Generator side block diagram 24
Figure 2.17: Grid side block diagram 24
Figure 2.18: The basic concept of geothermal energy system for power generation 25
Figure 2.19: Typical of Hydropower Plant with storage 26
Figure 2.20: Generation of Electricity using Biomass (Sugar mill in Nepal) 27
Figure 2.21: Micro-turbine-using CHP System Schematic 28
Figure 2.22: Schematic diagram of a diesel generator set 29
Figure 3.1: Flywheel energy storage advice 31
Figure 3.2: Schematic representation of a fuel cell 31
Figure 3.3: Schematic diagram of super-capacitors 32
Figure 3.4: Schematic diagram for a battery system operation 33
Figure 3.5: Buck converter circuit 37

Figure 3.6: Boost converter circuit 38
Figure 3.7: Booster converter on state 39
Figure 3.8: Booster converter off state 39
Figure 3.9: Buck boost converter circuit 40
Figure 3.10: Circuit diagram of Cuk converter 41
Figure 3.11: Bidirectional buck boost converter 41
Figure 3.12: Forward converter 42
Figure 3.13: Fly back converter 43
Figure 3.14: Push-pull type converter circuit 43
Figure 3.15: Circuit diagram of a half bridge converter 44
Figure 3.16: Hierarchical control architecture 44
Figure 3.17: Secondary control's principle on DC voltage restoration in DC micro-grids 46
Figure 4.1: Block diagram of the developed system 49
Figure 4.2: A single equivalent circuit model of a PV cell 52
Figure 4.3: Solar array equivalent circuit 54
Figure 4.4: The characteristics curve of Solar Cell 54
Figure 4.5: Characteristic curve of wind system 57
Figure 4.6: Equivalent circuit buck-boost converter 59
Figure 4.7: Developed Energy Management System Flowchart 67
Figure 5.1: Descripted DC micro-grid model system 69
Figure 5.2: Designed and Developed PV System Model 70
Figure 5.3: The PV System Model Output Voltage 71
Figure 5.4.: The PV System Model Output Current 71
Figure 5.5: The PV System Model Output Power 71
Figure 5.6: Developed wind power model 73
Figure 5.7: The Wind Power System Output Voltage 74
Figure 5.8: The Wind Power System Output Current 74
Figure 5.9: The Wind Power System Output Power 74

Figure 5.10: The output Torque from the Wind Turbine 75
Figure 5.11: The Rotor Speed of the Wind Turbine 75
Figure 5.12: Developed Biomass Power Model 77
Figure 5.13: Biomass power Output Voltage 77
Figure 5.14: Biomass power Output Current 77
Figure 5.15: Output Power of the Biomass power 78
Figure 5.16: The Rotor Speed of the Permanent Magnet Synchronous Generator 78
Figure 5.17: Developed Battery Energy Storage System Model 79
Figure 5.18: Battery $\boldsymbol{SoC}$ 80
Figure 5.19: Battery Output Voltage 80
Figure 5.20: DC-DC Bidirectional Converter Output Voltage 81
Figure 5.21: Output Power of the Battery 81
Figure 5.22: Output Power of the Battery from DC-DC Bidirectional Converter 82
Figure 5.23: Load voltage 82
Figure 5.24: Load Current 83
Figure 5.25: Load Power 83
Figure 5.26: Developed DC micro-grid including energy management system model 84
Figure 5.27: Production Power and Battery $\mathbf{SoC}$ 87
Figure 5.28: Output results from the energy management chart 87
Figure 5.29: Transition state from the Stateflow Chart 88
Figure 5.30: Production Power and Battery $\mathbf{SoC}$ 89
Figure 5.31: Output results from the energy management chart showing that the battery is charging 90
Figure 5.32: Transition state from the Stateflow chart 90
Figure 5.33: Output results from the energy management chart showing that the auxiliary load is connected 91
Figure 5.34: Production Power and Battery $\mathbf{SoC}$ 92
Figure 5.35: Output results from the energy management chart showing that the battery is discharging 92

Figure 5.36: Transition state from the Stateflow chart..... 93
Figure 5.37: Output results from the energy management chart..... 94
Figure 5.38: Transition state from the Stateflow chart..... 94
Figure 5.39: Output results from the energy management chart..... 95
Figure 5.40: Transition state from the Stateflow chart showing that the Load1 and the battery are supplied..... 95
Figure 5.41: Output results from the energy management chart..... 96
Figure 5.42: Transition state from the Stateflow chart showing that the Load1 is supplied..96
Figure 5.43: Output results from the energy management chart..... 97
Figure 5.44: Transition state from the Stateflow chart showing that the Load2 and the battery are supplied..... 97
Figure 5.45: Output results from the energy management chart..... 98
Figure 5.46: Transition state from the Stateflow chart showing that the Load2 is supplied.98
Figure 5.47: Output results from the energy management system chart ..... .99
Figure 5.48: Transition state from the Stateflow chart showing that the load is shutdown 100

LIST OF TABLES

Table 4.1: Type of appliances used in each house 49
Table 4.2: Type of appliances used in each office 49
Table 4.3: Required Values for the Developed DC Micro-Grid..... 50
Table 4.4: PV modules parameters..... 55
Table 4.5: The specification of the PV solar module based on standard test conditions ... 55
Table 5.1: Simulation Parameters 685
Table 5.2: Condition Table for the Energy Management System..... 85
Table 5.3: Action Table for the Energy Management System 86
Table 5.4: Summary of Scenarios and Results……101
Table 5.5: Economic Parameters……104

ABBREVIATIONS

A: Ampere

AC: Alternating Current

BESS: Battery Energy Storage System

BP: Boiling Point

BTB: Back to Back

CAES: Compressed Air Energy Storage

CdTe: Cadmium-Telluride

CHP: Combined Heat and Power

CIGS: Copper Indium Gallium Selenide

CO_2: Carbon Dioxide

DC: Direct Current

DFIG: Doubly Fed Induction Generator

DG: Distributed Generation

EDLC: Electrochemical Double Layer Capacitor

EGS: Enhanced Geothermal Systems

EM: Electromagnetic

EMF: Electromotive Force

EMS: Energy Management System

EES: Energy Storage System

FESS: Flywheel Energy Storage System

GW: Giga Watt

HFAC: High Frequency Alternative Current

Hz: Hertz

IC: Incremental Conductance

IM: Induction Machine

I – V: Current - Voltage

KCL: Kirchhoff Current Law

KVL: Kirchhoff Voltage Law

LCO: Li-Cobalt

LFP: Li-Phosphate

Li-ion: Lithium-ion

LCOE: Levelized Cost of Energy

LMO: Li-Manganese

LTO: Li-Titanate batteries

MG: Micro-Grid

MOSFET: Metal Oxide Semiconductor Field Effect Transistor

MPPT: Maximum Power Point Tracking

NCA: Nickel-Cobalt Aluminium

NiCd: Nickel-Cadmium

NMC: Nickel Manganese-Cobalt

NiMH: Nickel-Metal Hybrid

NOx: Nitric Oxide

PCC: Point of Common Coupling

PMM: Permanent Magnet Machine

PMSG Permanent Magnet Synchronous Generator

P&O: Perturbation and Observation

PV: Photo-voltaic

P- V: Power Voltage

PWM: Pulse Width Modulated

RFB: Redox Flow Battery

SoC: State of Charge

SMES: Superconducting Magnetic Energy Storage

STC: Standard Test Conditions

TV: Tele-Vision

UPS: Uninterrupted Power Supply

US $: United States Dollar

V: Voltage

Vdc: Direct Current Voltage

VRM: Variable Reluctant Machine

VSC: Voltage Source Converter

VSIs: Voltage Source Inverters

W: Watt

WTGs: Wind Turbine Generators

CHAPTER 1: INTRODUCTION

1.1. Background

1.1.1. Micro-Grids

The augmentation increase world electricity demand is one of the principal drives to the exhaustion of fossil fuels and expanded greenhouse gas emissions. To solve these problems, several countries have adopted actions for large deployment renewable energy generation, which are wind energy, solar power, biomass energy, tidal and hydropower (Lu et al., 2016). These sources are considered as significant in delivering clean energy and reducing greenhouse gas emissions for sustainable development (Lasseter & Paigi, 2016). Topić et al., reported that in 2019, a worldwide total of 2588 GW was achieved from the deployment of renewable energy resources, excluding hydropower. These renewable energy sources are often connected to the conventional power system through the distribution network near the loads, thus no transmission system is needed. In such a case, they are referred to as distributed generation system (Topić et al., 2021).

Distributed generation can impact negatively on the performance of the distribution network as the distribution network will no longer operate with a unidirectional power flow pattern (Peres & Lissitsa, 2018). The issues related with bidirectional power flow pattern are intensified by increasing levels of the distributed generation systems in the distribution network. Some of the known issues are known to affect voltage quality, protection equipment settings, desensitised relays, augmented fault currents, increased maintenance of equipment used, and affect a large portion of the distribution network (Maor, 2017). To address these issues, micro-grids are used as a platform to integrate distributed generation system, as they provide significant benefits to end-users and to the distribution network. Their benefits include improving the reliability of power supply, managing local loads with high power quality, mitigating carbon dioxide emission and reducing transmission and distribution network costs (Morstyn et al., 2018). Depending on the type of loads, micro-grids can supply power in DC or in AC form. Besides distributed generation systems, a typical micro-grid consists of a controllable load and an energy storage system.

1.1.2. Energy Storage Systems

An energy storage system refers to a device that converts energy from one form (usually electrical energy) to a storable form and that stored energy can be converted back in electricity when required (Parhizi et al., 2015). The utilization of energy storage system, especially in renewable micro-grids presents an exceptional benefit on the reliability of the electric power as it can smooth the power fluctuation, reduce power quality problems, control the micro-grid

frequency and voltage (Faisal et al., 2018), deliver initial energy when there is a transition between grid-connection and islanded mode operation of micro-grids and provides ride-through capability in case of dynamic variations in intermittent energy sources and enables distributed generations to operate as dispatchable units. They can also be used for energy arbitrage, whereby energy is stored at a lower cost and sold back when the market price is high. Various types of energy storage technologies are found in the market. Some of the attractive energy storage technologies are pumped hydropower, compressed air storage, superconducting magnetic storage, flywheel energy storage, super-capacitor and secondary batteries (Bradbury, 2015). Among these technologies, batteries, flywheels and super-capacitors are more attractive for micro-grid applications (Prashant & Atma, 2016). A typical flywheel can be utilised as a main storage system for the entire micro-grid, whereas super-capacitors would be an expensive choice to go for as compared to flywheels and batteries. On the other hand, batteries can be utilized either as the main storage system or supply capacity reserve for future energy demand (Nadeem et al., 2019).

Batteries are available in different sizes and power ratings, besides their use in micro-grids, other application areas include high tech electronic equipment and toys. Classical lead acid, NaS and LiH batteries are used in cars and solar systems. For industrial applications, batteries are mainly utilized as backup power in a UPS (Uninterrupted Power Supply) (Shalini et al., 2017). Some of the benefits of batteries include rapid response to load changes, low standby losses and high efficiency (60 – 95 %). Generally, the operation of batteries requires particular attention as they can be subjected to overcurrent, overvoltage or overcharging/discharging, which can significantly impact on their lifespan and on the micro-grid reliability. Hence, a battery management system is important to ensure the battery safety and optimise its performance.

1.1.3. Energy Management Systems

The energy management system (EMS) is a method utilized for monitoring and optimizing a system operation. Generally, the energy management system is utilized to control power generation and schedule programs for a group of power grid applications (Morstyn et al., 2019). However, energy management system may be considered as another way to control the electrical loads in micro-grids. Therefore, interest in improving the energy management system as the core of micro-grids has been greatly augmented to facilitate the integration of more renewable energy sources in the power system in a safe, stable, reliable, robust, optimal and coordinated strategy (Chowdhury et al., 2020). Specifically, more attentions have been focused on the optimization of the energy management system by seeking efficiency, economy

as well as environmentally friendly operation of micro-grids.

In the last years, much interest for the energy management system of micro-grids have been essentially augmented. Nevertheless, most of the researches are focused on the traditional platforms that cannot represent effectively the reality because of many purposes such as inexact models, deterministic estimations and balance conditions (Feng et al., 2019). To improve the performances of micro-grids and energy storage system (ESS), an advanced energy management system design and new control strategies are required (Totem, 2019). Depending on these aspects, several studies were reported focusing to enhance the proper action and operation of energy management systems, which still need much more interests.

1.2. Statement of the Research Problem

In micro-grids, batteries have been the favourite energy storage technology focus on addressing and accelerate United Nations Sustainable Development Goal 7 ‘Affordable and Clean Energy’ as well as contributing to the discussion around the long-term mitigation of climate change. However, their improper or non-effective operations can cause over-current, overvoltage or overcharging/discharging and significantly impact on their lifespan and on the micro-grid reliability. The problem in this research is the lack of a proper battery management system in a renewable DC micro-grid.

1.3. Motivation for Research

Due to the current generation methods based on fossil fuel, is driving increase in greenhouse gas emissions. To solve these problems, several countries around the world have engaged in large deployment of the renewable energy sources, which are wind energy, solar power, biomass energy, tidal and hydropower. This deployment facilitated by micro-grids, which serve as platforms for the renewable sources incorporation within utility grids. These micro-grids provide benefits such improving the reliability of power supply, managing local loads with high power quality, mitigating carbon dioxide and reducing transmission and distribution network costs. Three different types of micro-grids exist, which are the AC micro-grid, the DC micro-grid and the hybrid micro-grid. This research considers a DC micro-grid.

1.4. Aims and Objectives of the Research

The aim of this research is to develop a battery management system algorithm to control the charge and discharge of a battery bank linked to a DC micro-grid and to keep its SoC in admissible limits to avoid deep charge / discharge.

The objectives of the research are as follows:

- Develop DC micro-grid component models to be used in the simulation model using MATLAB/Simulink software
- Design and develop function block logic to be used for the simulation using State-Flow logical programming environment in MATLAB/Simulink software
- Develop a control system scheme for the DC micro-grid using State-Flow logical programming environment in MATLAB/Simulink software
- Develop an energy management system (EMS) algorithm for the DC micro-grid using State-Flow logical programming environment in MATLAB/Simulink software
- Develop a battery management system (BMS) algorithm using State-Flow logical programming environment in MATLAB/Simulink software
- Design and develop simulation of a DC micro-grid with battery energy storage using MATLAB/Simulink software

In addition, the research is to establish advantages of DC micro-grids employing the developed approach. The use of battery energy storage systems, especially in renewable micro-grids has an important role on the reliability of the electric power as it can smooth the power fluctuation, reduce power quality problems and control the voltage, in this regard an energy management strategy needs to be implemented. The software model must be flexible to enable the users to access and to change any control parameter within the DC micro-grid.

1.5. Methodology

The methodology adopted in this study is as follows:

1. Review of literature on micro-grids, their power electronics converters and control approaches,
2. Development of mathematical models of components of the DC micro-grid
3. Development of an algorithm for the battery management system
4. Development of a Simulink model of the DC micro-grid,
5. Simulation of the developed Simulink model and analysis of the results.

1.6. Research Questions

- How can battery energy storage systems in DC micro-grids be made more efficient by the energy management control algorithms?
- In order to balance the state of charge of each battery, how will the definition of the software model determine the control algorithm?
- Looking at the voltage drop of each battery, how will the SOC factor be adjusting in admissible limits?

- By introducing the energy management of a battery algorithm, will the system be able to avoid the deep discharge or the premature charge of a battery bank and increase lifespan of the storage system?
- Will this energy management of a battery contribute significantly to the reliability of micro-grids?

1.7. Significance of the Research

The use of batteries into DC micro-grids reduces the variation of power flow caused by fluctuating renewable energy sources. They contribute significantly to the reliability of micro-grids. Generally, the operation of batteries requires attention as they can be subjected to overcurrent, overvoltage or overcharging/discharging, which can significantly impact on their lifespan and on the micro-grid reliability. Hence, a battery management is important to ensure the battery safety and optimise its performance.

1.8. Plan of Development

Chapter 1: Provides the background, the statement of the research problem, aims and objectives. It presents also the methodology, the significant of this thesis.

Chapter 2: A literature review on micro-grids is presented in this section.

Chapter 3: This section gives the back ground on energy storage systems, power electronic converters for batteries and power electronic converters control.

Chapter 4: Describes the System and the modelling for the project.

Chapter 5: The results of simulation and analysis of the developed DC micro-grid model and energy management system algorithm are discussed.

Chapter 6: The conclusion of the research is presented in this section. A summary of the research is given and some future works are proposed.

CHAPTER 2: LITERATURE REVIEW ON MICRO-GRIDS

2.1. Overview

An overview on the concept of micro-grid using distributed generation (DG) systems based on diversity of sources both renewable and non-renewable is described through with its principal characteristics making it as an attractive option for electrification. There exist several types of energy storage system. In this research, only four types of technologies will be studying, which include chemical batteries, gravitational pumped storage systems, compressed pressurised air storage and mechanical flywheel.

A DC-to-AC VSI is utilised as an interface between the utility grid and the end user loads in the distributed energy sources. The inverter is used in a micro-grid to form an interface between the DC voltage of the renewable energy source with the AC voltage requirements of the load demand and the utility grid. The inverter is also utilised for stabilizing the grid by controlling the voltage, frequency, the active power and reactive power. Furthermore, the converter allows to connect battery energy storage system (BESS) to the grid, thus, a review on the basic power electronics converters and control used for batteries charging and discharging needs to also be discussed.

2.2. Concept of Micro-Grid

A typical micro-grid refers to a set of distributed generation (DG) systems based on renewable and/or non-renewable sources, incorporating an energy storage system (ESS) and local controllable loads, generally connected to the distribution system (Agrawal & Mittal, 2011). It may operate in both grid connected and isolated mode depending on the load condition. Micro-grids can be grouped into diverse categories depending on the location (such as campus, military, residential, commercial, and industrial), size (such as small, medium, and large scales), application (such as premium power, resilience-oriented, and loss mitigation), and connectivity (off-grid and grid-connected) (Lotfi & Khodaei, 2017). Generally, there exist three types of configurations, which are remote, grid-connected and networked.

A hybrid micro-grid integrates several distributed energies sources; the power from these sources is collected, converted and distributed according to the load requirements. A control system is needed to ensure a proper operation of micro-grid when power electronics interface with it to form a single unit. The control system is very necessary, besides providing flexibility, it also preserves the specific energy production and the power quality (Totem, 2019). A representative idea of a micro-grid can be given through Figure 2.1, where it is shown that a

micro-grid can be interconnected with the utility network, include a variety of energy assets and resources in order to provide different services to a range of facilities.

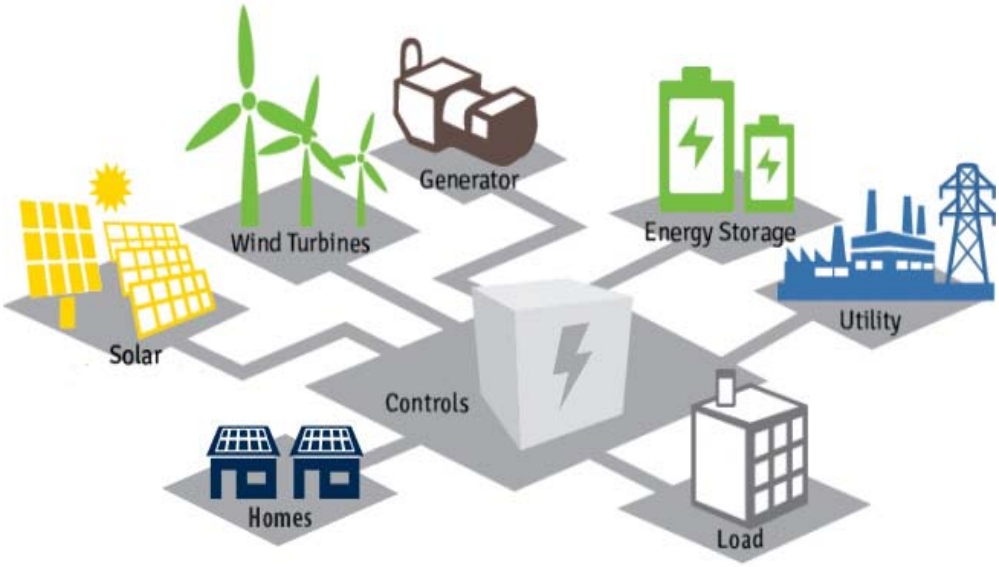

Figure 2.1: A typical micro-grid (Totem, 2019)

Based on the environmental interests (such as atmospheric, ground and water pollution, climate change), the utilization of fossil fuels, the finite and limited quantities of conventional fuels, the augmentation cost of electrical power, the necessity of energy security and the independence of some nations, reinforce the desire to adopt and develop renewable energy technologies (Chowdhury et al, 2019). The decentralization of electrical power generation brings production closer to the point of consumption, increasing system dependability, because if a fault happens somewhere and one part of the grid is isolated, that will not affect other sections. In addition, it raises the efficiency of the entire system, as transmission losses are reduced (Jones & Chowdhury, 2018).

All of the above obtain higher importance due to the unlimited augmentation in energy requirement around the world, with a varying rate between the nations and the continents. For practical and scientific benefits, significant motivations are deployed to encourage the integration of micro-grid projects for electrification in remote regions as well as nations in development (Hirsch et al, 2018). The great augmentation in electrical energy demand, requires more actions to optimize the grid, congestions alleviation and introduction of urgent auxiliary services. The significance and nature of the role of the micro-grid differ depending on the location where it is installed and the conditions (Carpintero-Rentería et al, 2019).

2.2.1. The Divergence between a Traditional Power Grid and a Micro-Grid

A conventional grid refers to a unidirectional grid, which produces power at one end and then transmits it to other areas where power is required. After long transmission, the power is distributed to each specific customer using a distribution transformer to decrease the voltage at consumer level. A micro-grid may operate connected to a conventional grid or autonomous, which is known as islanded mode (Islam et al., 2014).

Despite the fact that the conducting force and the objectives of the micro-grid in different countries are not precisely the same, the following elements below of micro-grids are generally characterized as the principal divergences compared to the traditional power grid (Feng et al., 2018):

- ✓ Improve the adequacy of discontinuous renewable energy sources and enable the electricity grid to adjust diverse power source structures.
- ✓ Virtually eliminates the risk of large-area and long-time power failure, except for large-scale physical damage.
- ✓ Promote the economy and reduce costs, energy consumption and emissions.

The distribution of the power grid is a fundamental factor to secure and stabilize the operation of the electrical system as well as to optimize the allocation of resources. According to the large-scale access of distributed generation (DG), periodic renewable energy resource, higher demands to the reliable power generation and economy, traditional power grid cannot achieve the requirement performed by the micro-grid improvement (Richter et al, 2012). Thus, the distribution of the micro-grid differs to the traditional distribution power grid. Based on the inappropriate restoration process of the traditional power system, this requires a rapid intervention, generally manual and in a real time, while in a micro-grid system the entire processing of the restoration is much more easier due to a limit number of controllable variables (Difference between traditional and MG) (Islam et al., 2014). Figure 2.2 shows the divergence between conventional and micro-grids.

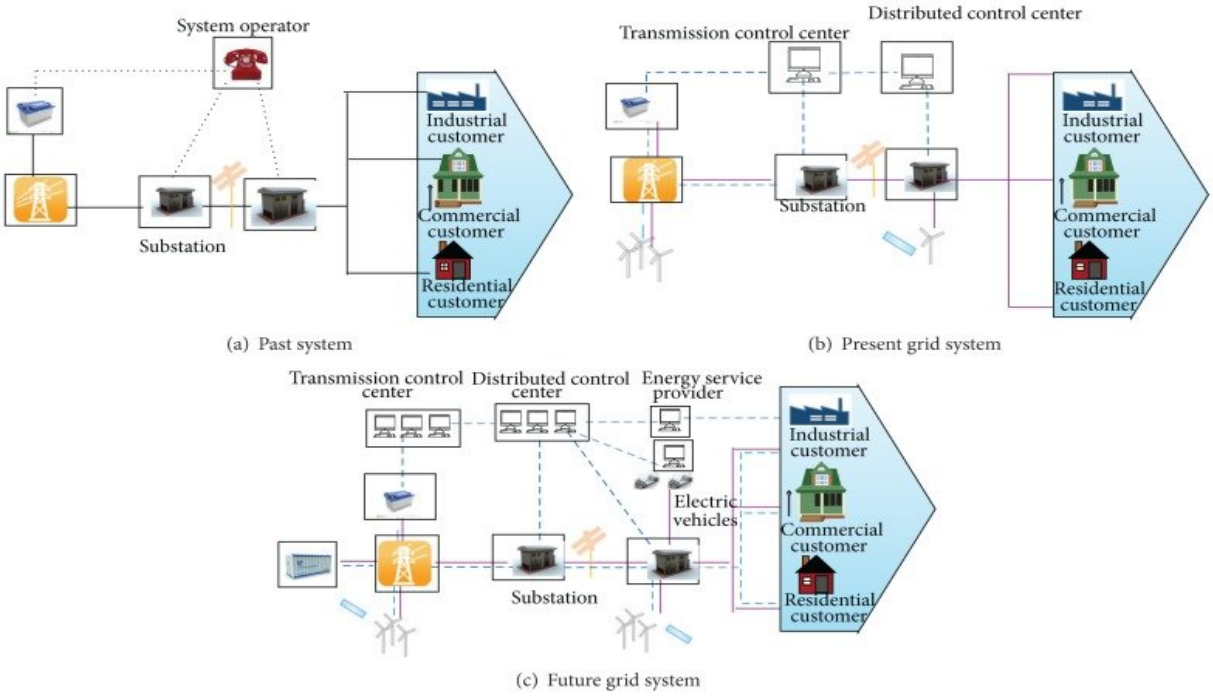

Figure 2.2: the divergence between conventional and micro-grids (Islam et al., 2014)

2.2.2. Some Benefits of a Micro-Grid

The development of micro-grid brings several gains compared to other technologies, as listed below (Chowdhury et al., 2019):

- According to the environmental protection, a micro-grid enables to reduce pollution due to it uses micro-source, which generate low or zero emissions.
- Micro-grids operate in parallel to the utility grid; this allows to take care of other loads by supporting the utility grid. The surplus of production generated by micro-grids may help to prevent overload issues and blackouts of the utility grid.
- Reduces the size of the transmission line and the installation. Micro-grids also reduce the use of fossil energy.
- The operation in both grid-connected and isolated mode, micro-grid provides uninterrupted power supply to the loads. This property gives it the ability to be more reliable and provide a high power quality to the critical loads.
- A micro-grid becomes more advantageous than the thermal energy saving when utilizing the combination of heat and power. This process is simple to reach with the micro-source in a micro-grid. The micro-source may be located closer to thermal and electrical loads to maximize energy efficiency.

2.2.3. Types of Micro-Grid

The micro-grid refers to a small power system that includes diverse elements, like DG sources, loads and storage systems, which are interconnected. There exist three types of micro-grid in terms of power, as an AC power system, a DC power system, or a hybrid system. Each of these three sorts of micro-grid presents advantages and disadvantages (Wang et al., 2012). The following Figure 2.3 presents the different types of micro-grids.

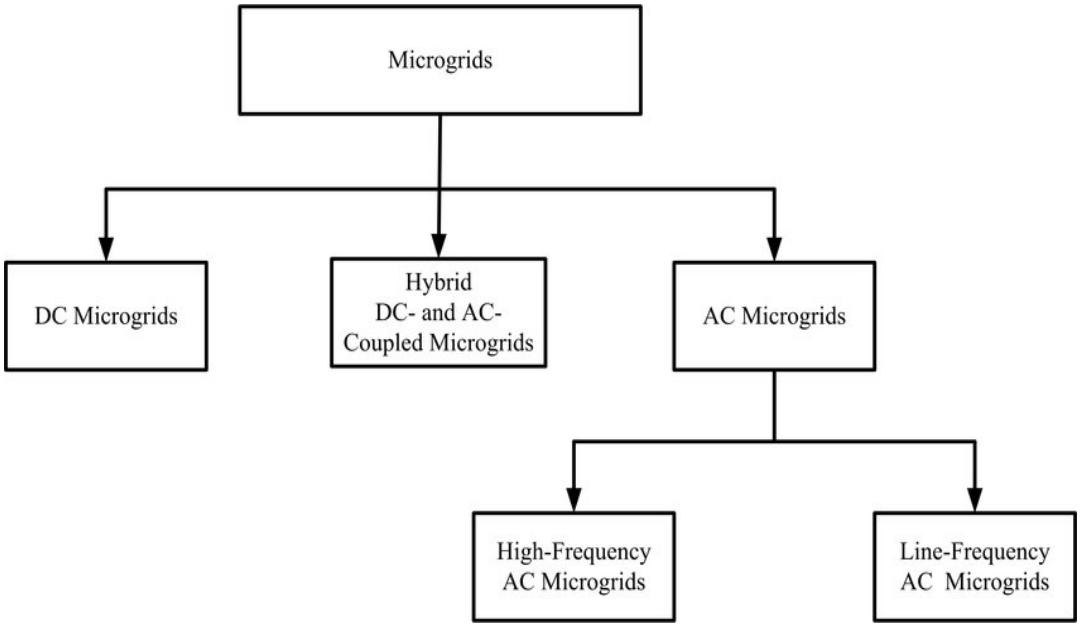

Figure 2.3: Classification of the micro-grid based on power type (Wang et al., 2012)

2.2.3.1. The DC Micro-Grid

DC Micro-grids have recently received much attention, especially for commercial and residential small-scale applications, as they provide an increased efficiency and controllability with additional power conversion stages being eliminated, synchronisation and compensation of reactive power no longer needed (Gu et al., 2014). In a typical micro-grid, the common bus is DC, hence, AC generators are connected to the DC bus through rectifiers, while inverters are used to supply AC loads (See Figure 2.4).

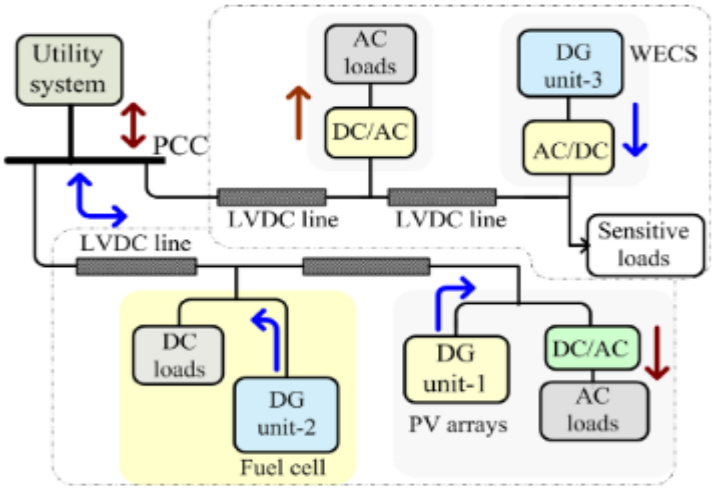

Figure 2.4: DC micro-grid with AC and DC loads (Justo et al, 2013)

The DC micro-grid can operate connected to the utility grid either isolated from it. It gives various operational advantages (Yadav et al., 2017).

- Many of the devices, which are connected to a DC micro-grid are generally electronic devices, such as TVs, computers, fluorescent lights, variable speed drives, households, businesses, and industrial devices. As there are directly connected to a DC type micro-grid, no power systems like AC-to-DC, DC-to- AC or AC-to-DC-to-DC are needed, which could be needed for an AC micro-grid.
- No transformer is used in a DC micro-grid; this characteristic makes it to be more efficient, reduced size, and more reliable in a DC power system. Moreover, a DC micro-grid has an ability to operate with twin wire cables, while an AC micro-grid operates with more wires (3 or 4).
- In DC micro-grids, there is no reactive power flow, therefore voltage control is assumed by the flow of active power, whilst in AC micro-grid the voltage control is associated to the reactive power flow and injects the active power, which mostly delimits the local power angle of the interfacing VSI.

However, a DC micro-grid still presents various issues that must be surmounted. There are no good practices implemented to manage fault situations and basic protective element such as circuit breakers, fuses and protection relays is lacking, like it can be seen in AC micro-grids (Lago & Heldwein, 2011).

2.2.3.2. The AC Micro-Grid

AC micro-grids are the most general type of micro-grids whereby distributed generation systems based on renewable and non-renewable are connected to the loads via a common

AC bus using power electronic converters (See Figure 2.5) (Justo et al., 2013). In such a case, DC generators and energy storage units are connected to the AC bus through DC to AC converters, while rectifiers are supplying DC loads (Camblong et al., 2009).

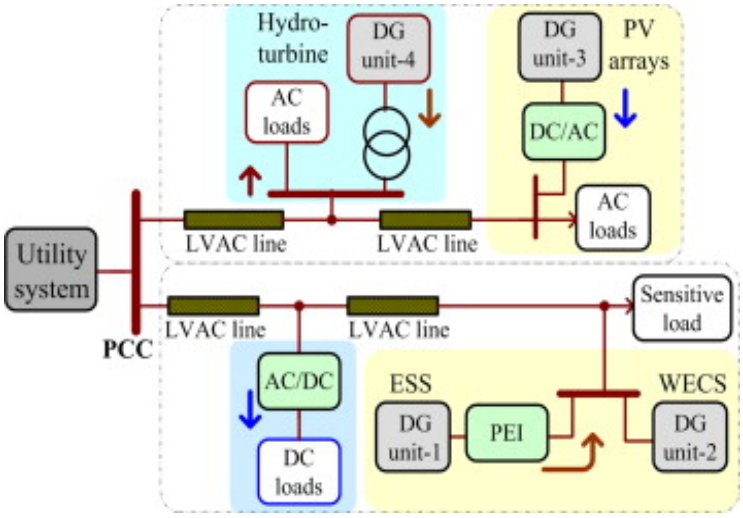

Figure 2.5: AC micro-grid with AC and DC loads (Justo et al., 2013)

All the distributed generation systems, which produce an AC output power, like wind turbine and biomass, may directly be connected to an AC-bus line of the micro-grid or through an AC/DC/AC power converter (Lotfi & Khodaei, 2017). The AC micro-grid has a facility of using the infrastructure that exists from the utility grid, because of its power system capability as well as the fact for being compatible with the utility grid. This implicates that the AC loads are directly linked to a AC micro-grid without needing power transformation converters (Justo et al., 2013).

2.2.3.3. The Hybrid Micro-Grid

A hybrid micro-grid includes an AC and DC micro-grid, it combines AC and DC buses types (See Figure 2.6) (Kishore & Ravikumar, 2016). A typical presentation of a hybrid micro-grid is illustrated in Figure 2.6; the red colour line describes the DC power flow and the blue colour line the AC power flow.

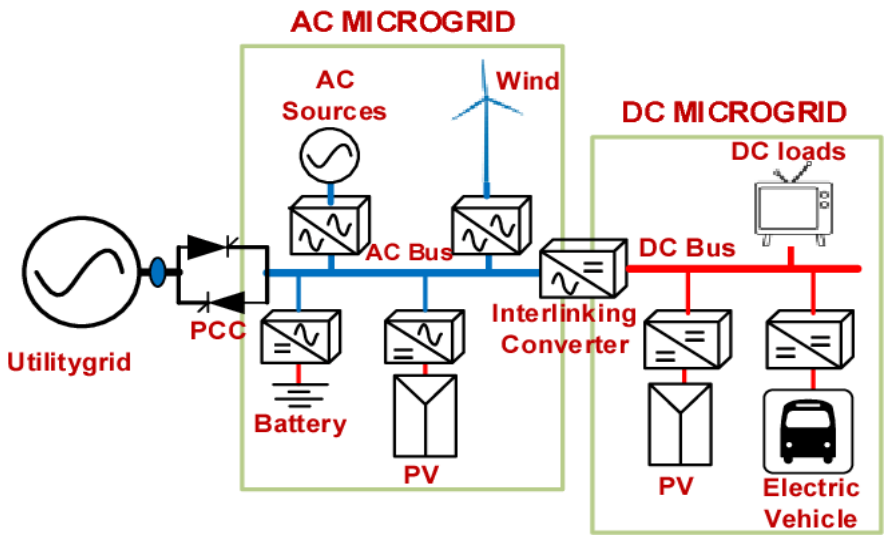

Figure 2.6: Conventional hybrid micro-grid (Kishore & Ravikumar, 2016)

For achieving the hybrid micro-grid configuration, bidirectional power electronics is utilized. The system offers more benefits in both side AC and DC micro-grid. An additional converter interface cannot be needed for supplying AC or DC loads, that augments the system efficiency and reliability. The coordination of a control algorithm can be required by the system to achieve the stability of the performance, which is a challenge for this type of configuration (Ortiz et al., 2019).

2.2.4. Micro-Grid Architecture

Figure 2.7 presents the architecture of a micro-grid and consists of the following components (Jadav et al., 2017):

- Distributed generations,
- Energy storage system,
- Control and communications modules

These equipments are linked to a low voltage grid dispatching. The low voltage dispatching integrates a diversity of micro-sources and diverse types of loads interfacing with the power electronic systems. To make sure of a good harmonization and control of the system, the Point of Common Coupling (PCC) can define the operating mode, which could be grid connected mode or autonomous mode. The PCC connects the micro-grid with the main medium voltage utility grid. The role of PCC is to connect or disconnect the micro-grid system from, or to the utility grid. To provide a total system stability, a micro-grid is supported and coordinated via diverse control levels, using micro-source and central controllers.

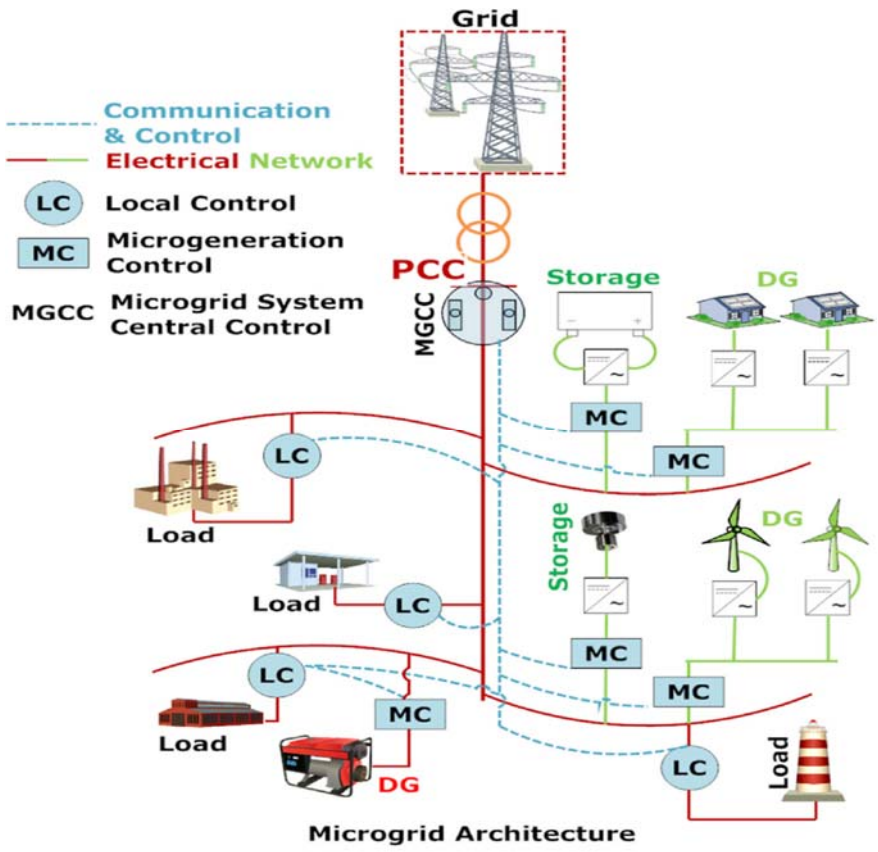

Figure 2.7: Micro-grid architecture (Mariam, Basu, & Conlon, 2016)

2.3. Distributed Generation Systems

Distributed generation includes a diversity of sources both renewable and non-renewable (Lasseter & Paigi, 2014). Renewable sources refer to generators that use renewable energy as the primary energy to produce electricity. They include technologies like photovoltaic, solar thermal power, wind power, biomass, tidal power, geothermal power, etc. Non-renewable sources use natural resources that are not naturally replenished to generate electricity see in Figure 2.8 (Ustun et al., 2011).

The power electronics are required to the source side of the output of a micro generator for converting power into its various forms; it may generate a fixed or variable frequency AC or DC. An inverter can be required for the conversion, or both rectifier and inverter to make sure that the frequency and voltage outputs concur to the grid one.

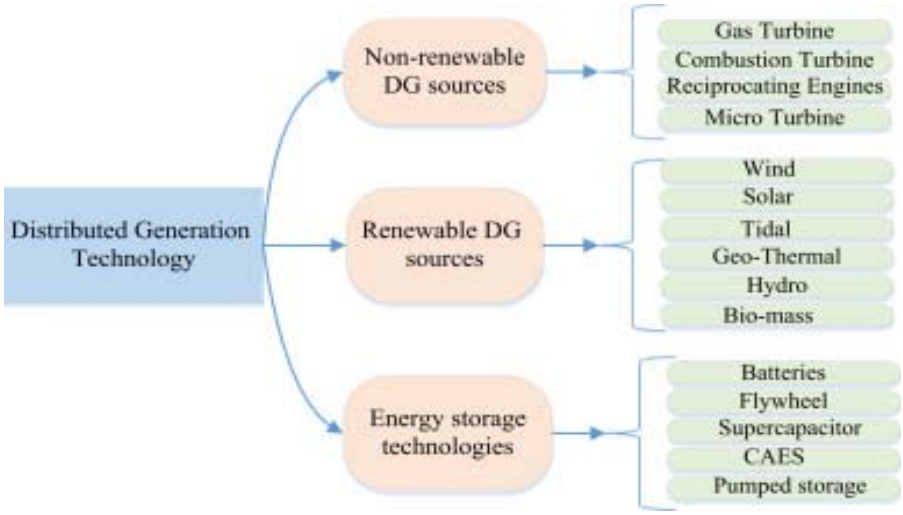

Figure 2.8: Distributed Generation Technologies (Muthuvel et al., 2017)

Based on power flow control, a micro-source may be classified as dispatchable or non-dispatchable system. The output operation set point of the dispatchable types is defined by the supervisory control system. Thereby, synchronous generators are conventional units, which allow external control and regulation (Muthuvel et al., 2017).

2.3.1. Solar Power System

Solar power can generate electricity into two different methods, which are solar thermal process and photovoltaic conversion. Solar thermal process converts solar power in heat, which drives a steam turbine as shown Figure 2.9 and produces electricity. Photovoltaic conversion consists of converting the photoelectric phenomena sunlight in electricity (Maghami et al., 2016). For photovoltaic systems, semiconductors such as silicon are used to form solar cells.

This generates an electrical voltage and the electrical current, which can drive a load. A solar cell constitutes an essential element of a photovoltaic system. These cells are connected in series and parallel to form modules, modules are connected in series to constitute strings and strings are connected in parallel to constitute arrays. On the other hand, solar thermal process uses solar collectors to collect heat; different types of collectors including parabolic through, concentrated solar collectors, etc. can be used (Cocco et al, 2016).

Because of the high cost and enormous losses of heat transport, solar thermal process is used for local domestic and industrial processes. The Combined Heat and Power (CHP) system achieves an efficiency of more than 80% comparing to a conventional power plant, which has an efficiency of approximately 35%; this big difference is because the CHP system is much closer to the user. The integration of a CHP system may participate to decrease the primary

energy use to up to 35% and reduce CO_2 emissions to 30% comparing to a large coal-fired power station (Nrel & Group, 2015).

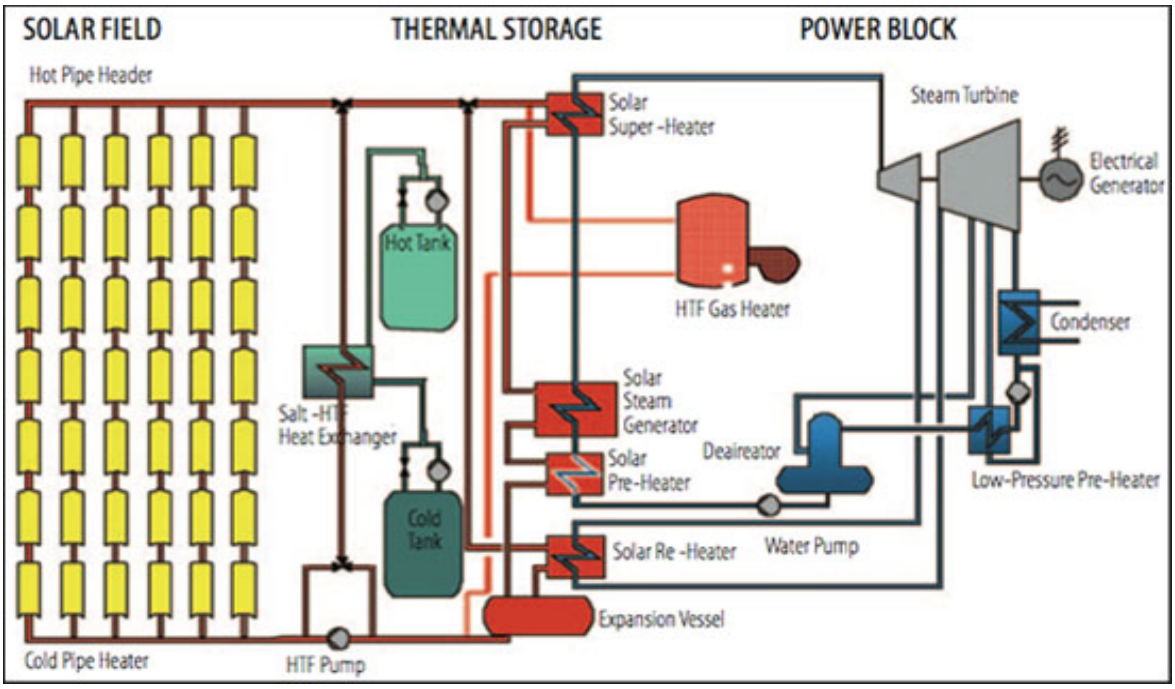

Figure 2.9: Block diagram of a concentrated solar power system (Cocco et al, 2016)

2.3.2. Photovoltaic System Presentation

By connecting the PV modules in an array unit is to generate a large quantity of electricity. Generally, a photovoltaic panel generates a constant DC voltage according to the irradiation of solar. Power electronics are principally needed, because they interface with the connection of micro-grid and an inverter is utilised to convert the produced DC voltage, in an adequate 50 Hz AC voltage. The weather fluctuations are very necessary to consider, because they enable to control the output voltage, which conduces to optimize the output voltage of the PV. The Maximum power point tracking is a specialized control technique improved, in order to extract the maximum generated power by the photovoltaic system. This controller allows to preserve the PV system operation at the highest possible efficiency to maximize the power extracted (Rajesh & Mabel, 2015).

2.3.2.1. Maximum Power Point Tracking Charge Controllers

The actual advanced technologies may allow the PV panels to operate at their maximum performance. Some aspects like temperature and diverse ambient states furnish disagreeable conditions for the operation of photovoltaic panels. A maximum power point tracking (MPPT) controller allows to make adjustments, according to the input generated by the PV systems and enable to control the output charge signal, which can conduce to the collected power

optimization from the PV systems. These controllers ensure the protection of the battery from over-charging (Sharma & Purohit, 2015). Based on the Solar-Electric (2015) brochure, an MPPT controller performs digital electronic tracking. MPPT utilises a technical method to sample the PV cells output voltage and provides a variable load to conserve the maximization of the output. This controller is utilized to adjust the PV module output, so that the maximum energy can be transferred to the batteries (Du Plooy, 2016).

2.3.2.2. Algorithms for Maximum Power Point Tracking

Various algorithms are implemented to track in a spontaneous way the peak power point from a solar panel. The principal used algorithm is the MPPT, which allows to extract the maximum power possible (Majid et al., 2011). The following controllers are the most developed for PV systems that use MPPT strategies:

- The perturbation and observation (P&O) algorithm
- Incremental conductance (INC)
- Parasitic capacitance
- Voltage-based peak power tracking
- Current-based peak power tracking

2.3.2.3. Photovoltaic Cell System Operation

The main operating mode of a PV cell refers to the conduction in a semiconductor such as silicon. Figure 2.10 illustrates the operation of a PV cell, as it is seen, the sombre area of solar cell is exposed to sunlight. When electromagnetic (EM) radiation hits the surface of the cell, this stimulates the electrons and induces them to move from a given energy stage (orbit) to another level, which leaves holes afterward (Molykote, 2017).

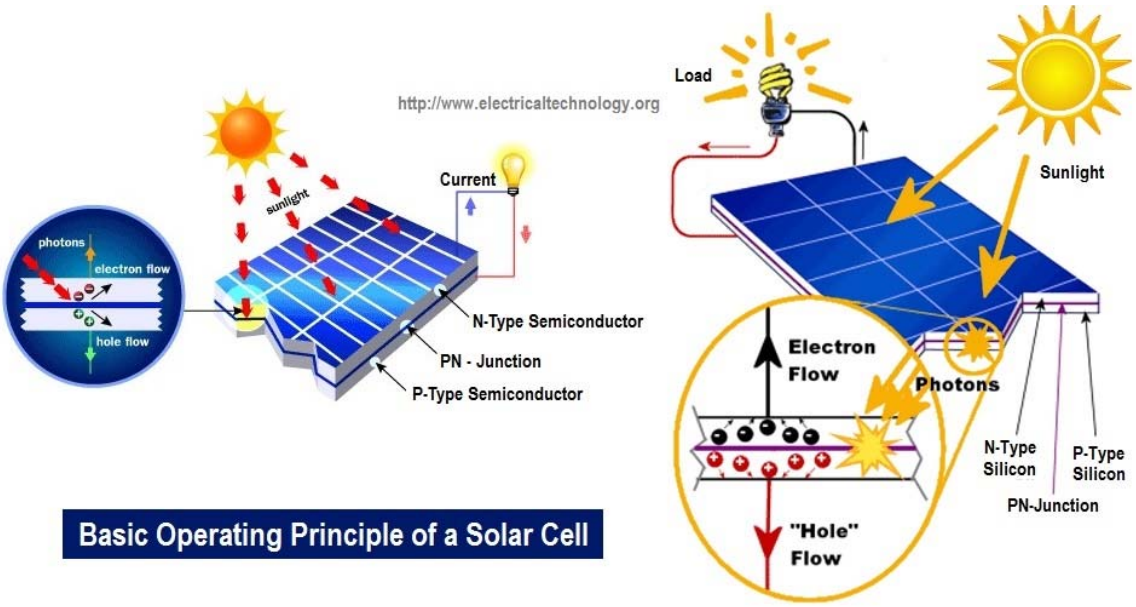

Figure 2.10: Photovoltaic cell operation (Molykote, 2017)

According to the proposed theory of operation of PV cell, the produced electric current is due to the relaxation of the excited free electrons within the PV cell by the incident photons. The PV cell refers to a device, which converts the incident solar energy in the electrical energy, therefore, there is electrical energy generated as long as there is incident solar energy on the PV cell and excitation of the free electrons within the PV cell. This explains how a PV cell can charge many capacitors without depletion, and can run a spark plug for a long time without weakening (Abdelhady et al., 2017).

2.3.2.4. Photovoltaic Module System

The electrical connection of photovoltaic cells is grouped in a series of rows and columns to form a module. To ensure the mechanical protection of cells against atmospheric agents, a glass pane is placed at the front of the module or by posteriorly placing isolating materials and plastics. A photovoltaic module is completely provided with high efficiency polycrystalline silica cells, which use a prismatic glass pane for optimizing light scattering as seen in Figure 2.11 (Strings et al., 2019).

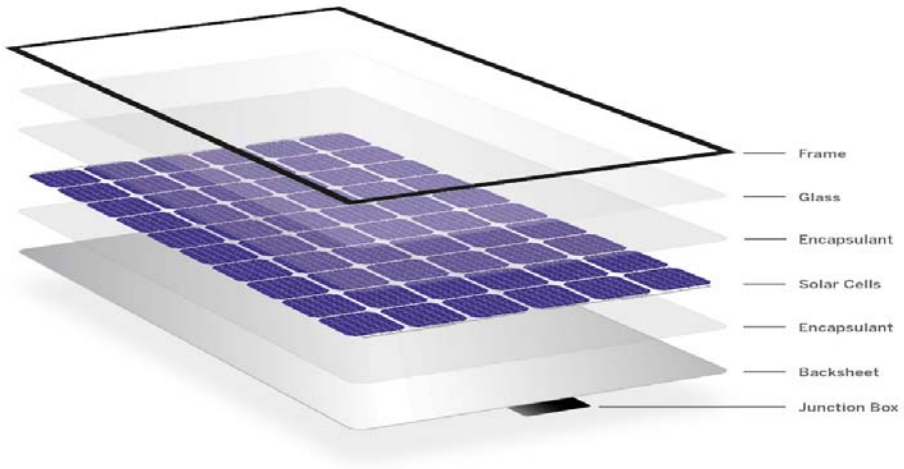

Figure 2.11: Photovoltaic module system (Strings et al., 2019)

2.3.2.5. Photovoltaic Array System

A photovoltaic array is a collecting link of photovoltaic modules, as it can be seen in the figure 2.12. Each photovoltaic (PV) module is made up of several interconnected PV cells (Singh & Rajput, 2016). The power that a module may generate is rarely sufficient to meet the needs of a home or business, so the modules are connected together to form an array.

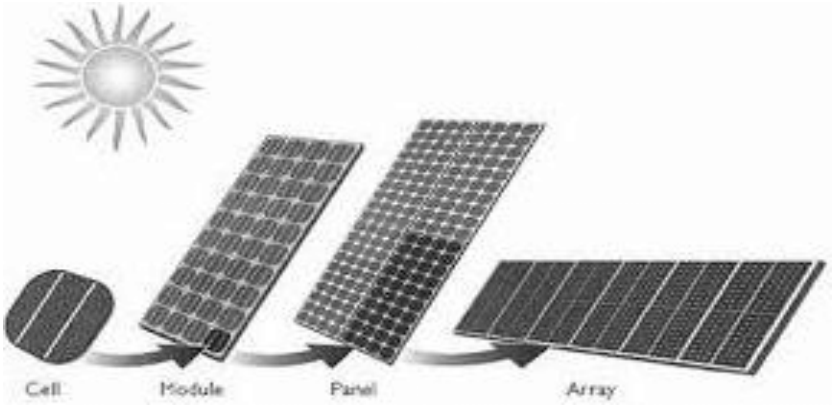

Figure 2.12: Photovoltaic array system (Singh & Rajput, 2016)

The modules of a photovoltaic array are firstly in general connected in series to reach the wanted voltage; the strings are after individually connected in parallel to enable the system to generate more current.

2.3.2.6. Solar cell efficiency

Over the past 10 years, the average efficiency of commercially available wafer-based silicon modules has augmented from approximately 12% to 17% (Super-mono 21%) and Cadmium-Telluride (CdTe) module efficiency raised from 9% to 18% (Salmi et al., 2012). Mono-

crystalline silicon is the most efficient module in the laboratory with an efficiency of 24.4%. Record efficiencies establish the potentiality of further efficiency augmentations at the generation level. High concentration multi-junction solar cells today reach an efficiency of over 47.1% in the laboratory (Freiburg, 2019).

2.3.3. Wind Energy Power System

The operational mode of wind turbines is characterized on two principles: Firstly, the conversion of kinetic energy of the moving air in mechanical energy, which is achieved through the use of aerodynamic rotor blades and mechanical power control. Secondly, the conversion of mechanical energy in electrical energy through a generator, which generates electricity (Knopper & Ollson, 2011). Based on their topology, wind turbines are grouped in horizontal axis and vertical axis (see Figure 2.13) (Tawfiq et al., 2019).

The vertical axis wind turbine has a set upright rotor shaft, which can capture wind from any direction (Shahariar & Hasan, 2014). Moreover, the vertical axis does not need an additional mechanism to capture the wind. A heavy generator device could be placed on the ground to consequently reduce the tower load (Schubel & Crossley, 2012). Different types of generators including induction generator, doubly fed induction generator, synchronous magnet generator, permanent magnet synchronous generator, etc. are generally utilized to convert the electro-mechanical energy in electricity (Parker et al., 2016).

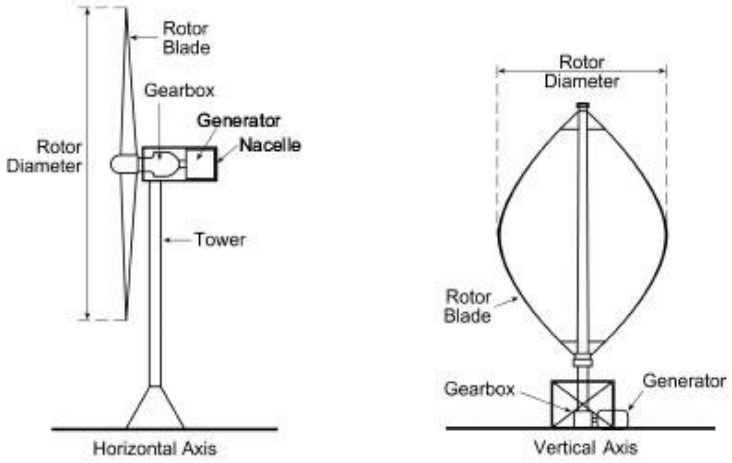

Figure 2.13: Vertical Axis versus Horizontal axis turbine (Salem, 2016)

Horizontal axis wind turbines present much more advantages then the vertical axis wind turbines. These advantages include:

- Providing a maximum amount of power; when the height increases the speed increases as well, consequently increasing the generator output power above the speed;
- Higher efficiency.

One of the disadvantages of the horizontal axis is that the generator is fixed on a tower, making the maintenance difficult (Tawfiq et al., 2019).

On the other hand, the vertical axis presents like advantages:

- Few moving parts simplifying the installation and maintenance, and raising the turbine efficiency;
- Low blade speed, less noise due to the low speed and less visual interference, because of the horizontal movement;
- No need for additional control compared to the horizontal axis.

However, the main disadvantage so far is their efficiency which is relatively smaller with slower rotation due to short towers (Shahariar & Hasan, 2014; Tawfiq et al., 2019).

2.3.3.1. Wind Turbine Characteristics

The characteristics of the included components therein (like rated output power and speed, cut-in and cut-out speed) affect the characteristics of wind turbines (Wrobel et al., 2018). Rated output power describes the maximum generated power of the rotor, which can describe the rate of the generator. Cut-in speed defines the minimum rotated wind speed of the turbine, the rated speed is the minimum wind speed allowing the turbine to start to generate the rated power and cut-out speed refers to the maximum wind speed that enables the turbine to develop power (Hossain et al., 2017). Beyond this speed, the wind turbine is stopped (Sumathi et al, 2015).

A common wind turbine extracts power from the wind, which is function of some parameters like wind power availability, wind turbine power curve as well as the ability to address the system variation (Barambones et al, 2019). In addition, the following equation (2-1) determines the captured wind turbine power (Bassols et al, 2016):

$$\mathrm{P_m}(\mathrm{v},\lambda,\beta) = \frac{1}{2}\mathrm{Cp}(\lambda,\beta)\,\rho\pi\,\mathrm{R}^2\mathrm{v}^3 \qquad (2\text{-}1)$$

Where $\mathrm{P_m}$ represents the power (W), R refers to the rotor radius (m), ρ is the air density (m^3), v is the wind velocity (m/s), $\mathrm{C_p}$ the coefficient of wind power, and β is the pitch angle

C_p refers to the extracted wind fraction of the wind turbine and their theoretical value limits to 59.7%, according to Betz rules (Sumathi et al., 2015). Similarly, Equation (2-2) as gives tip-speed ratio:

$$\lambda = \frac{R\omega}{v} \tag{2-2}$$

Where λ is tip-speed ratio for the wind turbine (radian), ω is the rotational speed of the rotor (radian / second), R is the rotor radius (m) and v is the wind speed (m / s).

2.3.3.2. Power Electronics Converters for Wind Turbines

Over the two past decades the investigation of diverse converter configurations has been performed depending on the power condition of the wind turbine generators. Most of the developed converters present some benefits and some challenges. Back to back bidirectional and diode rectifier based unidirectional converters represent the common converters topologies commercially utilized in the wind turbine generators (Blaabjerg et al, 2007).

1. Diode rectifier based converter

According to this topology, the wind turbine generator output frequency and magnitude AC power are converted in DC power through a circuit made up of a diode rectifier and afterwards by using a controlled inverter and after converted back in AC power at diverse frequency and voltage levels. The diode rectifier (uncontrolled rectifier) based converter system allows the transfer of power in one direction (like from generator to the grid). Diode rectifier topology is generally utilized in wind power generation system such as wound rotor synchronous generator (WRSG) or a permanent magnet synchronous generator (PMSG) instead of an induction generator (Islam et al, 2013). Figure 2.14 illustrates a diode rectifier using a step-up chopper system.

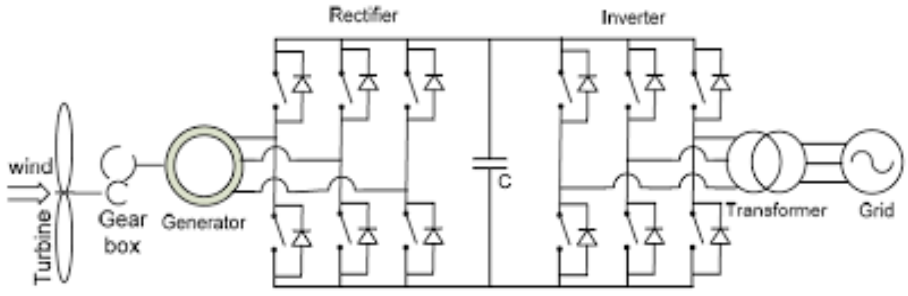

Figure 2.14: Diode rectifier based converter (Islam et al, 2013)

This converter presents as advantages: low system generation cost and easy implementation. In contrast, the diode rectifier presents as disadvantages: a large quantity of harmonics (input

current) affecting on the utility system performances, high harmonic losses (output voltage) and a single direction power manipulation ability.

2. Back to back converter

Back to back converter also refers to a controlled rectifier and a controlled inverter based converter and it is composed of two conventional pulse width modulated (PWM) voltage source inverter (VSI). The rectification stage makes it be differed to the diode rectifier based converter, by replacing the diode rectifier with chopper circuit by a controlled rectifier (see Figure 2.15). The bidirectional power flow ability is given by the controlled rectifier, which was impossible with the diode rectifier based converter (Mrcela et al, 2016). Furthermore, with the controlled rectifier the input current harmonics as well as harmonic losses are generally reduced.

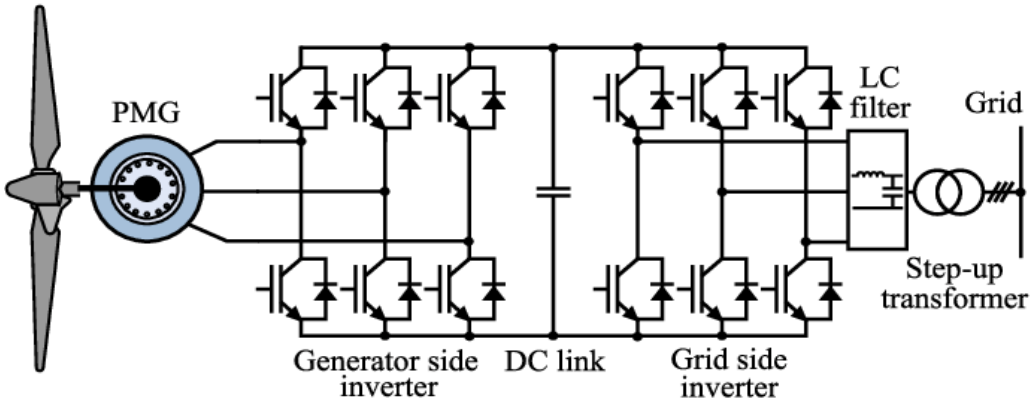

Figure 2.15: Back to back converter based wind turbine generator system (Mrcela et al, 2016)

This converter operates as a bidirectional power converter, it can boost the DC-link voltage to a higher level than the grid line to line voltage amplitude to reach the grid current full control, the decoupling control of the two inverters is assumed by the capacitor, which interfaces between the inverter and rectifier and this enables the asymmetric compensation on the grid and generator. This converter is composed of two inverters, which can make the switching losses to even be more accentuated, an extra EMI-filters may also be required for a higher switching speed to the network, and the combining control of the controlled rectifier and inverter is a bit complicated (Islam et al., 2013).

2.3.3.3. Voltage Source Converter and Current Source Converter Wind Turbine

The voltage source rectifier can operate as a power conversion topology. While the current source is considered a double part of a voltage source rectifier (Bao et al, 2012). When the voltage source drives the system, the topology is characterised by a capacitor (dc link voltage), which composes a direct link voltage with the bulk capacitor. The current source topology allows the control of the wind variable by either the inverter or the rectifier side (Lumbreras et

al., 2016). One of the important elements to be controlled in current source converter topology is the direct current link. This direct current link characteristic allows power flow from the generator to the network.

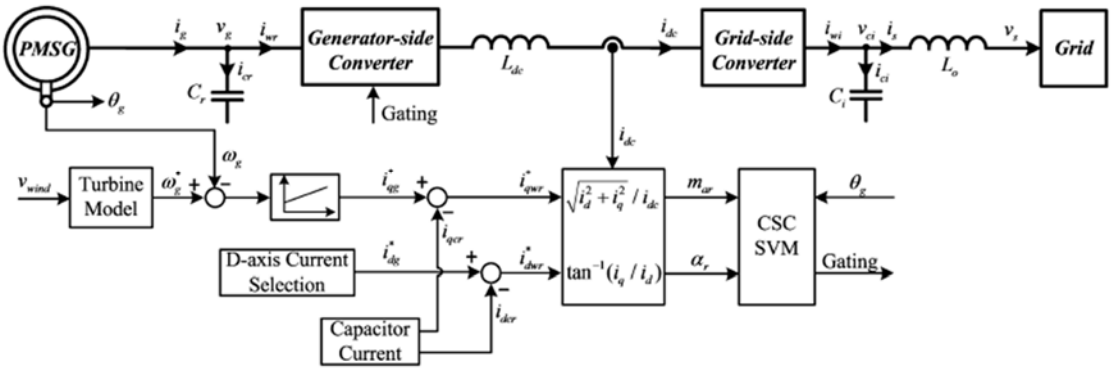

Figure 2.16: Generator side block diagram (Lumbreras et al., 2016)

The generator side needs to be controlled, as there are some elements like the generator stator, which requires the control of the current to set the torque and consequently the rotating speed as shown in Figure 2.16. For the network side, the objectives of the control consist of regulating the dc link current as well as manipulating the injected reactive power to the grid (see Figure 2.17). In addition, the converter must be capable to support the generator output variable frequency and voltage in order to control the speed (Blaabjerg et al, 2012).

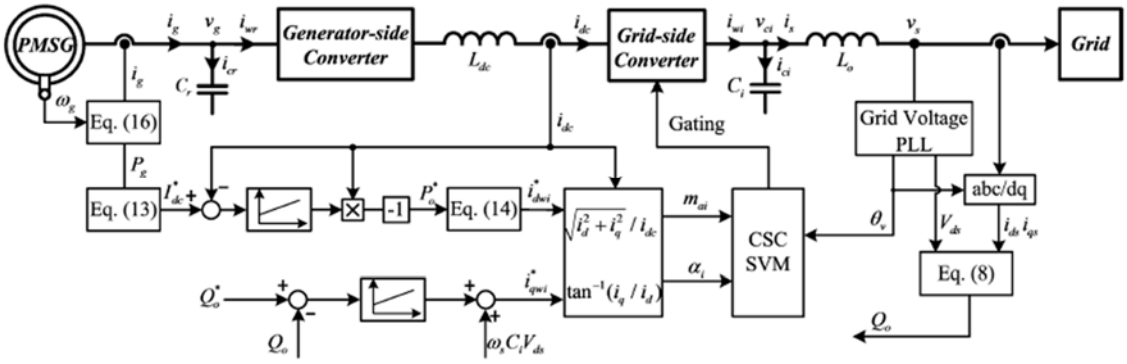

Figure 2.17: Grid side block diagram (Lumbreras et al., 2016)

2.3.4. Geothermal Power

Geothermal power consists of converting the containing energy in the hot rock in electricity by utilizing water to absorb heat contained in the rock and transporting that heat to the surface of the earth and converting it in electric energy via turbine generators as seen in Figure 2.18. High temperature water (> 240 ° C) is partially vaporised in steam and the conversion of heat to mechanical energy is realized by using low-pressure steam turbines (Sheth &

Shahidehpour, 2004). Exploitable geothermal reservoirs are located in highly permeable, high temperature, fluid-filled rocks in the upper part of the crust of the earth, usually in areas combined with young volcanic rocks (Valishin & Variamova, 2008).

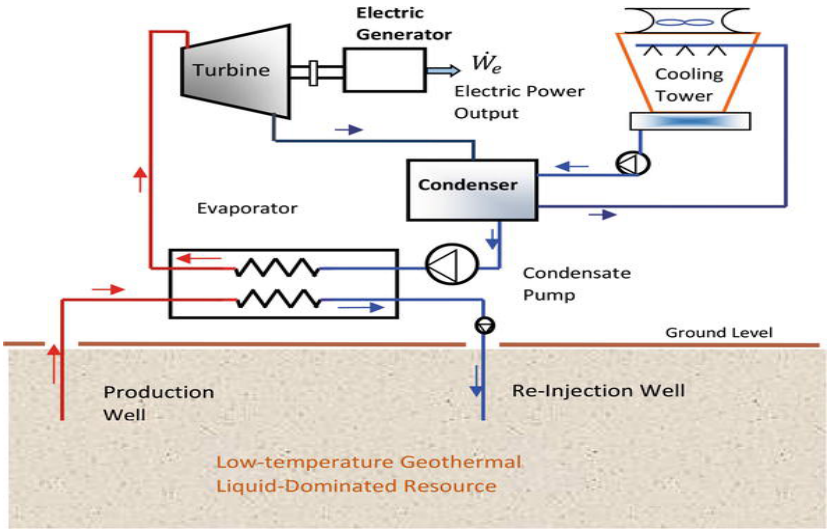

Figure 2.18: The basic concept of geothermal energy system for power generation (Subia, 2010)

The production well extracts the geo-fluid (brine) from the geothermal energy resource and the extracted brine transports the heat extracts from the liquid resource, which in return is efficiently transferred to the low boiling point (BP) organic working fluid through a heat exchanger. The heat is absorbed by the low boiling point organic liquid and boiled at a practically a bit lower temperature (comparing to water), which results to a developed vapour pressure that can run the axial flow or the radial inlet turbine (Subia, 2010). The turbine is connected to an electrical machine that converts the mechanical energy from the turbine shaft to an electric energy (Qxodeghhq et al., 2019).

The most current operating geothermal power plants include dry steam plants or flash plants (which can be single, double and triple) and operate with temperatures above 180 ° C. But, medium temperatures are generally utilized for power production either for a production combination of heat and power through a binary cycle technology improvement, wherein a geothermal fluid is utilized through heat exchangers to heat a closed loop process fluid (Anderson & Rezaie, 2019).

2.3.5. Hydropower

The greatest renewable energy source is the Hydropower as it approximately generates 16 % of electricity in the world and about 80 % of the renewable energy of the world (Mo et al, 2015). Hydropower is a process referring to the generation of electricity from the water flowing in a

river either an ocean. The objective of hydropower production is to generate clean energy, which contributes to climate change (Basar et al., 2015).

The hydropower plant is generally constituted by the following equipments, which are a generator, a turbine, a penstock and a wicket gate as shown in Figure 2.19. The turbo-generator is driven by water and the rotating generator generates electricity. The water that is stored in the reservoir has a potential energy at the initial stage, while crossing the penstock and progressively before attaining the turbine, potential energy is lost and kinetic energy is gained (Kuenzer et al., 2013).

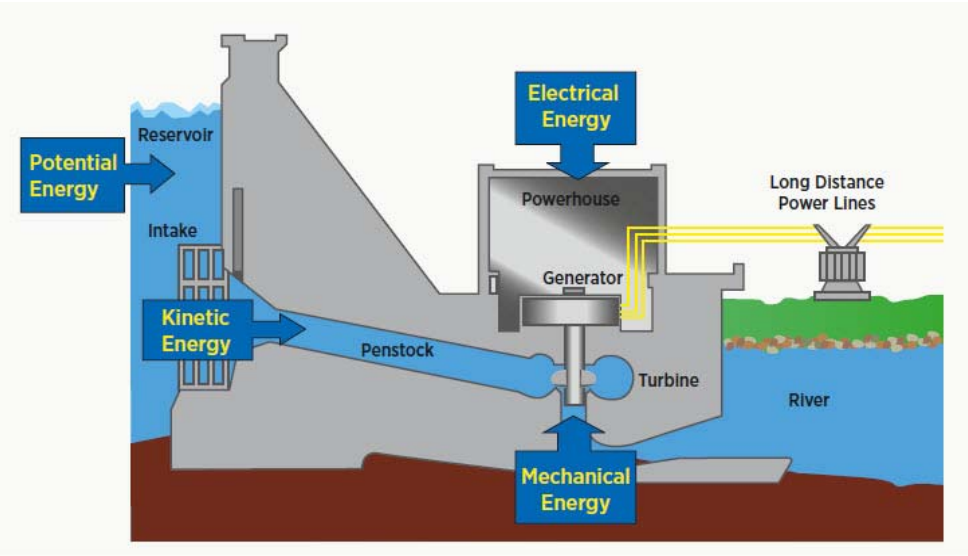

Figure 2.19: Typical of Hydropower Plant with storage (IRENA , 2012)

Hydropower is the transformation of the potential energy contains in the water that flows into a river or ocean with a certain vertical falling in an electric energy, which may be injected to the grid. The head and flow of water determine the potentiality of annual power production of a hydropower project. Hydroelectric power plants utilize a comparatively simple concept to convert the potential energy of water that flows in a river to run a turbine, which in return generates the mechanical energy needed to run a generator that produces electricity like it can be seen in Figure 2.19 (Pérez et al., 2017).

Generally, hydropower plants have very long lifetimes and particularly based on the component, they can be of the order of 30 to 80 years. Many examples exist, showing the hydropower plants that operated for over hundred years with regular upgrades of electrical and mechanical systems (Edenhofer et al., 2017). The using water to run hydropower turbines is not consumed but is returned to the river system. This cannot be instantly ahead of the dam

and may sometimes be several kilometres or further downstream, having a not insignificant effect on the river system in that zone.

2.3.6. Biomass Power

Biomass power uses the biomasses to generate biogas and the generated biogas is utilized as fuel in a biomass generator (see Figure 2.20) (Das, 2009). The used biomass comprises energy crops and wastes, like forest residues and a scope of other agricultural and industrial produces. Currently, biomass is becoming a more attractive system of global renewable energy representing a higher level for increasing the share of the world's electrical capacity (Rahman et al., 2015). Actually, the world's needs for renewable energy are increasing, it is to be expected that a new conventional thermal energy production plant from biomass will be deployed. Drax in North Yorkshire demonstrates the successful feasibility of the large-scale biomass power, showing in 2016 that it was capable to provide nearly 2GW of power from biomass alone (Mason et al, 2014).

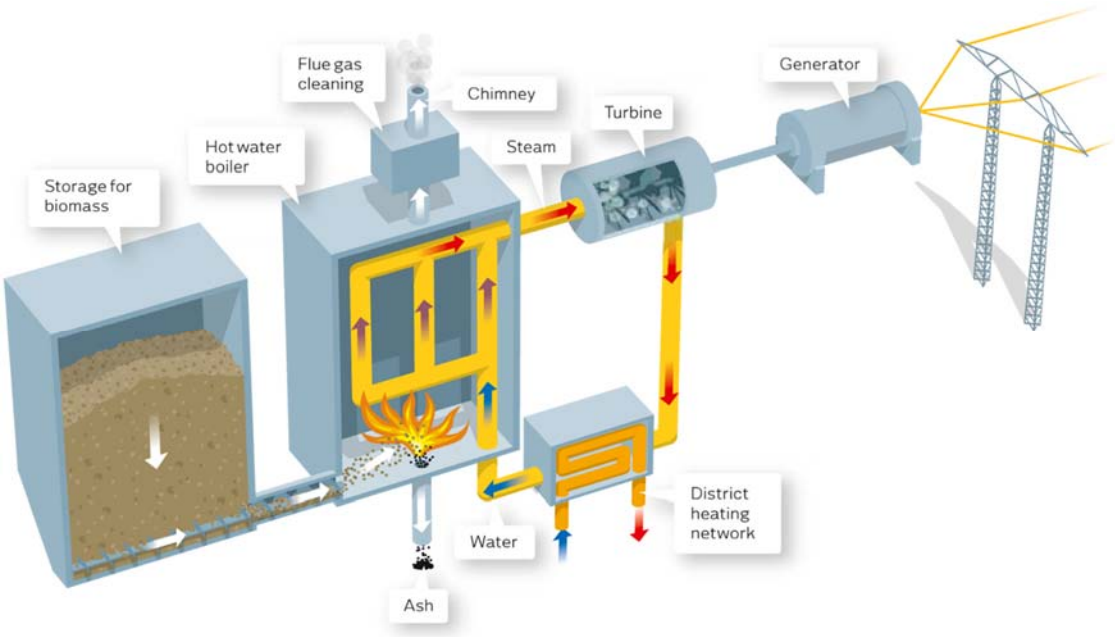

Figure 2.20: Generation of Electricity using Biomass (Sugar mill in Nepal) (Adhikari, 2020)

The process begins all on board by storing the waste and then transferred it in the boiler where is burned and produce heat. Under high heat temperatures, the water in the boiler becomes high pressure steam which is utilized to turn the turbine and the turbine drives the generator (Sharma & Goyal, 2015). The generator produces electricity which circulates in the network. The use of biomass power plant is very beneficial and can present many advantages such as less expensive, the environmental protection and climate change (Adhikari, 2020).

2.3.7. Micro-Turbines

Micro-turbine refers to an energy generator with a capacity ranging from 15 to 300 kW. Its operating mode is based on an opened cycle gas turbine (Hamilton, 2011). For small-scale distributed power production, micro-turbine generators have been presenting suitable perspectives. They present a good reliability factor and an easier design (high potentiality according to large-scale and low-cost manufacturing). Despite the fact that micro-turbines are not feasible to furnish power during peak periods this based on the results, but they can at least meet peak demand and ameliorate the reliability of power supply as they may furnish standby abilities if the power grid fails (Nascimento et al., 2013).

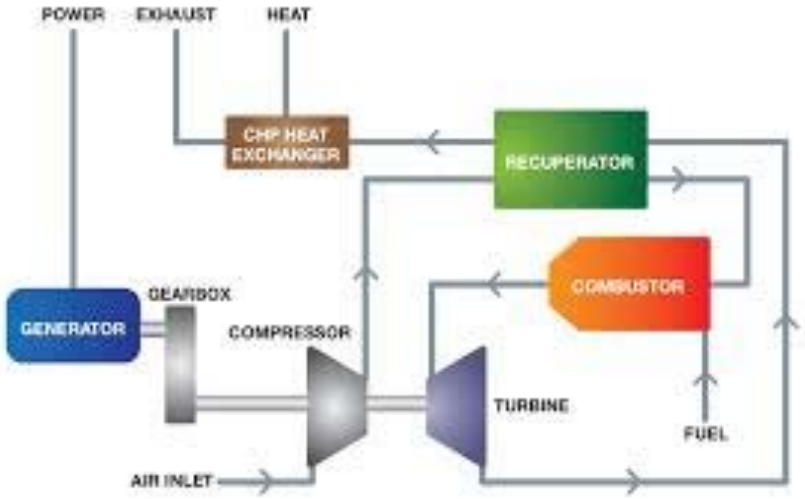

Figure 2.21: Micro-turbine-using CHP System Schematic (Darrow et al, 2015)

The block graphic of the principal components of the micro-turbine including the combination of compressor/turbine system, combustor, generator, CHP heat exchanger and recuperator is shown in Figure 2.21. The combined compressor-turbine unit constitute the core of the micro-turbine (or turbo-compressor) (Darrow et al., 2015). The micro-turbine generates electric power through a rotating high speed generator on a single shaft of the turbo-compressor either via a speed reducer, which drives a conventional 3600 rpm generator. The recuperator is a heat exchanger using the hot exhausting gases from the turbine (approximately 1,200ºF) to preheat the compressed air (approximately 300ºF) entering to the combustion chamber, thus decreasing the needed fuel that heats the compressed air to a required turbine inlet temperature (Padhi, 2010). Micro-turbines provide a supplementary heat exchanger package for the CHP operating mode.

2.3.8. Diesel Generators

A diesel generator (also known as genset) is constituted of two components an internal combustion engine and a synchronous generator both coupled on a shaft (see Figure 2.22). The diesel generator is extensively used as a commercially and industrially back-up either an emergency power system. They are also widely used for the new zones that present a difficulty to be supplied by the utility grid or expensive to implement (Krishnamurthy et al, 2018).

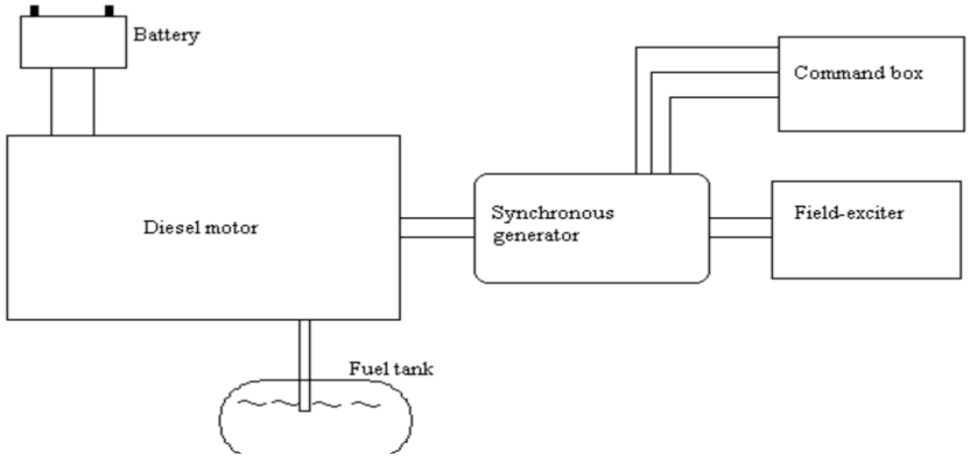

Figure 2.22: Schematic diagram of a diesel generator set (Jones & Chowdhury, 2008)

CHAPTER 3: BACK GROUND ON ENERGY STORAGE SYSTEMS

3.1. Energy storage Systems

A summary based on energy storage systems (ESSs), a review on the basic power electronics converters and control used for batteries charging and discharging are discussed. ESSs have a significant impact in a micro-grid, they serve to (Chakraborty & Simões, 2019):

- Balance power despite load fluctuations and other transients.
- Provide crossing capability and allow distributed generation systems to function as units that can be routed.
- Provide initial power for a transition between grid-connected or/from island-based micro-grid operations.
- Ensure uninterrupted power supply.
- Contribute in increasing the stability of the micro-network and improving power quality (Rai et al., 2015).

In general, energy may be stored into four distinct forms like:

- Chemicals (battery and fuel cell),
- Electrical (superconducting magnetic energy storage (SMES) and super or ultra-capacitor),
- Mechanical (pumped hydro, flywheels and compressed air energy storage (CAES) systems),
- Thermal (superheated oil or molten salts).

The most popularly energy storage devices used for micro-grids include batteries, flywheels, fuel cells and super-capacitors (Ustun et al., 2011).

3.1.1. Flywheel

Flywheel energy storage comprises a flywheel, bearings set, an electrical motor/generator, a power electronic converter, a vacuum chamber and containment or housing as illustrated in Figure 3.1. Energy is stored using accelerating rotor at a high-speed rate and stored in the system as kinetic energy. The stored energy in the flywheel energy storage system is generally taken from a given electrical source coming from the network either some other electrical energy sources. The common flywheel energy storage has the potential of charging and discharging faster without the influence of the variation of their operating temperature (Bolund, Bernhoff, & Leijon, 2017; Mousavi et al., 2017).

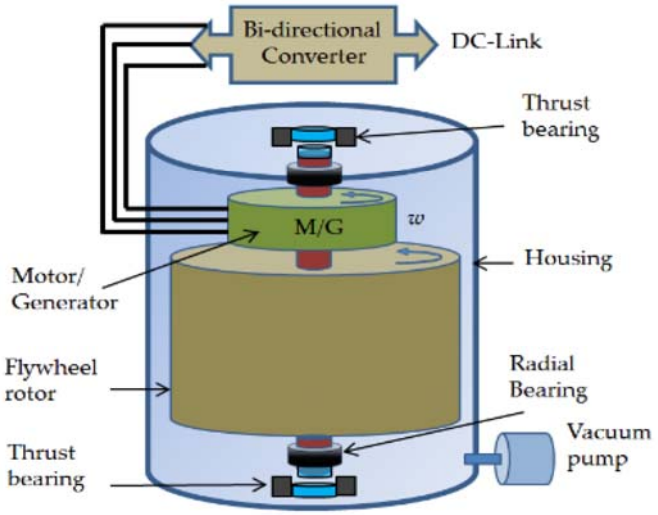

Figure 3.1: Flywheel energy storage advice (Amiryar & Pullen, 2017)

The electric machine or the incorporated motor / generator is coupled to the flywheel to allow the conversion of energy and the flywheel charging operation. The electric machine acts in two different ways. Firstly, as a motor, this operation allows to charge the flywheel by an acceleration movement and extracts an electrical energy from the source. Secondly, the same machine, reacts as a generator by extracting the stored energy on the flywheel and thus, during discharge the flywheel is slowed down (Amiryar & Pullen, 2017).

There are different electrical machines utilized in flywheel energy storage system, where the most popular include permanent magnet (PM) machine, induction machine (IM) and variable reluctant machine (VRM). The selection of the switching devices for the power converters depends on their operational characteristics and application. The back to back (BTB) or AC-DC-AC configuration is the power converters configuration largely used in FESS and it is connected to a DC link capacitor (Arani et al, 2017).

3.1.2. Fuel Cell

To generate electricity from fuel cell requires the combination of hydrogen and oxygen, heat, and water. It converts the energy generated by a chemical reaction in utilizable DC electric power like a battery. However, by providing fuel (hydrogen), it allows the fuel cell to generate electricity, without ever losing its charge (Yahyaoui et al, 2018). The best operation of fuel cells is with pure hydrogen and is considered for best utilization in combustion engines and fuel cell electric systems (Roca et al, 2019).

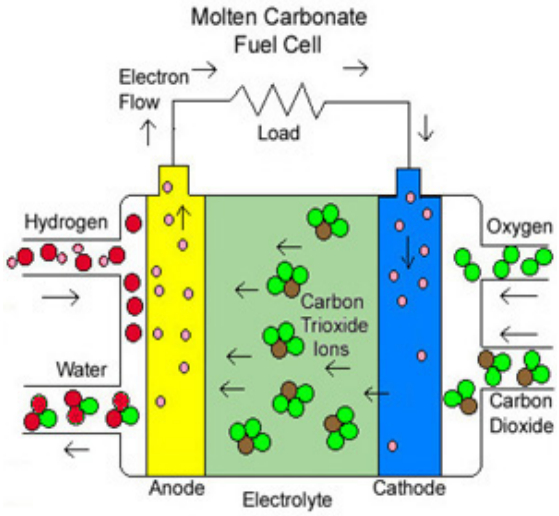

Figure 3.2: Schematic representation of a fuel cell (Sonian, 2017)

Fuel cell as illustrated in Figure 3.2, has as goal to generate an electrical current, which could be oriented outside the cell to accomplish a task, like supplying an electric motor, lighting a lightbulb. Due to the electricity nature, the generated current goes back to the fuel cell, to complete an electrical circuit. Various types of fuel cells exist, and they operate a little differently depending on the technology of each other (Sonian, 2017).

3.1.3. Super-capacitors

Super-capacitors refer to electrochemical energy storage units having great characteristics such as (high-power density, very low internal resistance, high cycle lifetime and cycling efficiency). The energy is stored through physical separation of positive and negative charges. The system uses two parallel plates separated by an insulating material to store these charges as shown in Figure 3.3 (Shi et al., 2014). They utilised polarized liquid layers placed between conductive ionic electrolytes and a conductive electrode allow to augment the capacitance. Their most significant characteristic is comparatively the low state of charge depending on the maximum voltage of 2.5 V and they are more efficient (approximately 95%) (Amrouche et al, 2016). Their output power is lower compared to electrolytic capacitors and it could achieve up to 10 kW/kg (Raza et al., 2018).

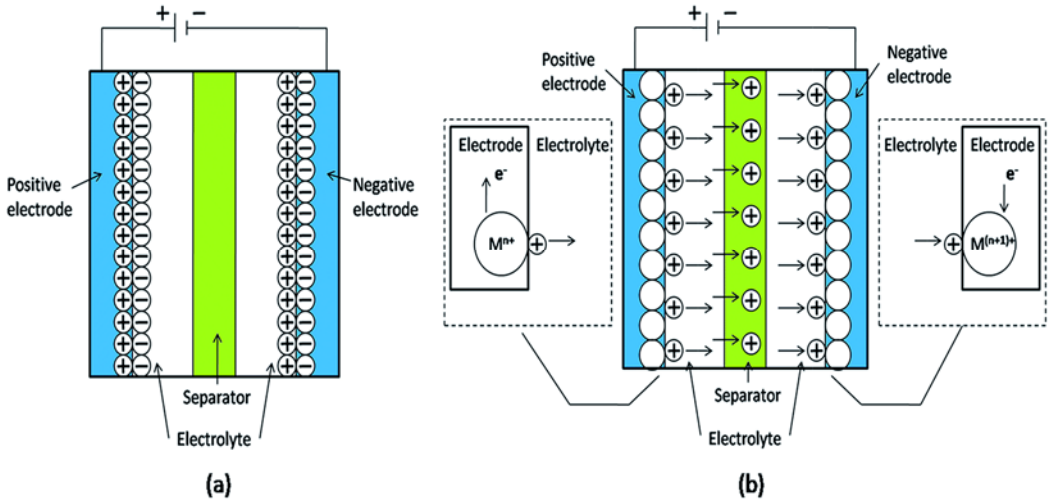

Figure 3.3: Schematic diagram of super-capacitors (Shi et al., 2014)

3.1.4. Secondary batteries

Secondary either rechargeable batteries are the oldest energy storage; they are electrochemical devices capable to generate energy (electrical energy), in which the electrochemical reactions allow to produce chemical energy to generate electrical energy. These electrochemical reactions are reversible and this reversibility enables the batteries to recharge by applying a voltage to their electrodes (Ibrahim et al., 2008). Figure 3.4 depicted the applications of commonly used batteries for grid energy storage applications.

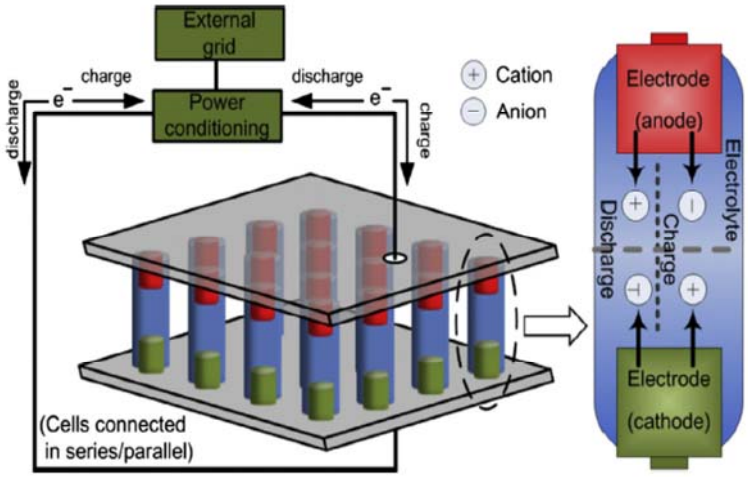

Figure 3.4: Schematic diagram for a battery system operation (Akinyele et al, 2017)

The battery system consists of electrochemical cells wired in series. Each electrochemical cell comprises an anode, a cathode and an electrolyte (Luo et al, 2015). The electrochemical cell can operate in both conditions converting electrical energy into chemical energy or by using electrochemical reactions to produce electrical energy (Akinyele et al., 2017).

The most storage systems utilized are the batteries due to their easy design and manufacture ("Lead-Acid Batter. Technol.," 2015). This is also due to their lower cycling capacity comparatively to other energy storage systems using commonly for power quality objectives. Divers types of batteries are available in the market; the best-known ones are lead-acid batteries, nickel-based batteries, lithium-ion batteries, redox batteries (Achkari & Fadar, 2018).

3.1.4.1. Lead Acid Battery

The energy density of this type of battery is around 30 to 50 Wh/kg, with a 2V per cell, it is principally utilized for the vehicle engines starting and emergency power supplies (Azzollini et al., 2018). Its cost per cycle is lower of about US $ 0.10. The benefits of lead acid batteries are (Minani-ku, 2016):

- Cheap,
- Low self-discharge,
- High tolerance at the temperature of charging and discharging.

In contrary, it presents as disadvantages:

- Low energy density,
- Limited lifespan,
- Slow charge.

3.1.4.2. Nickel-Based Battery

This battery includes two technologies, which are nickel-metal hybrid (NiMH) battery and nickel-cadmium (NiCd) battery. Nickel-metal hydride batteries were the choice of electric vehicles in the 1990s, they present many benefits like a high self-discharge rate, a low voltage per cell (1,2V). These battery technologies have a good memory including nickel-cadmium rechargeable batteries as well as metal-nickel hydride, which allows to support less load (Vazquez et al., 2010). This type of battery presents a low cost per cycle of approximately US $ 0.12. Other characteristics such as rapid charge time of about 1 to 2 h, slow discharge time of about 15 h as well as a maximum discharge rate of 10 ° C. Moreover, nickel-cadmium (NiCd) battery offers the lowest cost per cycle (about US $ 0.04) and a longer lifetime cycle than nickel-metal hybrid (about 2,000 cycles). It has a disadvantage of requiring a complex recycling more important memory effect. This type of battery has been progressively substituted by nickel-metal hybrid battery and Lithium-ion battery (Lansburg & Mcdowall, 2016).

3.1.4.3. NaS Battery

This battery technology is composed of liquid sulphur and liquid sodium. The electrolyte allows only positive sodium ions to pass across, which are going to be combined with sulphur to compose sodium polysulphides as shown in equation (3-1):

$$2\mathrm{Na} + 4S = \mathrm{Na}^2\mathrm{S}^4 \quad (3\text{-}1)$$

The operation system of this battery is reversible. For the discharge mode, the positive sodium ions circulate in the electrolyte in the external circuit of the battery and produce a voltage of approximately 2V. During the charge operation, the sodium polysulphides are induced to return the positive sodium ions across the electrolyte to create a recombination of electrons and to form elemental sodium. To allow this process, the battery should be kept at a temperature of around 300° C. This battery technology is characterized by its efficiency (approximately 89%) and has a greater pulse power capacity, which is 6 times than their continuous rate (30s). The biggest NaS unit is in Japan it has a capacity of 6 MW. Many other systems have been developed like the combined power quality and the advanced shaving applications in the United States of America market.

3.1.4.4. Lithium-ion Battery

The common use of Lithium-ion (Li-ion) battery is in laptops, mobile phones and some other portative electronic appliances. Li-ion battery technologies are generally used in many applications because of their energy density capacity and in applications that needed a good lightness, which represent major preoccupations (Karfopoulos et al., 2016). The lithium-ion battery offers some benefits like high energy density, long lifetime as well as low self-discharge rate. According to these aspects, this battery is classified as the best battery for electric vehicles. However, its disadvantages include a high cost and a protection exigency for limiting the voltage and current (Daniel et al., 2018).

Li-ion batteries can be found in 5 diverse types depending on cathode materials. These types include Li-Cobalt (LCO), Li-Manganese (LMO), Li-Phosphate (LFP), Lithium-Nickel Manganese-Cobalt (NMC), Lithium Nickel-Cobalt Aluminium (NCA) and Li-Titanite batteries (LTO). The fast response characteristics, high power density and energy, and good scale ability (from 1kW to 100MW) in divers applications allow to consider Li-ion battery as a more reliable energy storage system comparatively to other technologies in micro-grid application (Miao et al., 2019).

3.1.4.5. Metal-air Battery

These batteries are characterized as the most conventional technology. They are generally known as the cheapest technology that exists. They present a harmless characteristic to the environment. The principal disadvantage of these batteries is the difficulty and inefficiency of recharging them electrically; few developers propose a rechargeable electric battery (Han et al., 2018). The lifespan of rechargeable metal air batteries in improvement is only a few 100 cycles and around 50% of efficiency. The anodes of these batteries are designed with high energy density metals, which is another advantage. The electrolytes are generally constituted of a good conductor of OH- ions like KOH (Wang et al., 2019). The electrolyte can be in liquid either solid polymer membrane saturated with KOH. The electric recharging function of metal-air batteries has to be further improved, which could allow them to be compared with other rechargeable battery technologies.

3.1.4.6. Redox Flow Battery

Flow battery is recent technology also known as redox flow battery (RFB). It has a cell voltage from 1.15V to 1.55V. These batteries have been designed to manage intense energy applications that need many deep charging / discharging cycles (over 10,000 cycles). Compact batteries have not been designed to provide a discharge cycle of several hours, especially for 1000 deep discharge cycles and this characteristic is considered as a benefit of these batteries. A large quantity of battery cells would be required for big applications such as 100 MW over 10 hours of discharge. In addition, Redox flow batteries may quickly respond to the changing in load either input, and these batteries present a single capability to separate power from energy (Hiksas & Aninditio, 2017).

The size of the reactor enables to determine this battery output power, whereas the energy can be defined by the quantity and concentration of reactants including the size of the reagent reservoir. According to this characteristic, redox flow batteries present a capability to generate a large power ranging to energy ratios. The fact that the storage of the active reactants is made in separated tanks, the discharge of the batteries is inherently safer than conventional batteries, which is an advantage (Sánchez-Díez et al., 2021). All of these aspects render the redox flow battery comparatively adapted for large energy storage systems having a great number of deep discharge cycles (Chalamala et al., 2014). However, RFBs have a lower energy density (25 to 35 W/kg), a medium power density and their system is more complex than conventional batteries. Above all, however, these batteries have very high prices. At present, their cost is comparatively the same to a Li-ion battery (about $500/kWh).

3.1.5. Battery Energy Storage System Control

3.1.5.1. Basic Operation Modes of the Distributed Battery Energy Storage Systems

When the micro-grid provides a sufficient amount of input power as required by the load, the excess of production goes to supply the battery, at this moment; the battery operates in charging mode. During the charging process, to quickly reach the full charge state, the battery energy storage systems are loaded with maximum input power. If the battery energy storage systems (BESSs) are totally charged, it is unplugged and waiting for the discharge process.
In the case where the supplied energy from the renewable sources could not meet the load, the surplus is provided by the battery energy storage systems (BESSs), which go into the discharge mode and become power sources. The discharge process requires the balancing of each battery SoC and output power. The suggested SoC balancing method based on the droop control is generally used. Based on this method, the power load is distributed according to the SoC. During this process, the SoC in each battery is equal (Xiaonan et al., 2013).

3.6. Power electronics converters for batteries

The basic power electronics converters used for batteries charging and discharging consists of buck converter, boost converter, buck-boost converter, Cuk converter and bidirectional converter, which constitute non-insulated converters. Non-insulated converters are cheap and often utilized for small voltage conversion; they cannot offer protection for high input voltages. Besides these converters, there are also isolated converters such as forward converter**,** fly back converter**,** push-pull converter**,** and half bridge converter (Ali et al., 2014).

3.6.1. Non-Isolated Converters

3.6.1.1. Buck converter

This converter helps to decrease an input voltage to a lower output voltage. During the switching cycle, the input voltage V_{IN} is supposed to remain constant. The inductor current I_L and the output voltage V_O do not significantly change during one switching cycle due to the sufficiently large inductor L and capacitor C (Ghosh et al., 2018). The resistor R represents the load (Figure 3.5).

The inductor current in steady state operation is always supposed to be greater than zero. The activation of the metal oxide semiconductor field effect transistor (MOSFET) depends on the control signal for T_{on} =DTs, where D is the steady-state duty cycle. Based on this period V_A=V_{IN} and I_{in}=I_L. The inductor current starts to flow via the diode D_d when the MOSFET is turned off, which conduces to V_A=0 as well as I_{IN}=0. As the average voltage through the Inductor is equal

to zero, V_L=0 (inductor voltage), thus, the average output voltage is written as follows (Jayaswal & Palwalia, 2018):

$$V_0 = V_A = D.V_{IN} \tag{3-2}$$

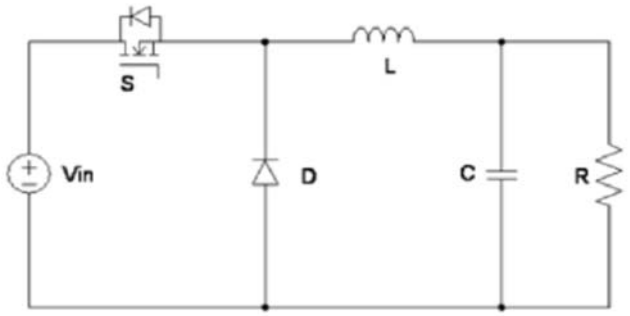

Figure 3.5: Buck converter circuit (Baharudin et al., 2018)

The average current across the capacitor C, I_C=0, therefore, I_L =Io and the input current is illustrated by the equation (3-3):

$$I_{IN} = D.I_0 \tag{3-3}$$

The equations below, present the instantaneous inductor current and capacitor voltage values during switching cycle:

When the MOSFET is on:

$$i_L = V_{IN} - V_0 \tag{3-4}$$

$$V_C = I_L - \frac{V_0}{R_L} \tag{3-5}$$

When the MOSFET is off:

$$i_L = V_0 \tag{3-6}$$

$$V_C = I_L - \frac{V_0}{R_L} \tag{3-7}$$

I_L represents the current across the inductor, V_C represents the capacitor output voltage, V_0 is the converter output voltage and V_{IN} is the input voltage.

3.6.1.2. Boost converter

A common boost converter (see Figure 3.6) allows stepping up an input voltage to a higher output voltage.

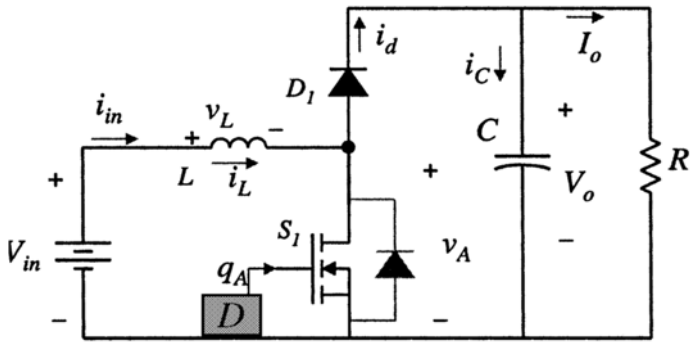

Figure 3.6: Boost converter circuit (Mohan, Undeland, & Robbins, 2003)

When the MOSFET is activated, according to a control signal, at this time the diode D1 is off, and the inductor current augments because of the positive voltage through it. The inductor current begins flowing across the diode D1 when the MOSFET is turned off, and its magnitude decreases (Ghanbari & Hosseini, 2008). The instantaneous values of the variables during the activation and deactivation periods are presented below:

When the MOSFET is on:

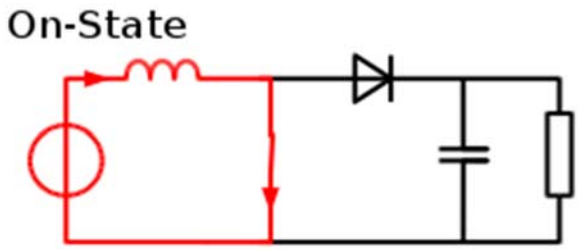

Figure 3.7: Booster converter on state (Hvljq et al., 2017)

$$V_A = 0 \tag{3-8}$$

$$i_L = V_{IN} \tag{3-9}$$

$$V_C = \frac{V_0}{R_L} \tag{3-10}$$

When the MOSFET is off:

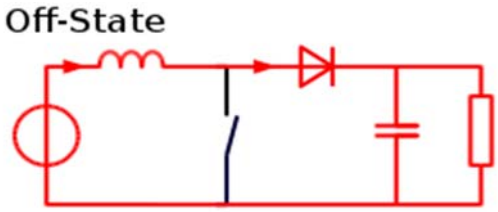

Figure 3.8: Booster converter off state (Hvljq et al., 2017)

$$V_A = V_0 \tag{3-11}$$

$$i_L = V_{IN} \tag{3-12}$$

$$V_C = i_L - \frac{V_0}{R_L} \tag{3-13}$$

With V_L=0 (inductor voltage), the average pole A voltage is given as:

$$V_A = V_{in} = (1 - D)\, V_0 \tag{3-14}$$

Further, by assuming I_C=0, obtaining the steady-state conversion ratios for the boost converter can be given by:

$$\frac{V_0}{V_{in}} = \frac{1}{1-D} \tag{3-15}$$

$$\frac{I_{in}}{I_0} = \frac{1}{1-D} \tag{3-16}$$

From equations (3-15) and (3-16), it is assumed that the output voltage be always higher than the input voltage, and the output current be always lower than the input current by the same ratio. D represents the buck converter duty ratio.

3.6.1.3. Buck boost converter

As illustrated below (Figure 3.9), this type of converter has two ways of operating; in one way it gives a possibility to step down the input voltage, another way it steps up the input voltage or vice versa (Mohan et al., 2013).

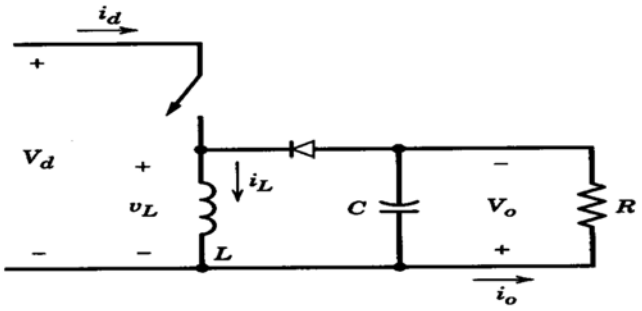

Figure 3.9: Buck boost converter circuit (Mohan et al., 2013)

Equation (3-17) gives the relationship between the input voltage and output voltage of this converter:

$$\mathrm{V_0} = \mathrm{V_d}.\mathrm{D}/\left(1-\mathrm{D}\right)\mathrm{V_0} \qquad (3\text{-}17)$$

During the activated state, the switch is on; there is isolation between the load, the inductor and input side. The load is fed from the energy stored by the capacitor in the off state. When the switch is in deactivated state, the input side is isolated from the circuit while the inductor supply energy to the capacitor and the load (De Sousa et al., 2015).

3.6.1.4. Cuk converter

The Cuk converter (Figure 3.10), refers to a DC / DC converter and its output voltage may be greater either lower than its input voltage amplitude. This converter is fundamentally a combination of boost and buck converters (Han et al., 2015). The Cuk converter is generally used to generate a different polarity output voltage. This means that the output voltage amplitude can be larger or smaller than the input voltage, and there is an inverse output polarity. The input inductor behaves as a dc supply filter that is used to prevent high harmonic current. The capacitor allows the transfer of energy to the Cuk converter (Ilman et al., 2019).

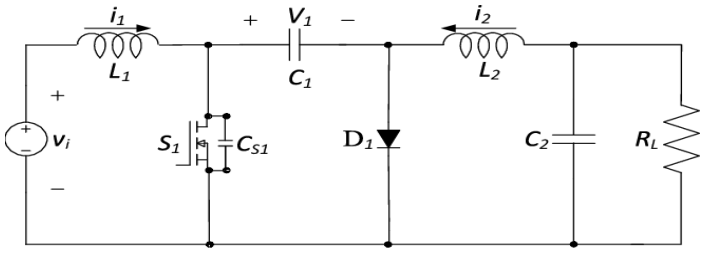

Figure 3.10: Circuit diagram of Cuk converter (Han et al., 2015)

3.6.1.5. DC-to-DC Bidirectional converter

In DC-to-DC Bidirectional converter (Figure 3.11), the power flows into two directions as it operates in two modes, which are the buck mode and the boost mode. This converter is mostly utilized to charge and discharge the battery relating on the battery voltage and load voltage (or

grid voltage) respectively (Fong, et al., 2016). In this type of converter, the inductor serves as the energy transfer element. The inductor charges via source side and actives switch in each switching cycle depending on the time T_{ON}=DT, with T=1/f_{sw} as the switching period and D represents the duty cycle. The absorbed energy discharges through the load during T_{OFF} = (1 - D)T (Karshenas & Daneshpajooh, 2011;Mohan et al., 2003).

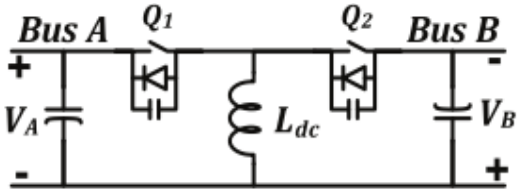

Figure 3.11: Bidirectional buck boost converter (Karshenas & Daneshpajooh, 2011)

3.6.2. Isolated Converters

Isolated converters are used isolating floating connections between input and output, its circuit is more complex and require higher number of components.

3.6.2.1. Forward converter

This converter derived from buck converter and using a transformer to raise or diminish the output voltage depending on the ratio of the transformer. This converter cannot store energy during switching conduction phase. The Figure 3.12 illustrates the scheme diagram of a forward converter.

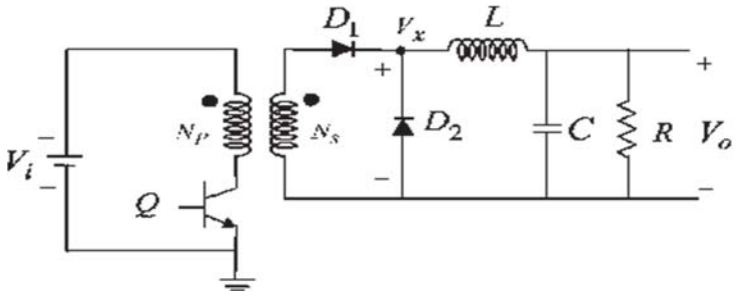

Figure 3.12: Forward converter

The above figure represents the forward converter schematic diagram, with V_i and V_o representing the converter input and output voltages, D_1 and D_2 represent the diodes, L is the inductor, C is the output capacitor, R is the load resistor, and Q is the transistor that controls the converter circuit operation in diverse modes. Vi appears through the primary side when the transistor is activated, by after generating. The switching states area of the inductor voltage must be equal; this area is used to calculate duty cycle.

$$\left(\frac{N_s}{N_p}V_i - V_o\right)DT_s = -(-V_o)(1 - DT_s) \quad (3\text{-}18)$$

$$\frac{V_o}{V_i} = \frac{N_s}{N_p} D \quad (3\text{-}19)$$

Where N_p and N_s represent the turns of primary and secondary power windings, *D* refers to the duty cycle. This converter is a simple and mostly used converter. The forward converter has the ability to deliver multiple outputs through an isolation transformer, which is an advantage (Mcfowland, 2012). Forward converter provides non-pulsating current loading and is well suited for high output current applications.

3.6.2.2. Fly back converter

This converter refers to a power supply converter using a coupled inductor; this converter is comparable to a buck boost converter. Fly back converters are mostly used for low power applications, where the output voltage must be insulated from the input voltage and it has a simple circuit than other converters (Rgpv, 2014). The circuit can deliver single or multiple independent output voltages and may work over a large range of input voltage variations (Das et al,, 2018). The Figure 3.13 illustrates the circuit of the fly back converter.

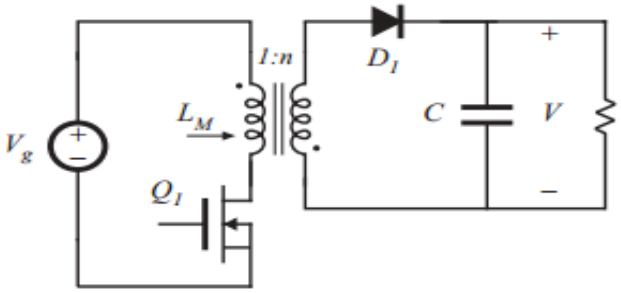

Figure 3.13: Fly back converter (Das et al., 2018)

When there is no current flowing across an inductor the energy stored is released by a sudden terminal voltage. Fly back converter transfers energy to the secondary side when the primary switch is deactivated. The diode is used to rectify the voltage while the capacitor smoothens the rectified in the secondary (Ponzo et al., 2019).

3.6.2.3. Push-pull converter

This converter (Figure 3.14) refers to a DC-DC converter using a transformer to convert the supplied DC power voltage. In this converter, the current between the two switches allows to produce power at the transformer primary side. Push pull converters are effective in high power applications and create less noise on the board (Petrocelli, 2018).

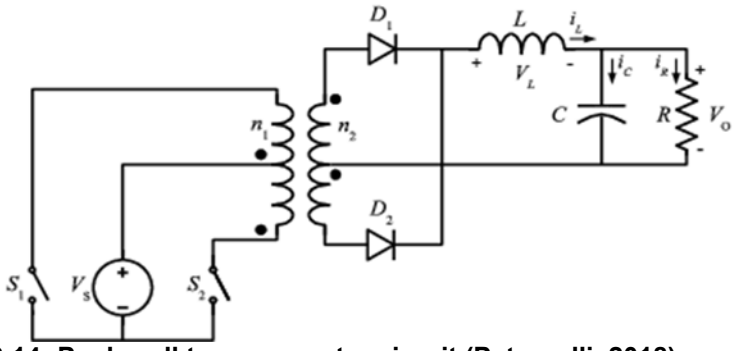

Figure 3.14: Push-pull type converter circuit (Petrocelli, 2018)

In addition, these converters are part of forward converter family and have two switching devices to control the energy flow through the transformer. The two switches must not be on at the same time. If the transformer saturates, it will destroy both switching devices. This means that the conduction times of the switching devices should be equal (Chandrasekaran & Karthikeyan, 2019).

3.6.2.4. Half bridge converter

Half bridge converter (see Figure 3.15) is similar to a push pull converter, but there is no requirement of a middle-tapped transformer. This converter produces more or lower output voltage than input voltage and have high output power. These converters are used in high power applications and their circuit is complex and uses two switches (Deng, 2015).

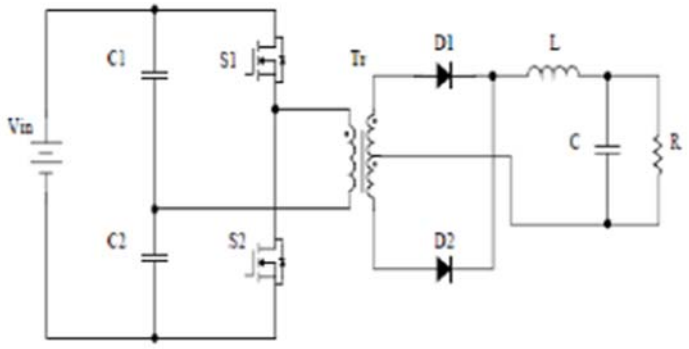

Figure 3.15: Circuit diagram of a half bridge converter (Deng, 2005)

There is no gap of magnetic field in these converters and magnetic cores are small which are advantages for this converter. It operates at half of the supply, which is a disadvantage, and it is not suitable for current mode control (Zhao et al., 2020).

3.7. Power electronics converters control

Figure 3.16 illustrates the hierarchical control architecture including the primary, secondary and tertiary controls. The primary control deals with basic power sharing control and current/voltage regulations, while the ssecondary control is higher than the primary level and

handles voltage compensation and improved sharing performance. Lastly, the tertiary control concentrates on the power management, energy management and economic dispatch (Bidram & Davoudi, 2012).

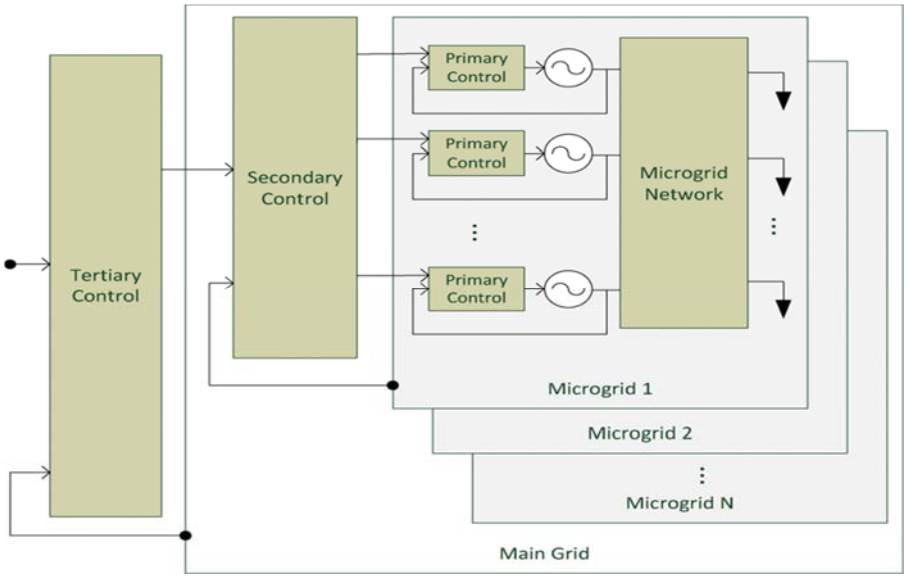

Figure 3.16: Hierarchical control architecture (Olivares et al., 2014)

3.7.1. Primary Control

The primary control includes inner loops (current / voltage regulation) and droop control (basic power sharing) depending on the control in the power converters.

3.7.1.1. Inner loop

A. AC to DC converter

Considering for instance a three-phase voltage source converter (VSC), centred on the vector control, the inner loop regulates the AC current in a synchronous rotating machine. Thus, the current is adjusted by the linear controllers based on a defined range and generate the required voltage, after the transformation of the measured currents of the synchronous rotating machine. Thus, pulse-width modulation (PWM) is utilised to reversely convert the voltage demands in three-phase modulation indices (Olivares et al., 2014).

B. DC to DC converter

There exist different types of DC to DC converters, however, their control can be classified in two ways, generally voltage and current controls (power control mode) (Chen et al., 2016). DC-to-DC converters voltage control modes define the reference voltage and operate like a controllable voltage source. Generally, the converters operating in current / power control

mode act like a controllable current / power source. To meet reference condition, the current / power output must be adjusted.

3.7.1.2. Droop control

The voltage droop control is largely admitted because it does not depend on the communication lines. Frequently, "droop control" is achieved by including a "virtual resistance" to the existing system. The operating conditions do not affect the virtual resistance, which represents an ideal value, like temperature. There is no possibility to produce real power loss, the variability of the real resistance value can be modified by the environmental factors and this would create "real" power losses that should be minimized. The droop control has been used in alternative current systems (Guerrero et al., 2013). The active power can be defined by the power angle d in a dominant inductive distribution grid, dynamically controlled by the frequency, and the alternating voltage V generally determines the reactive power. Moreover, the droop concept was successfully used in DC systems.

3.7.2. Secondary control

The reason of introducing secondary control in the micro-grid is to keep the bus voltage of a droop-controlled DC micro-grid at a nominal value that defines the reference on the primary control, which keeps the controlled parameter in an optimum range (Dragicevic et al., 2014). The Figure 3.17 illustrates the operating principle of secondary control in DC micro-grids. As it is shown, by implementing the main control, the operating point of the system goes from V_o (no-load voltage) to OP1 in load conditions $\mathrm{i_{dc1}}$ and from V_o to OP2 respectively within the load conditions $\mathrm{i_{dc2}}$. The functioning changes from OP1 to OP1_new and OP2 to OP2 new, as the system always operates at the rated voltage level after activating the secondary command.

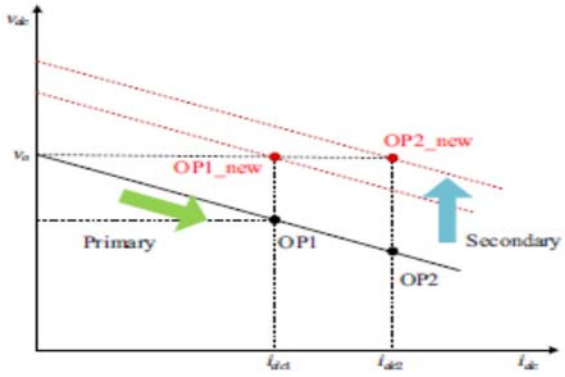

Figure 3.17: Secondary control's principle on DC voltage restoration in DC Micro-Grids (Naeinian, 2016)

Thus, in contrast to the voltage / frequency regulation in the AC micro-grids, the main role of the secondary control is to eliminate the voltage difference as well as ameliorate power quality. According to the communication link, secondary control can be put into practice with a centralised, distributed and decentralised control policy (Sahooet al., 2018).

3.7.3. Tertiary control

The principal function of tertiary control is to manage power and energy under specified targets, such as energy storage balance, reduction of energy flow losses and minimised operating costs. In the tertiary control, the control of the power flow may be improved by regulating the frequency (phase change in steady state) and the voltage amplitude in the micro-grid, when it operates in grid connection mode. In autonomous operating mode, the tertiary control references have to be disconnected to avoid voltage instabilities (Meng et al., 2017).

The role of tertiary control is to deal with the energy and power management including local controls. The energy management involves making decisions for the operation of renewable energy systems with uptime from several hours to several days, while the power management acts to ensure suitable operation of a micro-grid by behaving on the prompt operating principles towards some ideal parameters like voltage, current, power, and frequency (Rajesh et al., 2017).

CHAPTER 4: SYSTEM DESCRIPTION AND MODELLING

4.1. Introduction

The following chapter treats the description of the isolated DC micro-grid modelling. The designed and developed model includes a PV array, a Wind turbine, a Biomass generator and two battery banks designed for remote cities, a DC-DC converter. The developed energy management system control algorithm is also presented. The remaining part of the chapter is classified as following: System description of the design and developed DC micro-grid is presented in section 4.2. Section 4.3, presents the Modelling of main components of the system. In section 4.4, the Energy Management System Control algorithm is presented.

4.2. System Description

The DC micro-grid architecture developed was applied to power a small town. Different loads such as commercial load, industrial load, and residential load can be found in a town. The capacity of the power generation for each DG source is 210kWp for solar, 150 kW for wind energy and 150 kW for biomass, 576 kWh for battery bank. The generated power from the PV and battery bank are DC, but for wind and biomass is AC, therefore, the generated power from the AC sources are converted in DC by using a rectifier. The DC bus voltage for the system is 380 Vdc and the battery voltage is 240V.

To reduce voltage fluctuation, each DG source is equipped with a converter. Thus, battery is used to assure power supply to consumers without any interruption. For this developed model, two battery banks are considered. These battery banks do not operate at the same time. One can start by operating while another can be in standby. Another battery bank can be used when available power in distributed generation is not sufficient to supply the load.

4.2.1. Load Profile of the System

The DC micro-grid feeds the load directly by 380Vdc and three types of loads are considered commercial load, industrial load and residential load. The power system grid comprises production, transmission, and distribution. Based on production, the entire produced power, such as PV, Wind and biomass, are connected in parallel. In the stage of the transmission grid, the industrial load, which is the water treatment plant and commercial as well as domestic consumers are connected to the 380Vdc distribution bus. Battery banks will be used as back up during peak demands and variations in the power produced by renewable sources.

The load profile was selected from a publication of the US Department of energy, which contains the average of the DC power devices that can be found in a home and an office in a

Town. According to the Table 4.1 and Table 4.2 below, the load demand per day is generally low if all of appliances operate. Figure 4.1 shows the block diagram of the developed system.

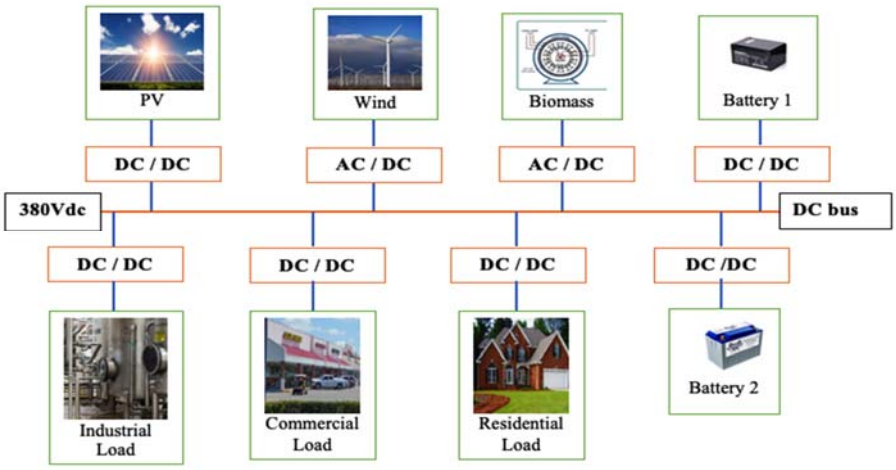

Figure 4.1: Block diagram of the developed system

Table 4.1: Type of appliances used in each house

Appliances	Units	Voltage (V_{dc})	Power Rating (W)
Lamp	9	12	98
Heater	1	12	600
Sandwich Maker	1	24	550
Refrigerator	1	24	72
Coffee Maker	1	12	135
Washing Machine	1	24	70
Dryer	1	24	2100
Fan	2	24	90
Iron	1	12	150
TV	2	12	30
Water Heater	1	12	660
Microwave	1	12	600
Computer	1	12	170

Table 4.2: Type of appliances used in each office

Appliances	Units	Voltage (V_{dc})	Power Rating (W)
Lamp	10	24	90
Lap Top	5	12	325
Printer	5	12	450
Desktop computer	2	12	300
Ceiling Fan	2	12	40
Air Conditioner	3	24	2400
Coffee Maker	1	12	135
Heater	3	12	1800
Microwave	1	12	600
Refrigerator	1	24	72

Every house in the Town requires 5.29 kW / day peak power, 6.21 kW / day for each office and a limit of 50 houses are considered in the study, 10 offices are considered and the industrial load which is a water treatment plant needs 180 kW. Thereby, the total power required to supply the city is 507 kW. The Table 4.3 provides the summary of all the values/variables for the developed DC micro-grid.

Table 4.3: Required Values for the developed DC Micro-Grid

System	Capacity	Number of Unit	Total
PV power	210kWp	1	210kWp
Wind energy	150kW	1	150kW
Biomass energy	150kW	1	150kW
Battery storage	288kWh	2	576kWh
Residential load (house)	5.29kW / day	50	265kW
Commercial load (Office)	6.21kW / day	10	62.1kW
Industrial load	180kW / day	1	180kW

4.2.2. Operation of the Designed and Developed System

Energy storage systems ensure a proper operation of micro-grids because of the irregular form of renewable sources. A proper operation of energy storage systems allows to consider micro-grid as an excellent, reliable and less expensive system for producing energy. For the use of battery system, the rapid discharge either premature charge of a given battery in the battery bank would reduce the life of the storage system and if this is not controlled, it would reduce the credibility of the micro-grids.

Furthermore, in the case of the solar and wind, since these sources are not permanent, the energy produced by these sources must be stored to be reused during peak demand. The work is concentrated on the battery energy management. The system is made up of two battery banks and these two battery banks do not operate at the same time, it will depend on the demand of the network.

In this work, several aspects will be considered for the management of battery energy such as in the case where there is equality of production, an abundance of production and finally a low production. The system will be founded on the individual monitoring of charging and discharging of each battery in the bank finally to balance their state of charge and make the system efficient.

4.3. Mathematical Modelling of Main Components of the Developed DC Micro-Grid System

The concern in this point is to design a dynamic model of the developed DC micro-grid, which helps to verify the justness of the designed controller. The MATLAB/Simulink mathematical

modules have been used to build the DC micro-grid model including battery system, which use the component equivalent circuits. Four diverse power supply are considered in this model (PV, wind, biomass, and battery). A generator is considered for the case of biomass.

4.3.1. Modelling of Solar Power

The aim of the modelling is to penetrate the characteristics of a system, in the case of solar power two parameters are considered, precisely the irradiation and ambient temperature. Many research documentations have shown that a PV model could be complex depending on the systems.

As it can be seen in Equation (4-1), the PV output power depends on the solar irradiation and the area of PV module (Gunasekaran et al., 2018).

$$P_{solar} = \eta_g i_r A \tag{4-1}$$

Where, η_g is the production efficiency, i_r radiation of solar in w/m^2 and A the area. The Equation (4-2) represents the PV efficiency.

$$\eta_{ce} = \eta_{ref}\eta_{ce}[1 - \beta(T_{cell} - T_{cellref})] \tag{4-2}$$

Where, η_{ce} represents the production efficiency, β = Temperature coefficient *C* ((0.004–0.006)/*C*), η_{ref} is the reference module efficiency, T_{cell}: reference cell temperature, and the temperature (T_C), which is given as follows:

$$T_C = T_a + \left[\frac{NOCT-20}{800}\right] G_t \tag{4-3}$$

With T_C representing the cell absolute temperature in Kelvin, T_a=temperature in ℃, NOCT is the nominal operating cell temperature in ℃; G_t is the solar irradiation in tilted module (W/m^2). Total radiation in the solar cell including normal and partial solar radiations is determined by the following equation.

$$T_I = I_D R_D + (I_b + I_d)R_r \tag{4-4}$$

With T_I the total irradiation (kW/m^2), I_D is the diode current (A), R_D is the diode internal resistance (Ω), R_r is the referred cell resistance (Ω) and $(I_b + I_d)$ represent the total cell current (A).

4.3.1.1. Photovoltaic module modelling

The output characteristic of a PV array is determined by cell temperature, solar irradiation and output voltage. The operation mode of a PV either solar cell resembles to the PN junction diode operation, which converts light energy in electricity by the photovoltaic effect (Mandelli et al., 2016). Figure 4.2 represents the configuration of a single PV cell. Based on this representation, solar irradiance is described through a current source I_{ph}, and (diode current $\mathrm{I_d}$, output current I_{pv}, series resistance $\mathrm{R_s}$, parallel resistance $\mathrm{R_p}$, and output voltage V_{pv}) represent the remaining circuit parameters of the configuration.

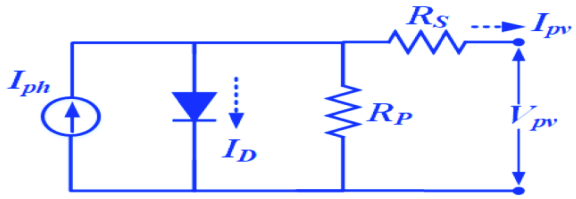

Figure 4.2: A single equivalent circuit model of a PV cell (Azzouzi et al., 2016)

The output current is given by the following formula:

$$I = \mathrm{N_p}\left[\mathrm{I_{ph}} - \mathrm{I_{rs}}\left(\frac{\mathrm{expq(V+IR_s)}}{\mathrm{AKTN_s}} - 1\right)\right] \tag{4-5}$$

$$\mathrm{I_{RS}} = \mathrm{I_{rr}} - \left[\frac{1}{\mathrm{T_K}} - \frac{1}{\mathrm{T}}\right] \tag{4-6}$$

Where, $\mathrm{N_p}$ and $\mathrm{N_s}$ are numbers of cell connected in parallel and series, K is Boltzmann's constant, 1.380658e–23 J/K, A ideal diode factor between 1 and 5, $\mathrm{IR_s}$: inverse cell current saturation at T, $\mathrm{I_{RS}}$ represents the solar cell reverses saturation current and $\mathrm{I_{rr}}$ represents the reverse saturation current at $\mathrm{T_r}$.

$$\mathrm{I_{ph}} = \left[\mathrm{I_{scr}} + \mathrm{K_i}(\mathrm{T} - \mathrm{T_r})\frac{\mathrm{S}}{100}\right] \tag{4-7}$$

Where, I_{scr} represents the short circuit current at the base temperature of the cell, $\mathrm{K_i}$ the coefficient of the short circuit temperature, $\mathrm{T_r}$ is the referred cell temperature, S: solar radiation in $(\mathrm{w/m^2})$. According to this configuration, the shunt resistance in parallel to the ideal shunt diode and the I-V characteristics are described by the following equation:

$$\mathrm{I} = \mathrm{I_{ph}} - \mathrm{I_D} \tag{4-8}$$

The Equation (4-9) below, gives the mathematical model of the PV array voltage-current characteristic:

$$\mathrm{I} = \mathrm{I_{ph}} - \mathrm{I_o}\left[\exp\frac{\mathrm{q(V+IR_S)}}{\mathrm{AKT}} - 1\right] - \frac{\mathrm{V+IR_S}}{\mathrm{R_{sh}}} \tag{4-9}$$

Where, I_{ph} refers to the Irradiance current (A), $\mathrm{I_D}$ is the diode current (A), $\mathrm{I_o}$ represents reverse saturation current (A), $\mathrm{R_s}$represents series resistance (Ω), $\mathrm{R_{sh}}$ is the shunt resistance (Ω), I is the cell current (A), q is the charge of electron, 1.60217733e–19 Coulomb (Cb) and V is the cell voltage. The formula below, shows the PV cell output current, which uses a single diode model:

$$\mathrm{I} = \mathrm{I_{PV}} - \mathrm{I_{D1}} - \frac{\mathrm{V+IR_S}}{\mathrm{R_{sh}}} \tag{4-10}$$

The simplified PV system allows to obtain the open circuit voltage and the PV module maximum power. The voltage and power with series resistance values ($\mathrm{R_s}$) is determined by fill factor (Gunasekaran et al., 2018).

$$\left.\begin{aligned} FF &= FF_o\left[1 - \frac{R_s}{\frac{V_{oc}}{I_{sc}}}\right] \\ FF_o &= \frac{V_{oc}\ln(V_{oc}+0.72)}{1+V_{oc}} \end{aligned}\right\} \tag{4-11}$$

$$\left.\begin{aligned} \mathrm{P_{max}} &= \mathrm{FF \times V_{oc} \times I_{oc}} \\ \mathrm{P_{max}} &= \frac{\mathrm{V_{oc}-\ln(V_{oc}+0.72)}}{\mathrm{1+V_{oc}}} \times \left(1 - \frac{\mathrm{I_{sc}\times R_s}}{\mathrm{V_{oc}}}\right) \times \frac{\mathrm{V_{oco}}}{\mathrm{1+\beta \ln\frac{G_o}{G}}} \times \left(\frac{\mathrm{T_o}}{\mathrm{T}}\right)^{\delta} \times \mathrm{I_{SO}}\left(\frac{\mathrm{G}}{\mathrm{G_o}}\right)^{\alpha} \end{aligned}\right\} \tag{4-12}$$

Where,

- FF is the fill factor of the ideal PV module without resistive effects;
- $\mathrm{V_{oc}}$ normalised value of the open circuit voltage to thermal voltage.

The PV modules enable to obtain the power conversion in the PV system. The PV performance ability depends on the temperature and its characteristic curves (power &*V*, *I* curves) under standard test condition as illustrated in Figure 4.4. Depending on the nominal value of a solar cell, the entire power demands cannot be produced by a single solar cell (Kinhekar et al., 2016). Therefore, multiple PV arrays are generally connected in series and parallel as illustrated in Figure 4.3 this scaling up to produce the expected PV power. Scaling up PV modules provides voltage and current and is represented by the following equation:

$$\left.\begin{aligned} \mathrm{I_A} &= \frac{\mathrm{N_P}}{\mathrm{I_M}} \\ \mathrm{V_A} &= \mathrm{N_S \times V_M} \\ \mathrm{P_A} &= \mathrm{FF \times V_A \times I_A} \end{aligned}\right\} \tag{4-13}$$

With,

- I_A and V_A are PV cell voltage and current.
- I_M and V_M are PV module voltage and current.
- P_A and P_A are PV cell power and module power.

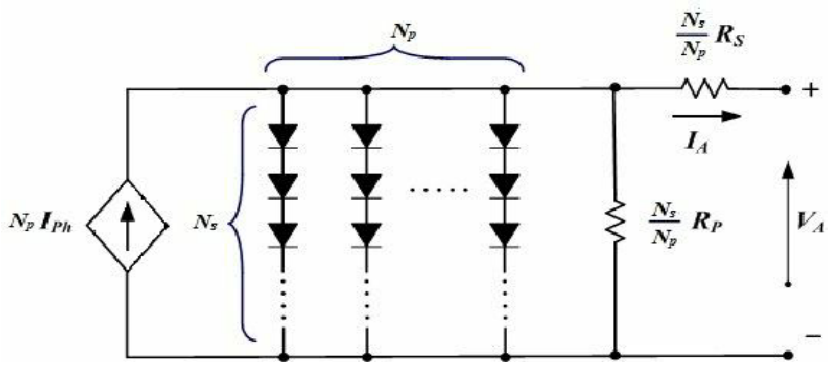

Figure 4.3: Solar array equivalent circuit (Ravi et al., 2014)

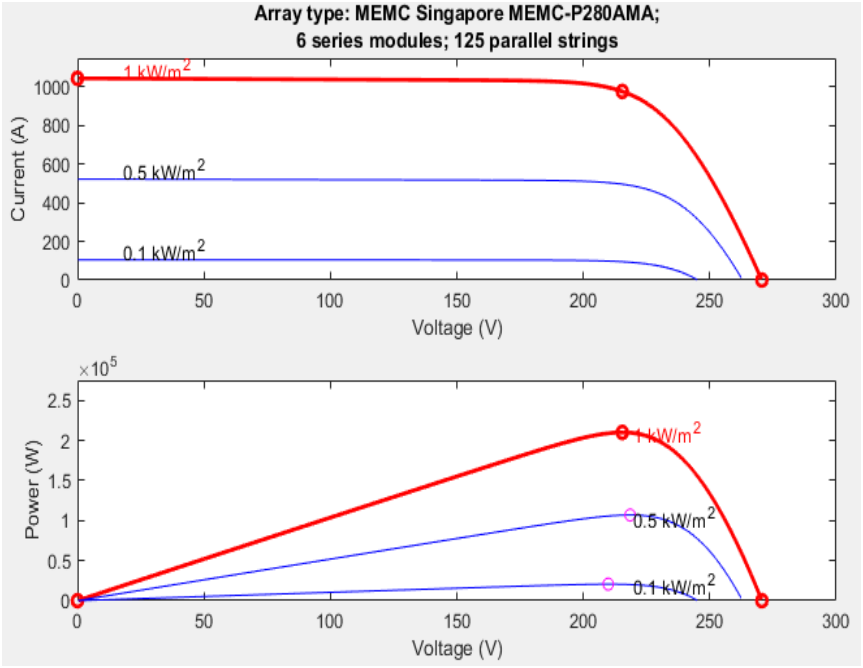

Figure 4.4: The characteristics curve of Solar Cell (voltage vs. current and power)

4.3.1.2. Photovoltaic System Design

The design requirement is that a 215.4 kW_p photovoltaic system delivers 35.9 V_{dc} to the output. To meet the requirements, the number of modules must be calculated. Thus, the number of solar panels needed in series is calculated as:

$$\frac{215.4}{35.9} = 6 \ PV \ panels$$

Indeed, the number of panels in series, which must be utilized is estimated to be 6.

So, the new PV system output voltage is therefore: $6\times 35.9 = 215.4\ \mathrm{V_{dc}}$. The following formula determines the PV system output current:

$$\mathrm{P = VI}$$

$$\mathrm{I_{total}} = \frac{210000}{215.4} = 974.93\ A$$

The number of solar panels in parallel is calculated as follows:

$$\frac{974.93}{7.8} = 125\ PV\ panels$$

Hence, the new power is determined by the following formula:

Actual power = $(125 \times 7.8 \times 6 \times 35.9) = 210.015\ \mathrm{kW}$

Table 4.4: PV modules parameters

Module type	MEMC Singapore MEMC-P280AMA
Number of cells per module	72
Number of solar panels in series	6
Number of solar panels in parallel	125

Table 4.5: The specification of the PV solar module based on standard test conditions

$\mathbf{V_{oc}}$	**45.1 V**
$\mathbf{I_{sc}}$	8.34 A
$\mathbf{V_{mp}}$	35.9 V
$\mathbf{I_{mp}}$	7.8 A

4.3.2. Modelling of Wind Power

This supply power model is characterized by the variation of wind speed with gust and wind speed (Gunasekaran et al., 2018).

$$\mathrm{W_v} = \mathrm{V_w} + \mathrm{V_g} + \mathrm{V_{wr}} \qquad (4\text{-}14)$$

With,

- $\mathrm{V_w}$ is the base wind velocity (m/s);

- V_g the gust wind velocity (m/s);
- V_{wr} the ramp wind component (m/s).

The gust speed is expressed as follows:

$$V_{wg} = \begin{Bmatrix} 0\ t < T_1 \\ C_2\left\{1 - \cos\pi\left[\frac{t-T_1}{T_2-T_1}\right] T_1 \le t \le T_2\right\} \\ 0\ t \ge T_2 \end{Bmatrix} \quad (4\text{-}15)$$

$$V_w = \begin{Bmatrix} 0\ s < T_3 \\ C_3 = \left\{\left[\frac{s-T_3}{T_4-T_3}\right] T_3 \le s \le T_4\right\} \\ 0\ s \ge T_4 \end{Bmatrix} \quad (4\text{-}16)$$

Where,

- C_2 represents the maximum gust value,
- C_3 *the* maximum wind speed induced by the ramp,
- T_3 and T_4, ramp start and stop times.

Wind power is given by the following expression:

$$P_w = \frac{dW_w}{dt} \quad (4\text{-}17)$$

The energy drawn by the wind turbine is determined by the formula below:

$$\left.\begin{aligned} W_w &= V_a \times \frac{1}{2}\rho\left({V_1}^2 - {V_3}^2\right) \\ P_w &= d\frac{V_a \times \frac{1}{2}\rho\left({V_1}^2 - {V_3}^2\right)}{dt} \end{aligned}\right\} \quad (4\text{-}18)$$

Where,

W_w is the energy drawn by wind turbine and ρ the air density. Based on Betz, the maximum output power wind turbine is given by:

$$P_M = \frac{16}{27} A_R \frac{3}{2} V^3 \quad (4\text{-}19)$$

The substitution of the value for V_1, and V_3 enable to obtain the Equation (4-19).

$$V_2 = \frac{2}{3} V_1 \quad (4\text{-}20)$$

$$V_3 = \frac{1}{3} V_1 \quad (4\text{-}21)$$

The modelling of wind turbine helps to describe the captured output power of the turbine (Bhayo et al., 2017). The characteristic curve of wind speed is presented on Figure 4.5, which varies in function of power. The wind power according to a given area is calculated as follows:

$$P_w = \frac{1}{2}\rho A W_v^{\,3} \tag{4-22}$$

$$P_M = P_w C_p \tag{4-23}$$

$$C_p = \frac{1}{2}[\delta - 0.22\beta^2 - 5.6]e^{-0.17\delta} \tag{4-24}$$

Where,

- β is the pitch angle of the blade (degrees);
- δ is the tip speed ratio of the turbine;
- C_p is the power coefficient.

The maximum produced power by a wind turbine is calculated by the following Equation:

$$P_G = V_G I_G \tag{4-25}$$

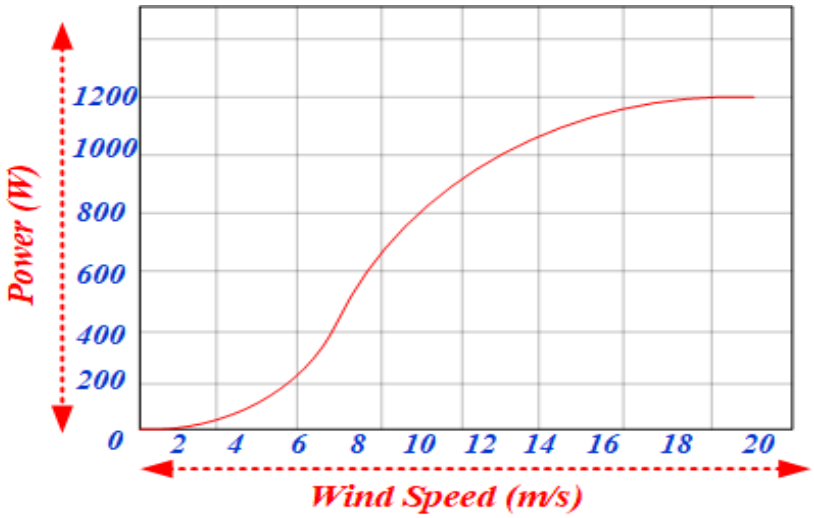

Figure 4.5: Characteristic curve of wind system (wind speed vs. power) (Bhayo et al., 2017).

The design requirement is thus for a 150 kW wind energy generation delivering 380 V_{dc}.

4.3.3. Modelling of the Battery

The principal focusing parameters of battery mathematical model are the voltage and current. The current can be determined by the changing of the terminal voltage of the battery (Yu et

al., 2016). The current production is driven by the transmission of electrons from one electrode to another (Camacho & Mihet-Popa, 2016). The potential difference between the positive and negative electrodes determines the open circuit voltage of the battery (Gunasekaran et al., 2018). The following equations present the charging and discharging voltages of battery.

$$V_{discharge} = E_0 - V_{op}{}^{+} - V_{op} - IR_{pol} \quad (4\text{-}26)$$

$$V_{charge} = E_0 + V_{op}{}^{+} + V_{op} + IR_{pol} \quad (4\text{-}27)$$

$$V_{battery} = E_0 - K\left[\frac{Q}{Q-it}\right] i - R_0 i \quad (4\text{-}28)$$

$$V_{battery} = E_0 - \left(\frac{K}{s_{oc}}\right) i - R_0 i \quad (4\text{-}29)$$

$$V_{discharge} = E_0 - Kd_r \frac{Q}{Q-it} i_1 - R_0 i - Kd_v \frac{Q}{Q-it} it + e(t) \quad (4\text{-}30)$$

$$V_{charge} = E_0 - Kc_r \frac{Q}{it+\lambda Q} i_1 - R_0 i - Kc_v \frac{Q}{Q-it} it + e(t) \quad (4\text{-}31)$$

$$e(t) = Bi[e(t) + Au(t)] \quad (4\text{-}32)$$

$$V_{discharge} = E_0 - Kd_r \frac{1}{s_{oc}} i - R_0 i - Kd_v \left(\frac{1}{s_{oc}} - 1\right) + e(t) \quad (4\text{-}33)$$

Equation (4-28) could also be rewritten by utilizing the SoC because of the polarization ohmic voltage. The composed relation model allows to modify the Equations (4-30) and (4-31). E_0 is the open circuit voltage of the battery expressed in (Volt); K is the polarization coefficient (Ω); Q represents the battery capacity (A/h) and R the internal resistance.

The Equations (4-30) and (4-31) present some limitations such as (i) battery aging and self-discharge, (ii) the current amplitude does not have impact on the battery capacity, and (iii) no consideration of the temperature coefficient (Zhou et al., 2016). To surmount these limitations, it is crucial to consider the aspects that have impact on the life of the battery. The analyze of SoC condition is done at each instant and is calculated with threshold capacity by the help of the following Equation;

$$Soc = Soc_{in} - \int_0^t \left(i - \max(i_g, i_d)\right) \frac{d\tau}{Q} \quad (4\text{-}34)$$

The net power produced by a DC micro-grid structure can be calculated as follows:

$$P_{net} = P_{PV} + P_{wind} + P_{biomass} \quad (4\text{-}35)$$

4.3.4. Modelling and Design of Power Converter

In this study, the boost and buck-boost converters are utilized to perform an impedance spectroscopic measurement in parallel with the regulation of the PV output voltage and battery systems. The buck-boost converter utilizes switches (MOSFET) to convert the battery input from one level to another, which can be lower or higher. The control of the output voltage average value is controlled by ON and OFF commutators based on the times (t_{on} and t_{off}) over a constant frequency or constant period $T = (t_{on} + t_{off})$. This switching method is called Pulse-Width Modulation. The buck-boost converter results from a cascaded combination of a buck and boost converters and it is needed in the applications where the step-up and step-down converters abilities are required (Hong et al., 2016). The conversion ratio of the output to the input voltage in steady state refers to the product of the rational conversion of the both cascaded converters. If both switches for the two different converters have the same duty cycle, then equation (4-36) can be applied:

$$\frac{v_o(t)}{v_{batt(t)}} = D\frac{1}{1-D} \quad (4\text{-}36)$$

In continuous conduction mode, the duty cycle is expressed by the following equation:

$$D = \frac{V_o}{V_{in}+V_o} \quad (4\text{-}37)$$

The Duty Cycle D is given by the ratio of the ON time to the period. Depending on D, the output voltage can be lower either higher than the input voltage. The Figure 4.6 gives the representation of a buck-boost converter.

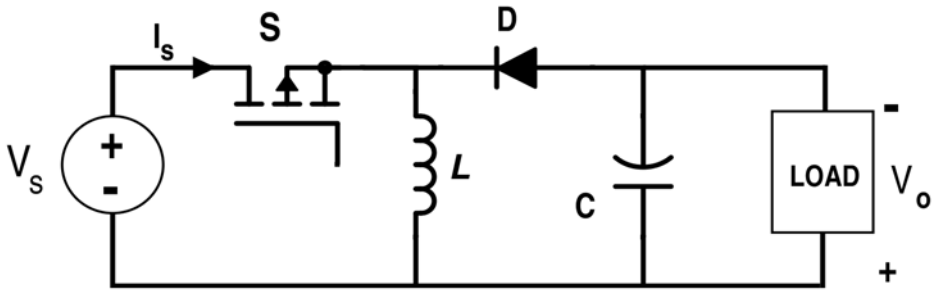

Figure 4.6: Equivalent circuit Buck-boost converter (Hong et al., 2016)

According to Figure 4.6, a large capacitor is used for filtering the output signal, which results in a stable output voltage $-v_o(t) \approx v_o$. The analyse of the both states ON and OFF is also estimated using the same configuration (Figure 4.6) by adopting Kirchhoff's Voltage and

Current Law (KVL and KCL). The power converter is considered to be in steady state, the switches are supposed to be ideal, the inductive and capacitive elements losses are ignored. The state variables of the circuit (inductor voltage, v_l and capacitor current, i_c) are expressed mathematically in the following equations.

$$v_l(t) = L\frac{dI_L(t)}{dt} \tag{4-38}$$

$$i_c(t) = C\frac{dV_C(t)}{dt} \tag{4-39}$$

In a deactivated state of the switch (ON state), the source generates power to the inductor and diode is inverse polarized. According to the figure 4.6, $V_s = V_{batt}$ and $V_o = V_L$. In the activated state, the input voltage becomes equal to the output voltage, which means:

$$V_{batt}(t) = V_L(t) \tag{4-40}$$

$$0 = i_c(t) + \frac{v_c(t)}{R_{load}} \tag{4-41}$$

$$v_o = V_{batt}(t) = L\frac{di_L(t)}{dt} \tag{4-42}$$

$$\frac{di_L(t)}{dt} = \frac{V_{batt}(t)}{L} \tag{4-43}$$

$$\frac{\Delta i_L(t)}{\Delta t} = \frac{\Delta i_L(t)}{DT} = \frac{V_{batt}}{L} \tag{4-44}$$

$$(\Delta i_{L-closed}(t)) = \frac{V_{batt}(t)DT}{L} \tag{4-45}$$

When the switched is opened (OFF state), the diode is polarized forward and the stored power into the inductor is supplied to the output, since there is no supply from the source.

$$v_c(t) = -v_L(t) \tag{4-46}$$

$$i_L(t) = i_c(t) + \frac{v_c(t)}{R_{load}} \tag{4-47}$$

$$v_L(t) = v_o(t) = L\frac{di_L}{dt} \tag{4-48}$$

$$\frac{di_L(t)}{dt} = \frac{v_0(t)}{L} \tag{4-49}$$

$$\frac{\Delta i_L(t)}{\Delta t} = \frac{\Delta i_L(t)}{(1-D)T} = \frac{v_o(t)}{L} \tag{4-50}$$

$$\left(\Delta i_{L-opened}(t)\right) = \frac{v_0(t)(1-D)T}{L} \quad (4\text{-}51)$$

For the operating steady state:

$$(\Delta i_{L-closed}) + \left(\Delta i_{L-opened}\right) = 0 \quad (4\text{-}52)$$

$$\frac{V_{batt}(t)DT}{L} + \frac{v_o(t)(1-D)T}{L} = 0 \quad (4\text{-}53)$$

$$v_o(t) = -V_{batt}(t)\left(\frac{D}{1-D}\right) \quad (4\text{-}54)$$

When *D* is greater than 50%, the output will be higher than the input and vice-versa.

4.3.4.1. Design of Converters

A. Buck-Boost Converter Parameters

A.1. Determination of Inductor Value

Inductor selection determines the ripple current in the power converter. The larger the inductor size, the lower the current ripple. More so, it is important that the chosen inductance significantly exceeds the calculated (required) minimum value to maximize efficiency of the power converter and to avoid unexpected issues (resulting in a transition from continuous conduction mode to a discontinuous conduction mode) that may arise because of the wide battery voltage input range.

By minimizing the power losses into the converter during operation, the power at the source equals the power at the load ($P_o = P_s$).

$$\frac{{v_0}^2(t)}{R_{load}} = V_{batt}(t)i_s(t) \quad (4\text{-}55)$$

$$i_s(t) = i_L(t)D \quad (4\text{-}56)$$

$$\frac{{v_0}^2(t)}{R_{load}} = V_{batt}(t)i_L(t)D \quad (4\text{-}57)$$

$$I_L = \frac{{v_0}^2(t)}{V_{batt}(t)R_{load}D} = \frac{P_o(t)}{V_{batt}(t)D} = \frac{V_{batt}(t)}{R_{load}(1-D)^2} \quad (4\text{-}58)$$

The maximum and minimum values of the inductor current are as follows:

$$I_{max} = I_L + \frac{\Delta I_L}{2} = \frac{V_{batt}(t)}{R_{load}(1-D)^2} + \frac{V_{batt}(t)DT}{2L} \quad (4\text{-}59)$$

$$I_{min} = I_L - \frac{\Delta I_L}{2} = \frac{V_{batt}(t)}{R_{load}(1-D)^2} - \frac{V_{batt}(t)DT}{2L} \quad (4\text{-}60)$$

The minimum inductance for continuous operation is:

$$L_{min} = \frac{R_{load}(1-D)^2}{2f} \quad (4\text{-}61)$$

According to the equation (4-36), the duty cycle value specified in the design is:

$D = \frac{V_{load}}{V_{batt}+V_{load}}$, in this study $V_{load} = 380\ V$ et $V_{in} = 240\ V$, then the duty of cycle is:

$$D = \frac{380}{240 + 380} = 0.61$$

In this study, a 20 kHz switching frequency was selected to avoid interference from audio noise. The load resistance is calculated as follow:

$R_{load} = \frac{V_{load}}{I_{load}}$, while

$I_{load} = \frac{P_{load}}{V_{load}}$ and $P_{load} = 510\ kW$, $V_{load} = 380\ V$, then

$I_{load} = \frac{510.10^3}{380} = 1342\ A$, so the $R_{load} = \frac{380}{1342} = 0.28\ \Omega$

Since R = 0.28 Ω and switching frequency f = 20 kHz.

$$L_{min} = \frac{R_{Load}(1-D)^2}{2 \times f} = \frac{0.28(1-0.61)^2}{2 \times 20000} = 1.07\ \mu H$$

For continuous operation it is important to select an inductor value that is 25% larger than L_{min}. Hence, the inductance must exceed:

$$(1.07) + \left(\frac{25}{100} \times 1.07\right) = 1.3375\ \mu H$$

$1.3375\ \mu H$ is the minimum value of the inductor, but a larger inductor should be connected to the output voltage to decrease the current ripple. A $6.7\ \mu H$ inductor was selected in this study. The inductor ripple current is calculated by the following equation, where L is the inductance, Fsw the switching frequency, V_{in} the input voltage and D the duty cycle.

$$\Delta i_L = \frac{V_{in} \times D}{L \times Fsw} = \frac{240 \times 0.61}{6.7\ 10^{-6} \times 20\ 10^3} = \frac{146.4}{134\ 10^{-3}} = \frac{1.09\ 10^3}{100} = 10.9\ A$$

A.2. Determination of Capacitor Value

$$|\Delta Q| = \left(\frac{V_0(t)}{R}\right) DT = C\Delta V_0 \quad (4\text{-}62)$$

$$\Delta V_0 = \frac{V_0(t)DT}{R_{Load}} = \frac{V_0(t)D}{R_{Load}\times C\times f} \quad (4\text{-}63)$$

$$r = \frac{\Delta V_0(t)}{V_0(t)} = \frac{D}{R_{Load}\times C\times f} \quad (4\text{-}64)$$

$$C_{min} = \frac{D}{\left(\frac{\Delta V_0(t)}{V_0(t)}\right)\times R_{Load}\times f} \quad (4\text{-}65)$$

With ΔV_0= 4% of V_0, thus ΔV_0 = 15.2 V and the ratio $\left(\frac{\Delta V_0(t)}{V_0}\right)$ = 0.04

$$C_{min} = \frac{D}{\left(\frac{\Delta V_0(t)}{V_0(t)}\right)\times R_{Load}\times f} = \frac{0.61}{0.04\times 0.28\times 2.10^4} = 2723.2\ \mu f$$

A larger capacitor is connected across the output voltage to decrease the output voltage undulation. An 8200μf capacitor was selected in this study.

B. Boost Converter Parameters

V_{in} = 215.4 V; f_s = 20 kHz; V_{out} = 380 V; Power = 210 kW; η= 0.9.

dv percent = 1 this is equal to percent of output voltage.

V_{in} is the minimum value of the input voltage; f_s: switching frequency; V_{out}: initial value of the output voltage; P: power converter; η: efficiency and D: the duty cycle.

D = $1 - \frac{(V_{in}\times\eta)}{V_{out}} = 1 - \frac{(215.4\times 0.9)}{380}$ = 0.4898

d_i: input current, $d_i = I_{ripple}\times I_{out}\times\frac{V_{out}}{V_{in}}$

I_{ripple}: The right evaluation of the inductor current undulation is between 20% to 40% of the output current.

$I_{out} = \frac{Power}{V_{out}} = \frac{210.10^3}{380}$ = 552.62 A, thus $d_i = 0.4\times 552.67\times\frac{380}{215.4}$ = 389.99 A ≈ 390 A

L: inductance (Henry) it is given by $\mathrm{L} = \frac{[\mathrm{V_{in}} \times (\mathrm{V_{out}} - \mathrm{V_{in}})]}{(\mathrm{d_i} \times \mathrm{fs} \times \mathrm{V_{out}})}$ = $\frac{215.4 \times (380 - 215.4)}{390 \times 20{,}000 \times 380}$ = 11.96 μH

ΔV: output voltage ripple; $\mathrm{d_V}$= $\mathrm{V_{out}} \times \frac{\mathrm{d_V\ percent}}{100}$ which is $\mathrm{d_V} = 380 \times \frac{1}{100}$ = 3.8 V

C: capacitor (Farad) it is given by $\mathrm{C} = \frac{\mathrm{I} \times \mathrm{D}}{\mathrm{f_s} \times \mathrm{d_V}}$ = $\frac{552.67 \times 0.4898}{20{,}000 \times 3.8}$ = 3562 μf

4.4. Developed Energy Management System Algorithm for Battery Energy Storage system

The energy management system (EMS) is a method utilized for monitoring and optimizing a system operation. Generally, the EMS is utilized to control power production and schedule programs for a group of power grid applications. However, EMS may be considered as another way to control the electrical loads in micro-grids.

The present system is designed to meet the load demands. As renewable resources are intermittent sources, the battery is used as a back-up system and this is also designed to meet the load as well. The developed DC micro-grid model has three different types of load (Industrial, Residential and Commercial Loads), in this developed model, the industrial load is assumed to be a priority load and an auxiliary load is used to absorb all the overproduction when the battery banks are fully charged. The system comprises three renewable sources with the energy storage system, which provides power to the loads when the power generation is insufficient. The net power generation and the load demands are calculated as follows:

$$\mathrm{P_G} = \mathrm{P_{pv}} + \mathrm{P_{wind}} + \mathrm{P_{biom}} \quad (3\text{-}66)$$

$$\mathrm{P_L} = \mathrm{P_{Ind}} + \mathrm{P_{Res}} + \mathrm{P_{Com}} \quad (3\text{-}67)$$

With, $\mathrm{P_G}$ the power generation; $\mathrm{P_{pv}}$ the power produced from PV; $\mathrm{P_{wind}}$ the power produced from Wind; P_{biom} the power produced from Biomass; P_L the load demands; P_{Ind} the Industrial load; P_{Res} the Residential load and P_{Com} the Commercial load.

The battery bank will charge when there is surplus of power generation and will discharge when the power generation is not capable to handle the load demands. Based on the developed architecture, the power generation will supply the load demands through four conditions and by the support of the battery bank. The developed flow chart architecture is presented in Figure 4.7.

Firstly, the load demand and the power generation through different sources will be measured

according to the following cases:

First condition: When the power generation is equal to overall load demands.

Based on this case, the loads are supplied by the power generation from PV, Wind as well as Biomass without any disruption.

Second condition: When the power generation exceeds the total load demands.

For this scenario, the power generation is higher than the load demands, thus the total load demands are provided by the power generation and the excess of production is used to charge the batteries. As the loads are provided by the power generation, at the same moment the SoC of the battery is measured. The condition is that, if it has a minimum value, which is < 100%, then the battery will be connected to charge until its SoC will attain the maximum value and the excess power will be supplied to the auxiliary load.

$$\mathrm{SoC_{min}} < \mathrm{SoC_{batt}} < \mathrm{SoC_{max}} = 20\% < \mathrm{SoC_{batt}} < 100\% \tag{3-68}$$

$$\mathrm{P_G} > \mathrm{P_L} = \mathrm{Charging} \tag{3-69}$$

Third condition: When the total load demands exceeds the power generation.

When the power generation is less than the total load demands, then the loads will be provided with the help of the battery bank. The EMS checks and calculates the difference between the power generation and loads. At the same time the SoC of the battery bank will be measured. In the case where the power in the battery is enough to provide the load demands, then the battery is discharged until its SoC will reach its minimum value.

$$\mathrm{P_G} < \mathrm{P_L} = \mathrm{Discharging} \tag{3-70}$$

$$\mathrm{P_L} = \mathrm{P_G} + \mathrm{P_{batt}} \tag{3-71}$$

$$\mathrm{SoC_{batt}} < 20\% = \mathrm{Disconnect} \tag{3-72}$$

Fourth condition: When the generation power is still less the load demands and the SoC of the battery is < 20%.

When the $\mathrm{SoC_{batt}} < 20\%$, the battery will be disconnected to the system and at this time the industrial load and the commercial load will be supplied by the available production from the renewable energy sources. The difference power between the power generation and the two

load demands will be calculated and after that, the available power generation will be checked to verify if it is enough to supply the two load demands (industrial and commercial loads). If yes, then the two loads will be supplied and if not, only the priority load (industrial load) will be provided by the power generation, which is the most estimated. The EMS will calculate the difference between the power generation and the priority load, and it will check the availability of the generated power to see if it can provide the priority load demand. If the condition is approved, then the priority load will be provided by the available power generation. In contrary, if the condition is not satisfied, then the difference between the residential load and the power generation will be calculated. The available power generation will be measured if it could supply the residential load. If the condition is approved, the residential load demand will be provided by the available power generation from the renewable sources, if not the system will be shut down and the available power generation from the renewable sources will be supplied to the battery bank. The system will permanently verify the power generation until the power generation becomes active or the SoC of the battery reaches 20%.

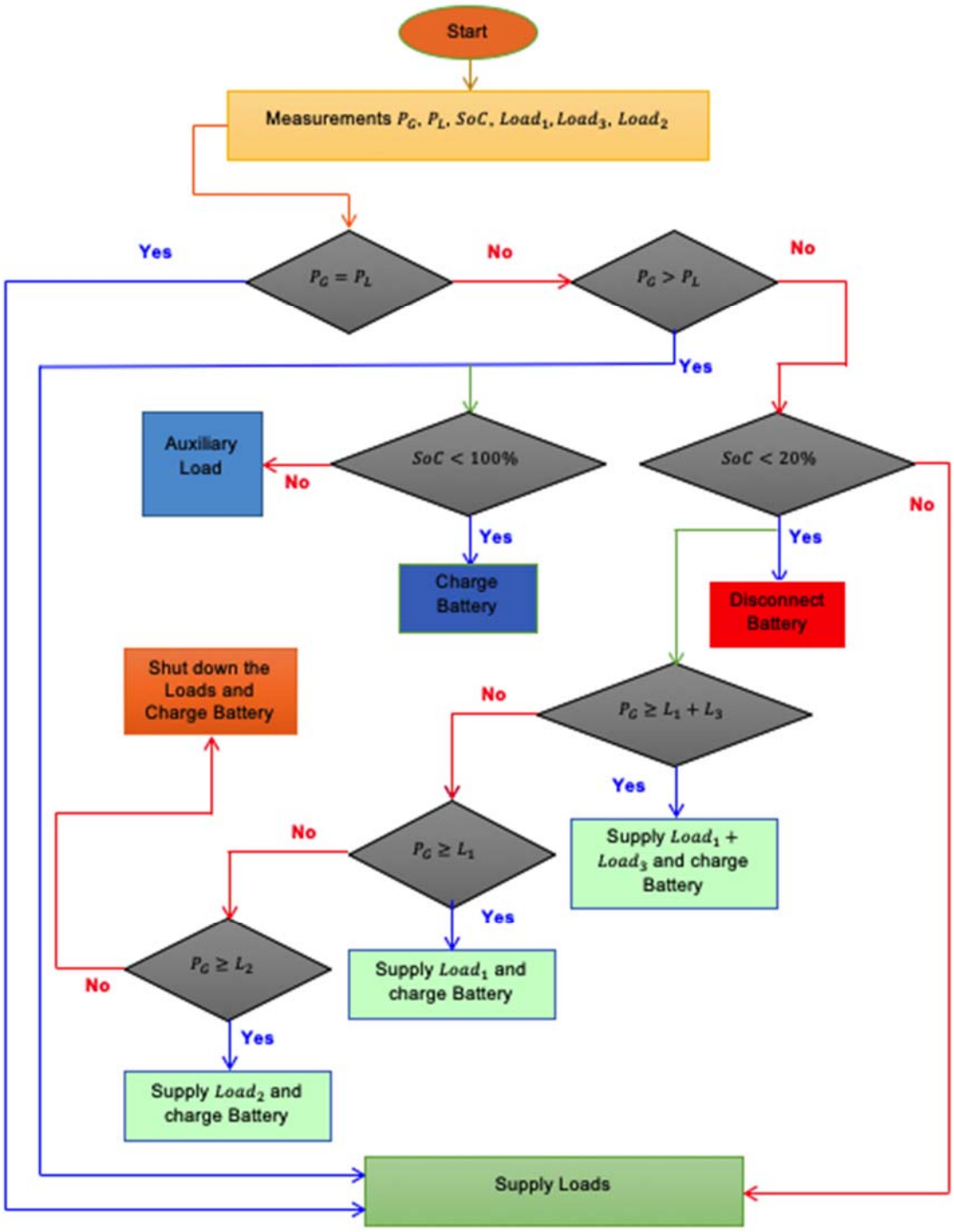

Figure 4.7: Energy Management System Flowchart

CHAPTER 5: RESULTS AND DISCUSSION OF THE DEVELOPED MODEL

5.1. Introduction

In the precedent section, the descripted model structure and diverse specified simulation procedures have been presented, so this chapter implicates the study of the simulation results. The designed and developed DC micro-grid simulation model was performed by the use of Simulink blocks available in the MATLAB / SIMULINK software. The blocks used included that of the photovoltaic, permanent magnet synchronous machine, battery and converters were designed in the SimPower Systems toolbox. Also blocks for circuit breaker, load, Measuring and display devices were also used.

The following sections present the organization of this chapter. In section 5.2, the description of the simulation model for the developed DC micro-grid is presented. The simulation results of a photovoltaic array model of the developed DC micro-grid are presented in section 5.3. In section 5.4, the results of the simulation of wind energy model for the developed DC micro-grid are presented. Section 5.5 gives the simulation results of biomass energy model for the developed DC micro-grid. The section 5.6 gives the simulation results of the battery energy storage of the developed DC micro-grid. The load demands results of the developed DC micro-grid are presented in the section 5.7. Section 5.8 is concentrated on the simulation of the developed energy management system algorithm. Section 5.9 focuses on the discussion of the simulation results of the entire model including the developed energy management system algorithm. Section 5.10 presents a brief summary on this chapter.

5.2. Description of the Designed and Developed Simulation Model for the DC Micro-Grid

Simulation model of the DC micro-grid was designed and developed on MATLAB/SIMULINK environment by physical modelling. All circuit elements and machines are represented by their respective model blocks available in the software. Figure 5.1 illustrates a complete system model of the developed DC micro-grid composed of model blocks of PV, Wind, Biomass, Battery, loads, switchgears, measuring and displaying devices. Table 5.1, presents the simulation parameters.

Table 5.1: Simulation Parameters

Description	Specification
PV power	210kWp, 380Vdc
Wind energy	150kW, 380Vdc
Biomass energy	150kW, 380Vdc
Battery storage	576kWh / 240V

Residential load	265kW
Commercial load	62.1kW
Industrial load	180kW
DC bus voltage	380Vdc

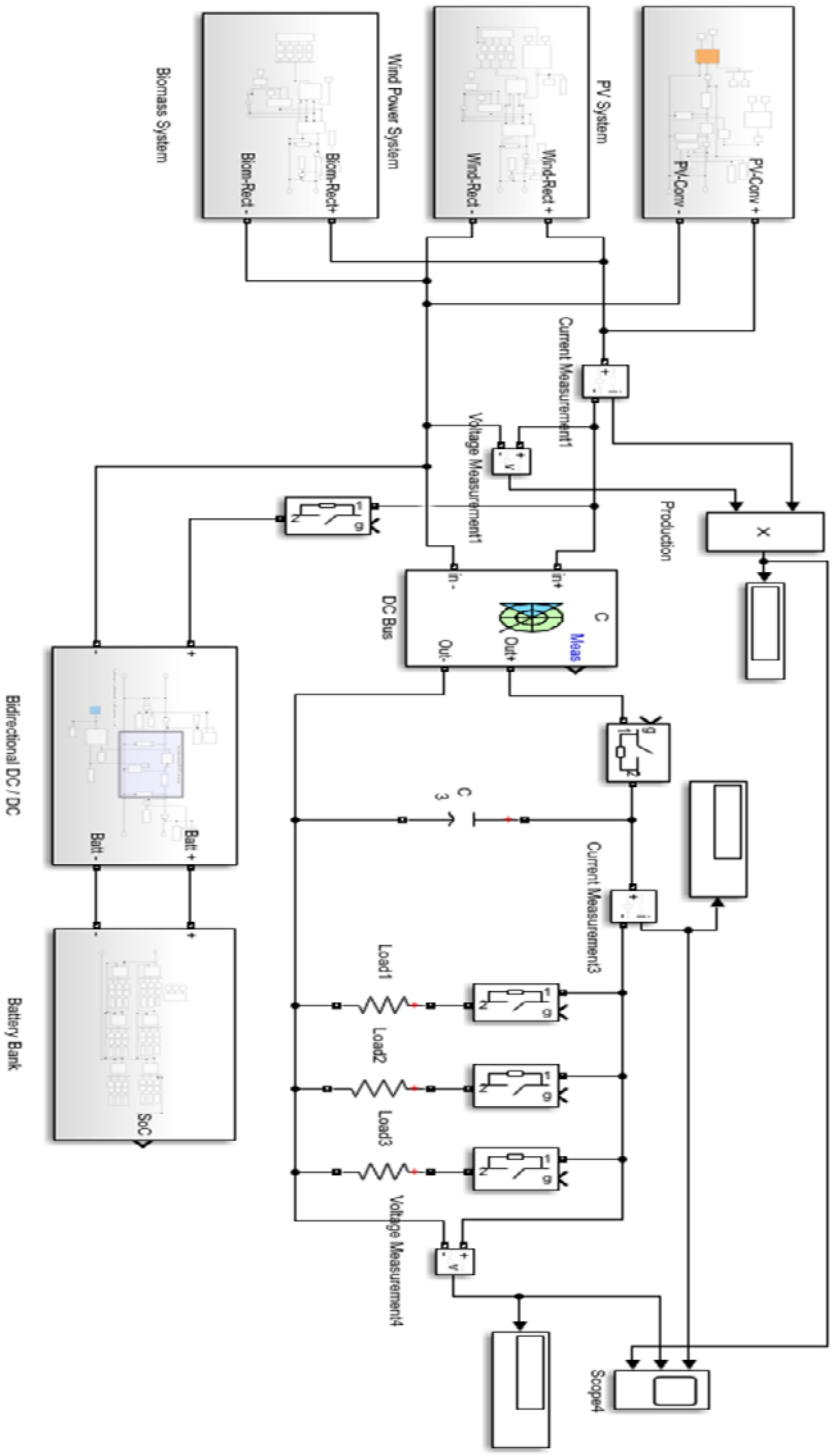

Figure 5.1: Descripted DC micro-grid model

5.3. Simulation Results of the PV Array Model for the DC Micro-Grid

The complete autonomous PV model was designed using MATLAB / SIMULINK software environment. The PV array model has been designed in SIMULINK and to step up the output voltage of the PV system from 215.4 V_{dc} to 380 V_{dc} , a DC-DC boost converter was designed and associated to the PV model utilizing physical electronic components, which include resistor, inductance, diode and a IGBT; this is presented in Figure 5.2. To generate the required power, a large number of solar cells has been connected in parallel and series to constitute a PV module. The solar irradiation was assumed constant at 1000 W/m^2 and the temperature constant at 25℃ in the simulation. As the PV output voltage is not constant, which means that it varies, therefore, the duty cycle control was implemented to maintain the output voltage from the DC-DC boost converter constant at 380 V_{dc} adopting the following Equation.

$$D = 1 - \frac{(V_{in} \times \eta)}{V_{out}} \quad (5\text{-}1)$$

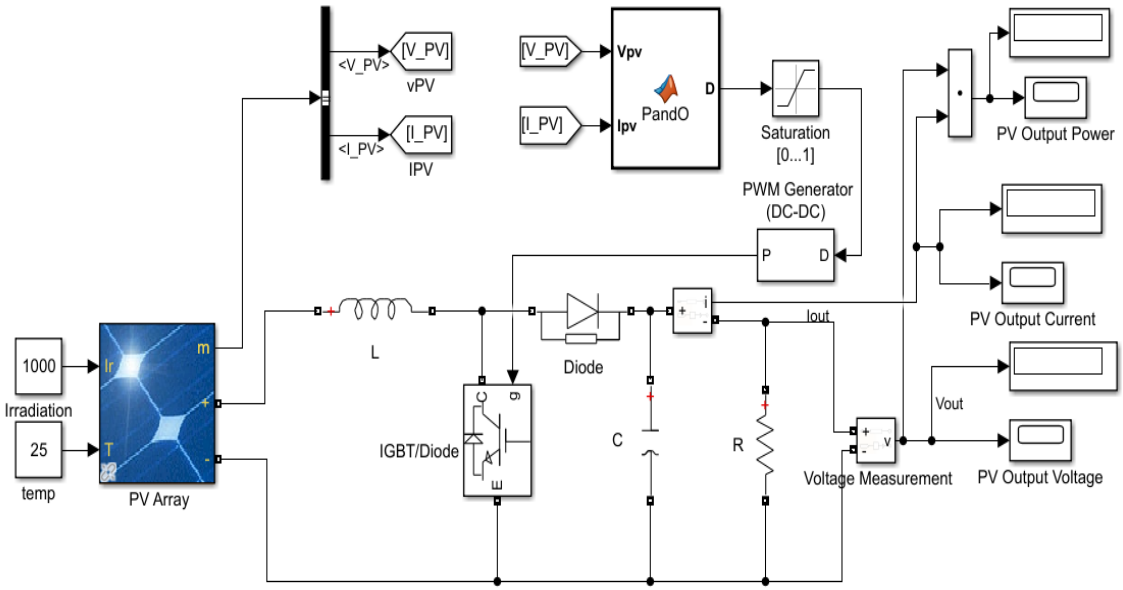

Figure 5.2: PV array model for the developed DC micro-grid

5.3.1. Simulation Results of the Developed PV Array Model for the DC Micro-Grid

Finally, to ensure that the design of this model is correct, the model can be simulated for its evaluation and analysation of its performances. This photovoltaic model consists of 750 identical solar cells, which are connected in parallel and series and able to deliver 35.9 V DC, 6 of which are in series and 125 in parallel. This system is designed to generate a maximum power of 210 kW, a voltage of 380 V_{dc} and a maximum current of 552.67 A at the DC-DC boost converter output.

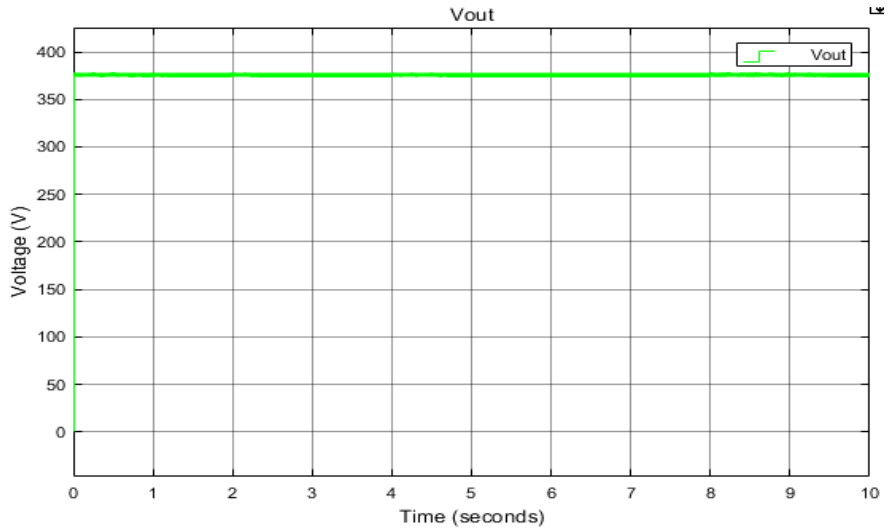

Figure 5.3: PV model output voltage for the DC micro-grid

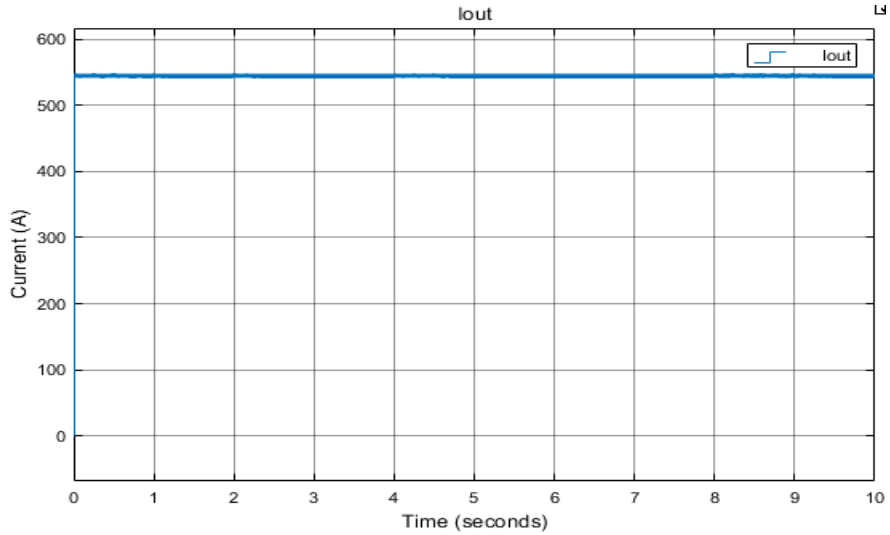

Figure 5.4.: PV model output current for the DC micro-grid

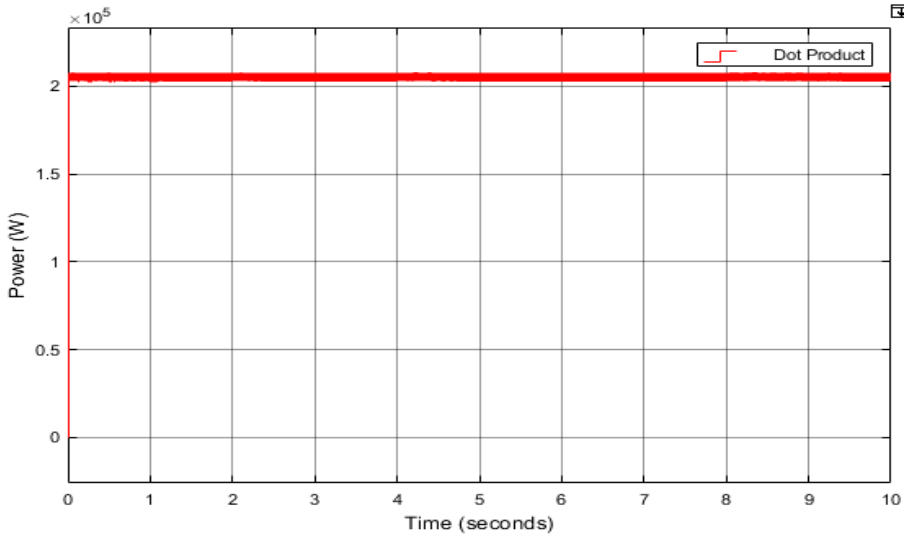

Figure 5.5: PV model output power for the DC micro-grid

The PV system output voltage from the boost converter as a function of the simulation time is illustrated in Figure 5.3 above. The output voltage remains constant at 380 V_{dc} with very small ripples; the designed model allows a ripple with 0.9% variation from the steady state.

The PV system model output current from the boost converter is presented in Figure 5.4. As it is shown, the value of the output current stays constant at 553 A with a very small ripples. The founded simulation results were identical to the calculations done in section 4.3.4.1 in the point B above of the photovoltaic model output current.

Figure 5.5 illustrates the generated photovoltaic model output power and as it can be seen, the output power remains constant. The produced power is 210.678 kW. This result refers and approves the calculated value of the photovoltaic model output power in the precedent chapter, Section 4.3.1.2.

5.4. Simulation Results of the Developed Wind Power Model for the DC Micro-Grid

The wind energy model was also designed in MATLAB / SIMULINK software environment and a AC-DC universal bridge rectifier was added to the permanent magnet synchronous generator (PMSG) block output, which converted the AC output voltage of the wind power model from 380 $\mathrm{V_{ac}}$ to 380 $\mathrm{V_{dc}}$; this is illustrated in Figure 5.6. The wind speed is kept constant at 12 m/s, pitch angle to 0°, rotor speed 12.08 rad/s and the torque of 12500 Nm in the simulation. The rotor speed and torque are calculated as follow:

Knowing that $\mathrm{P_{wind}}$= 150 kW, f= 50 Hz and the pair of poles considered is equal to 48.

The rotational speed is calculated by:

$$\mathrm{N} = \frac{60 \times \mathrm{f}}{\mathrm{p}} \tag{5-2}$$

$$\mathrm{N} = \frac{60 \times 50}{24} = 125 \text{ rpm}$$

The angular velocity is calculated by:

$$\omega = \frac{\mathrm{N} \times 2\pi}{60} \tag{5-3}$$

$$\omega = \frac{125 \times 2 \times 3.14}{60} = 12.08 \text{ rad/s}$$

The torque is calculated as follow:

$$\mathrm{C} = \frac{\mathrm{P}}{\omega} \tag{5-4}$$

Because of certain losses in the machines such as the losses of hysteresis, it is thus that in the calculations the power is fixed at 151 kW.

$$C = \frac{151\,000}{12.08} = 12500\ Nm$$

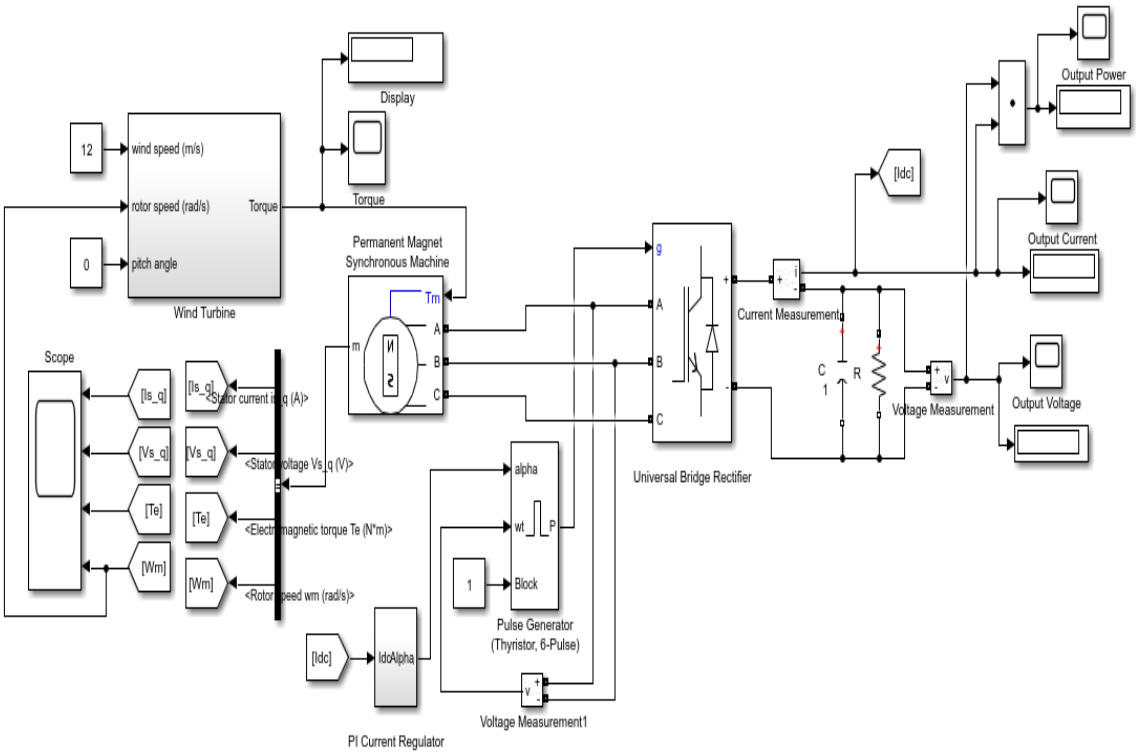

Figure 5.6: Developed wind power model for the DC micro-grid

5.4.1. Simulation Results of the Developed Wind Power Model for the DC Micro-Grid

To make sure that this design model is correct, the model can be simulated to estimate and analyse its performances and quality. The wind power model is constituted of a wind turbine, which turns at 12.08 rad/s and able to deliver a torque of 12500 Nm that runs a permanent magnet synchronous machine. This system is constituted of a maximum power of 150 kW, a voltage of 380 V_{dc} and a maximum current of 394.74 A at the output of the universal bridge rectifier. The following Figures, present the simulations results.

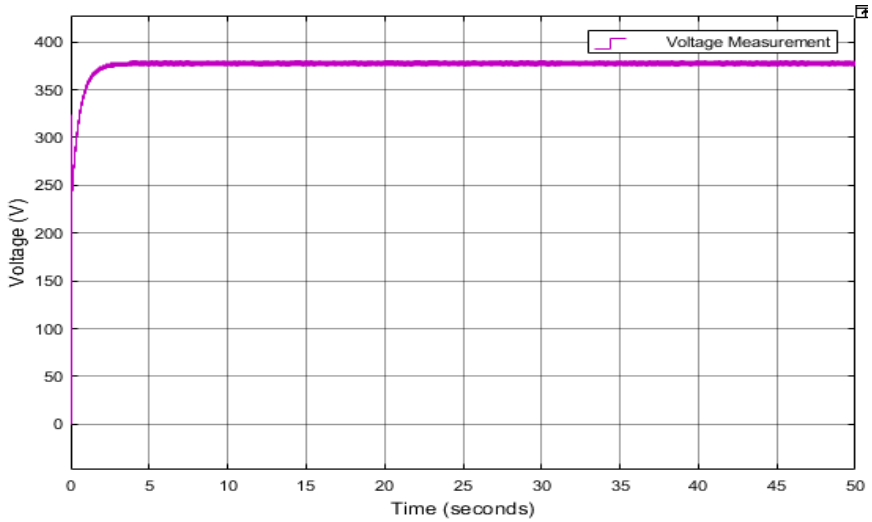

Figure 5.7: Wind power output voltage for the DC micro-grid

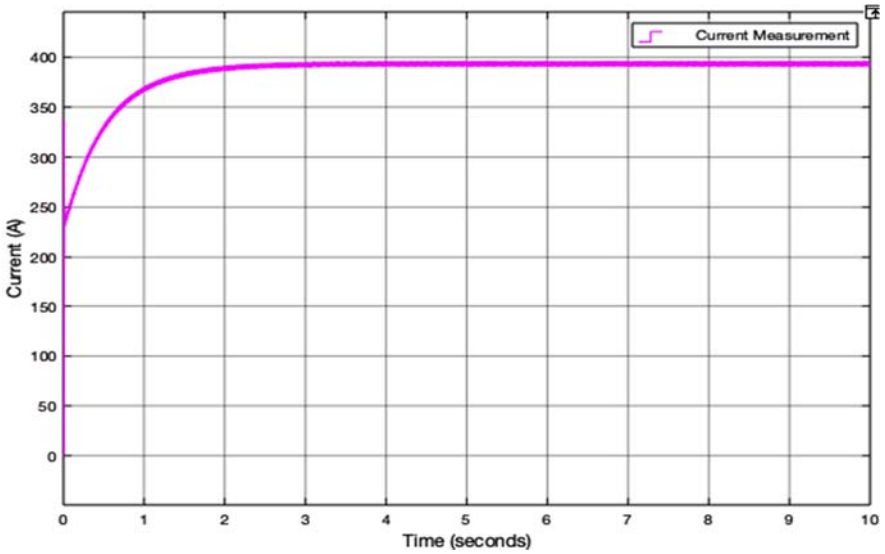

Figure 5.8: Wind power output current for the DC micro-grid

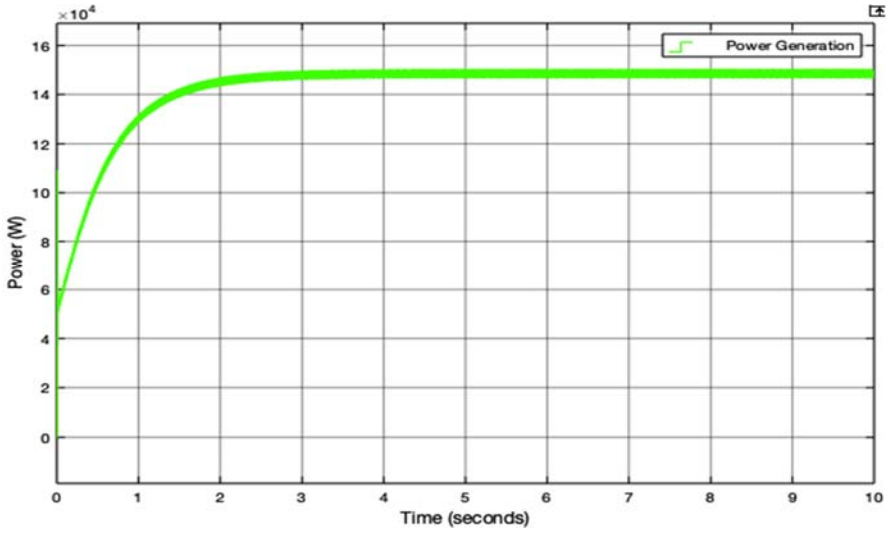

Figure 5.9: Wind power output power for the DC micro-grid

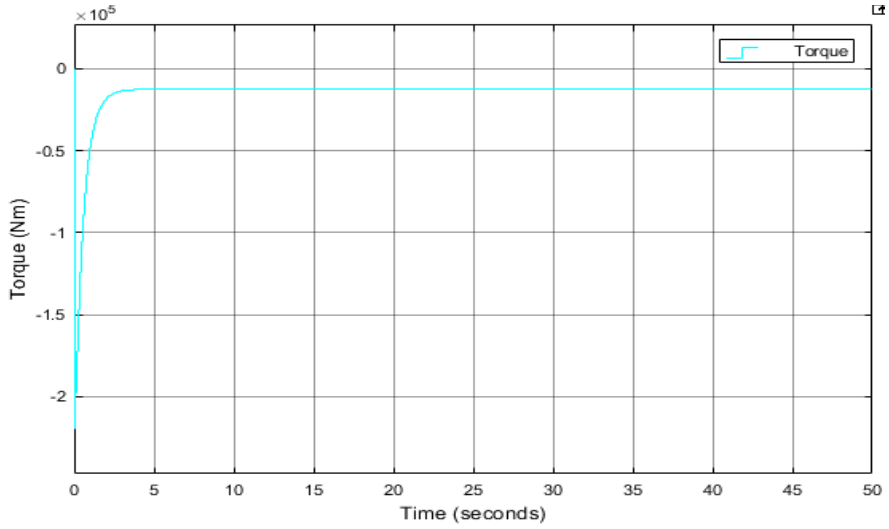

Figure 5.10: The output torque from wind turbine for the DC micro-grid

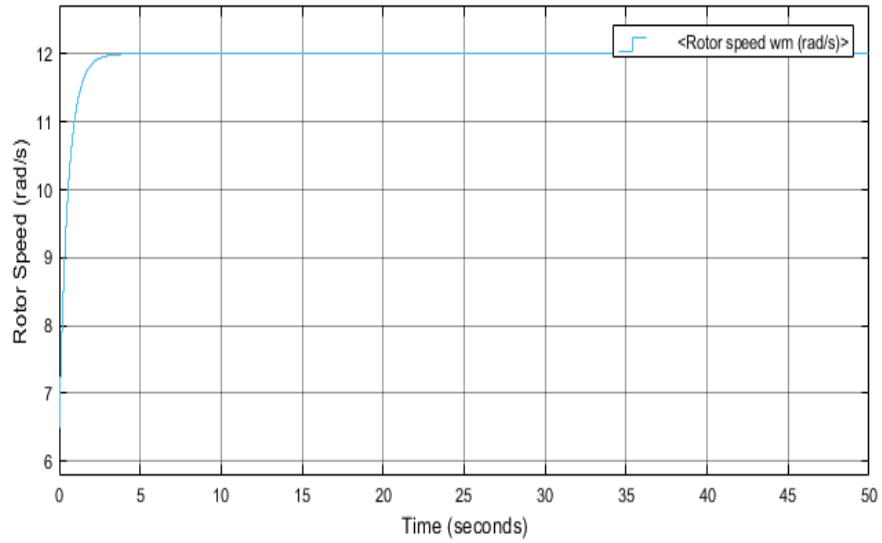

Figure 5.11: The rotor speed of the wind turbine for the DC micro-grid

Figure 5.7 presents the universal bridge rectifier output voltage of the wind power system. The steady state of the output voltage is attained at approximately 2.5s and after remains constant at 380 V_{dc} with very small ripples. The output current of the wind power system model from the universal bridge rectifier is shown in the Figure 5.8. As it can be seen, the steady state is reached at 2.5s and the output current stays constant with small ripples at 397 A as an average value. Figure 5.9 presents the generated output power from the wind model and the steady state of this power starts to be reached at 2.5s and remains constant with small ripples. The average value of the power produced is 148.778 kW.

Figure 5.10 above presents the torque curve. Figure 5.11 illustrates the rotor speed curve, the steady state is reached after 2.5s. The torque and rotor speed remain constant without any ripple. The generated torque is 12520 Nm and the rotor speed is 12 rad/s. These results

confirm the rotor speed and torque values of the wind turbine calculated in the Equation 5.4 above. Therefore, the founded voltage, current and power output values of the simulation results were identical and equal to the expected values of the output from the universal bridge rectifier.

5.5. Simulation Results of the Developed Biomass Power Model for the DC Micro-Grid

Since the biomass block does not exist in SimpowerSystems, the PMSG was considered for this case. The biomass power model has been implemented using MATLAB / SIMULINK software environment and a AC-DC universal bridge rectifier was added to the output of the PMSG block, which converts the AC output voltage from 380 V_{ac} to 380 V_{dc}; this is shown in Figure 5.12. The torque is kept constant at 2906.4 Nm and the rotor speed at 52.33 rad/s, in the simulation. The rotor speed and torque are calculated as follow:

The rotated speed is estimated at 500 rpm at a frequency of 50 Hz. Referring to the equations 5-2; 5-3 and 5-4, the rotor speed and torque can be calculated.

$$N = \frac{60 \times f}{p} \rightarrow p = \frac{60 \times f}{N} = \frac{60 \times 50}{500} = 6 \text{ poles}$$

$$N = \frac{\omega \times 60}{2\pi} \rightarrow \omega = \frac{N \times 2\pi}{60} = \frac{500 \times 6.28}{60} = 52.33 \text{ rad/s}$$

$$C = \frac{P}{\omega} = \frac{151000}{52.33} = 2906.4 \text{ Nm}$$

5.5.1. Simulation Results of the Developed Biomass Power Model for the DC Micro-Grid

To be sure with the design of the model made, this is simulated to estimate and analyse its quality performances. This model comprises a PMSG operating at 52.33 rad/s with a constant torque of 2906.4 Nm as illustrated in Figure 5.12. The characteristics of the system are (a maximum power of 150 kW, a voltage of 380 V_{dc} and a maximum current of 394.74 A at the output of the universal bridge rectifier. The following Figures, present the simulations results.

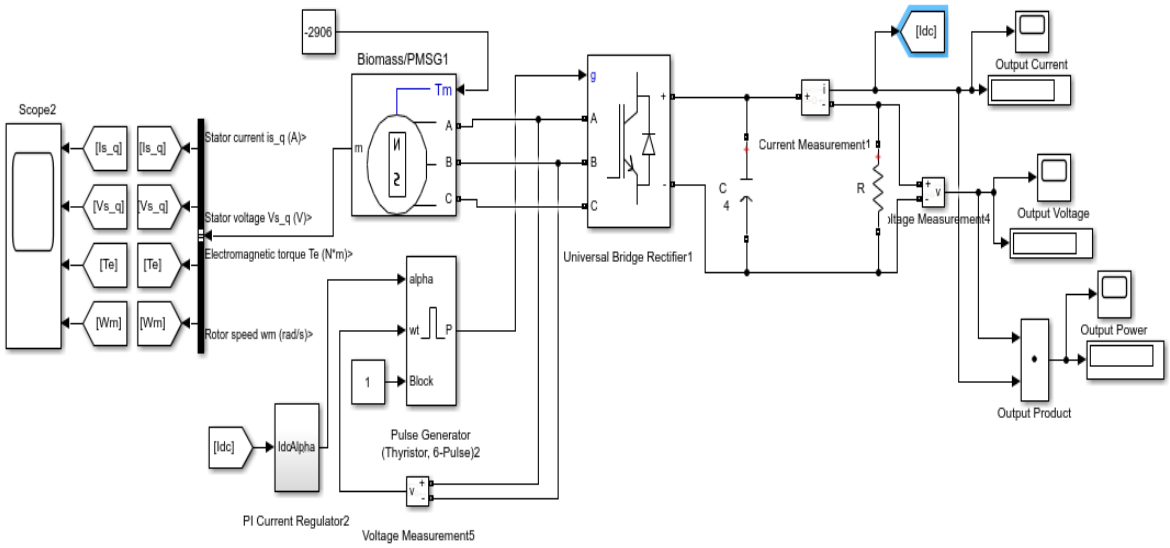

Figure 5.12: Biomass power model for the DC micro-grid

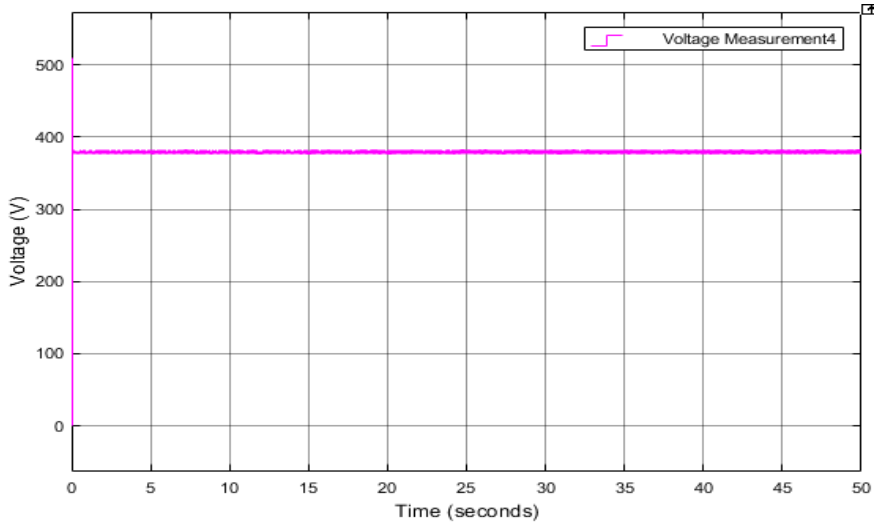

Figure 5.13: Biomass power output voltage for the DC micro-grid

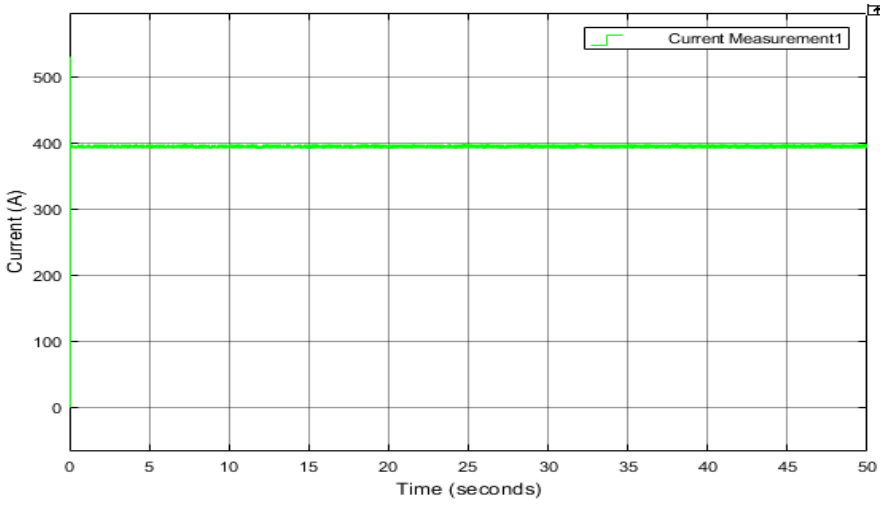

Figure 5.14: Biomass power output current for the DC micro-grid

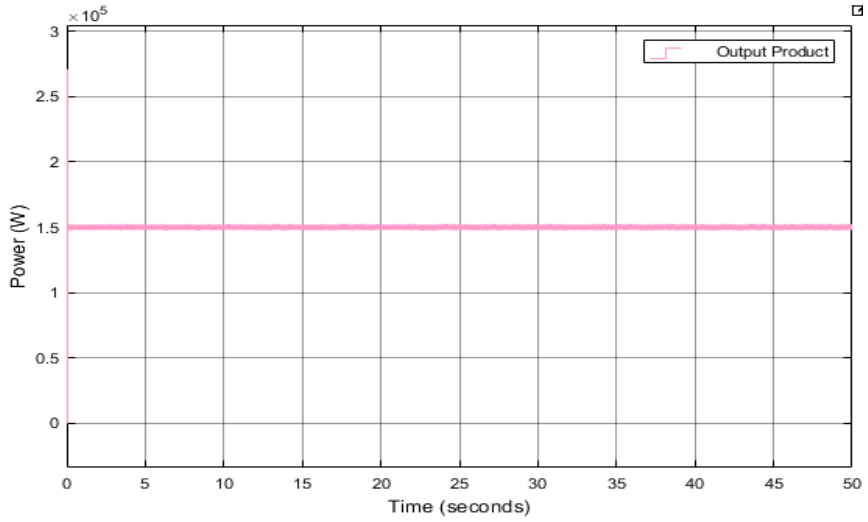

Figure 5.15: Output power of the biomass power for the DC micro-grid

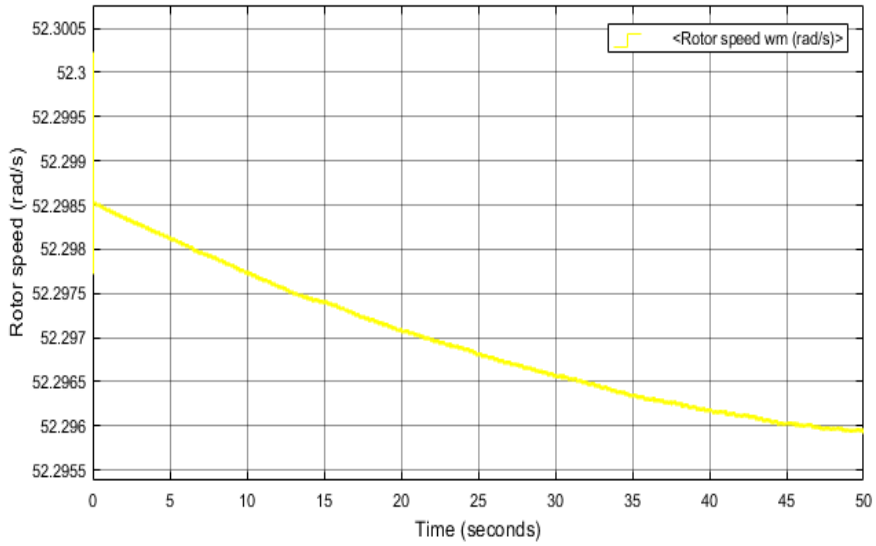

Figure 5.16: The Rotor Speed of the permanent magnet synchronous generator

The above Figure 5.13, refers to the universal bridge rectifier output voltage. This voltage value is constant at 380 V_{dc} with very small ripples. The output current of the model is presented in the Figure 5.14. As it can be seen, the output current stays constant at 398.7 A with a very small ripples. Figure 5.15 presents the generated output power of the biomass power system and this value remains constant. The power generated by the biomass system is 151.678 kW.

The rotor speed curve of the PMSG is presented in Figure 5.16 and its output value is 52.3 rad/s. Comparing the result of the simulation to the calculated value in Section 5.5, the simulated value of the rotor speed was found identical to the above value. Thus, these results approximately refer to the expected values of the designed model. The designed model allows a ripple with 0.87% variation from the steady state.

5.6. Simulation Results of the Developed Battery System Model for the DC Micro-Grid

The Battery model has also been implemented within MATLAB / SIMULINK software environment and a DC-DC bidirectional converter was utilized and designed utilizing physical electronic components like resistor, inductance, capacitance and a IGBT/Diode to step up the battery output voltage for the discharging mode and to step down the battery input voltage of the battery system from 380 V_{dc} to 240 V_{dc} for charging and vice versa, with a duty cycle equal to 0.61; this is presented in Figure 5.17. Two battery banks were considered in this simulation grouped in series and parallel. Each battery bank generates 288 kWh and the battery bank capacity is at 576 kWh. To maintain the DC-DC bidirectional converter output voltage, the duty cycle control is developed and that value is maintained at 380 V_{dc} adopting the following equation.

$$D = \frac{V_{out}}{V_{out} + V_{in}} \tag{5-5}$$

$$D = \frac{380}{380 + 240} = 0.61$$

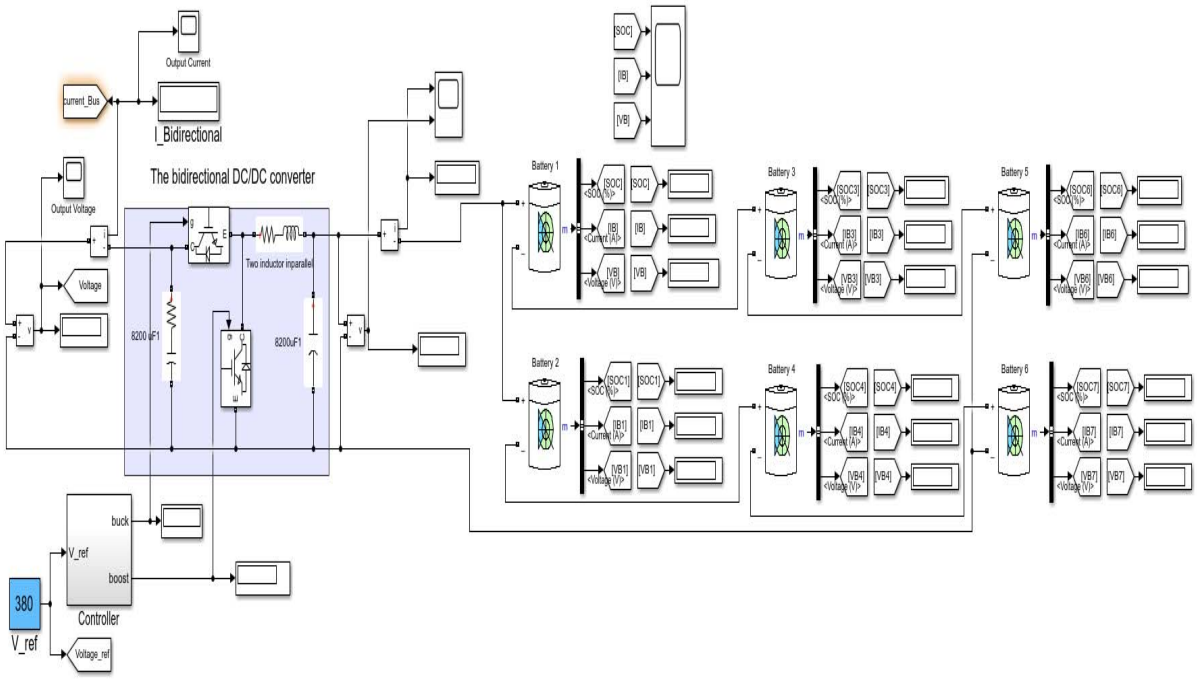

Figure 5.17: Battery energy storage system model for the developed DC micro-grid

5.6.1. Simulation Results of the Developed Battery System Model for the DC Micro-Grid

The battery bank is designed to first meet the total load demands and provide power to the priority load (industrial load), which is the most consideration in this research within at least five hours on its own when it is fully charged without any power generation. But the total load demands can also be supplemented by the battery bank for few hours. The battery bank model comprises 6 identical batteries grouped in parallel and series and able to deliver 80 V DC 1200 Ah each, 3 of which are in series and 2 in parallel as considered in the design. The characteristics of the modelled battery bank are (a maximum power of 576 kWh, a voltage of 240 V_{dc} and a maximum current of 2400 Ah). The expected generated values at the bidirectional converter output are 380 V_{dc} as voltage, 1345 A for the current and 511 kW as output power. The Figures bellow, present the simulations results:

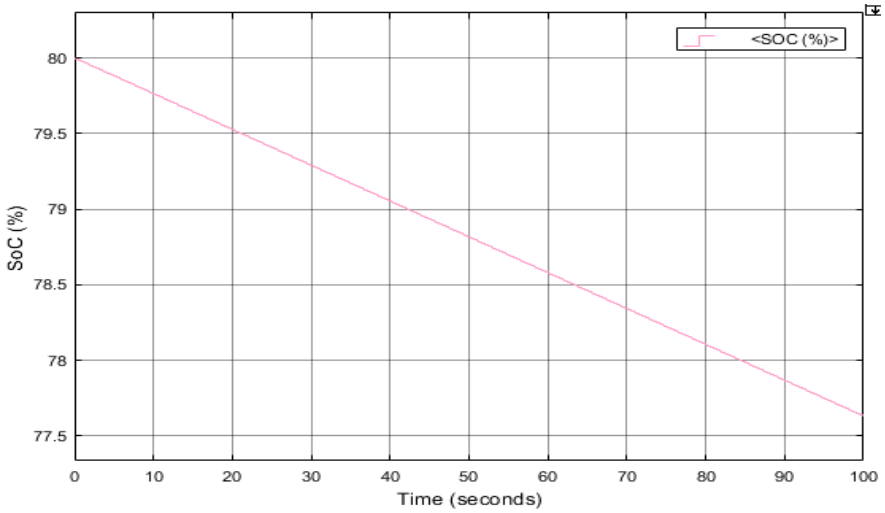

Figure 5.18: Battery SoC for the DC micro-grid

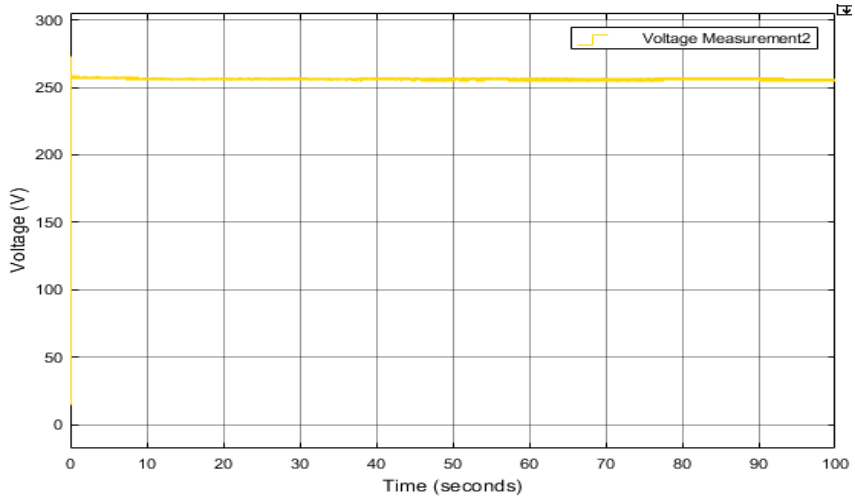

Figure 5.19: Battery output voltage of the DC micro-grid

Figure 5.18 presents the battery SoC, it can be seen that the battery is discharged gradually without knowing the problem of rapid discharge. The battery output voltage is presented in Figure 5.19. This output value remains constant at 256 V with very small ripples.

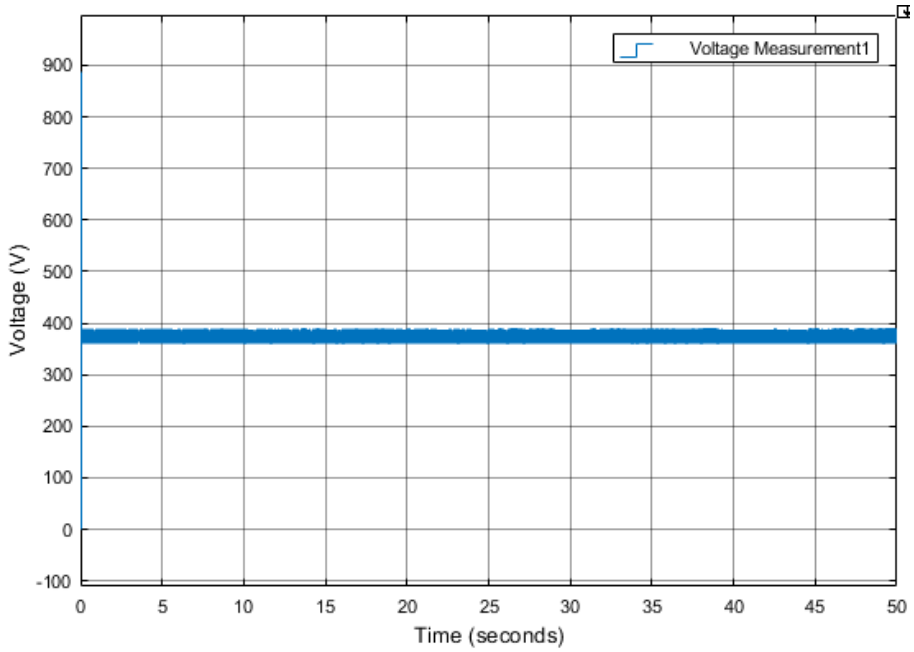

Figure 5.20: DC-DC bidirectional converter output voltage of the battery

Figure 5.20 illustrates the battery output voltage and its value stays constant with small ripples.

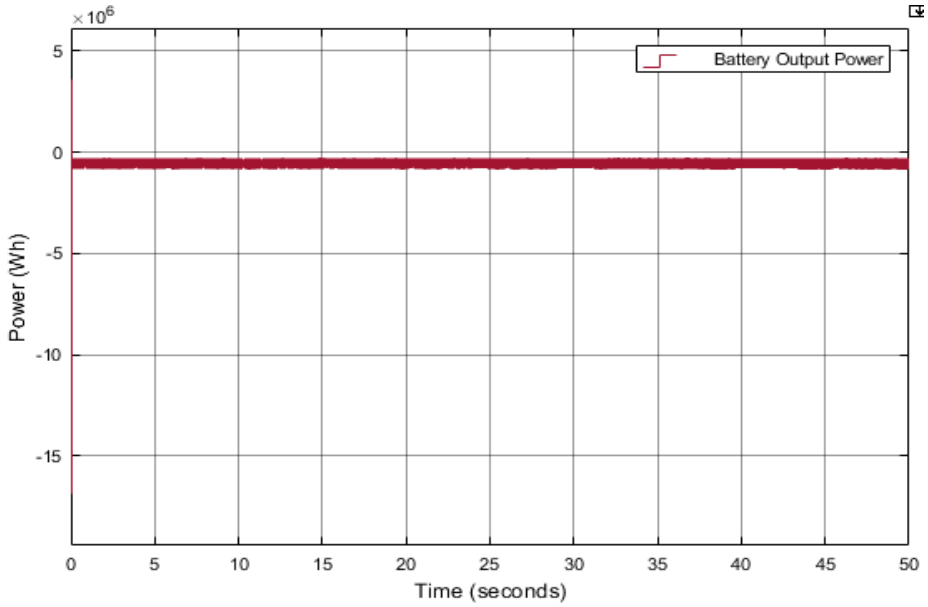

Figure 5.21: Output power of the Battery for the DC micro-grid

Figure 5.21 shows the generated battery bank output power, and the result demonstrates that this output power has a constant value with small ripples. The average value of the produced power is 563,45 kWh.

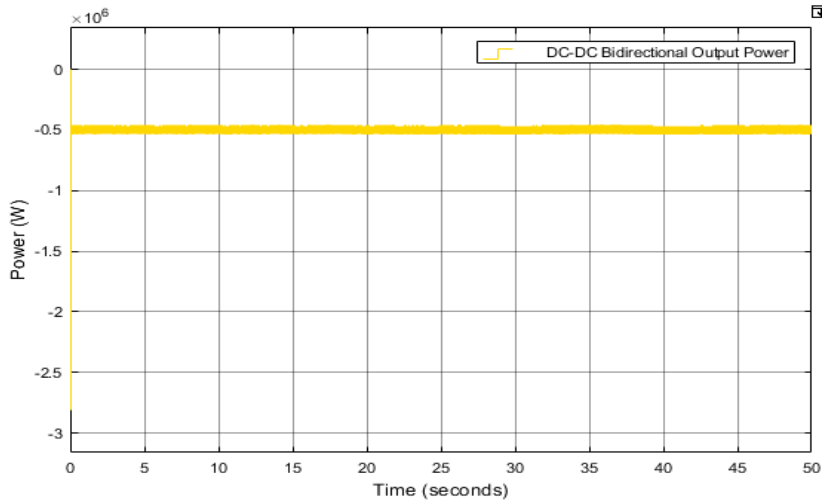

Figure 5.22: Output power of the battery from DC-DC bidirectional converter for the DC micro-grid

Figure 5.22 illustrates the output power from DC-DC bidirectional and the output power remains constant with very small ripples. Thus, the voltage and power output results of the simulation found were identical and equal to the expected values of the output from the DC-DC bidirectional.

5.7. Simulation Results of the Load demands for the DC Micro-Grid

The designed and developed system is constituted of three different types of loads (Load1 = Industrial load, Load2 = Residential load and Load3 = Commercial load), which are connected in parallel and represented by the resistors in the model. The industrial load is considered as a priority load in this system and an auxiliary load is used, which will be supplied when the battery storage will be fully charged. The entire load comprises 510 kW, with Industrial load 200 kW, Residential load 150 kW and Commercial load 160 kW. The following curves show the different measures of the load, which are power, voltage and current.

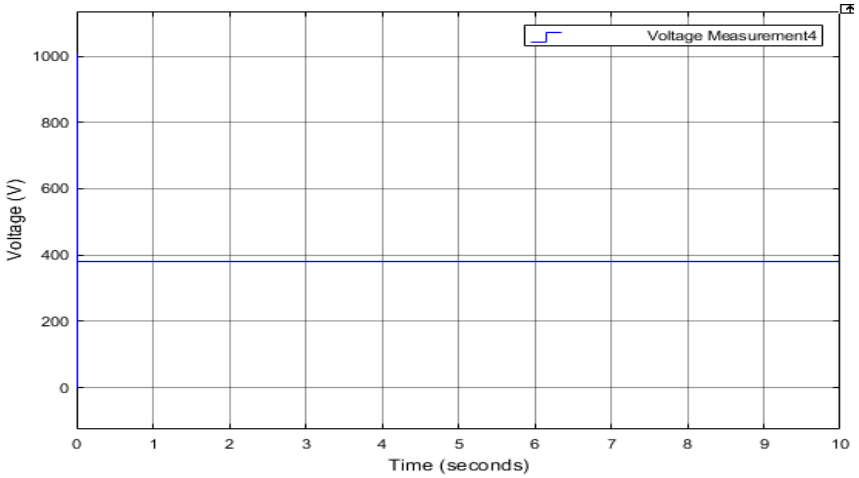

Figure 5.23: Load demands voltage for the DC micro-grid

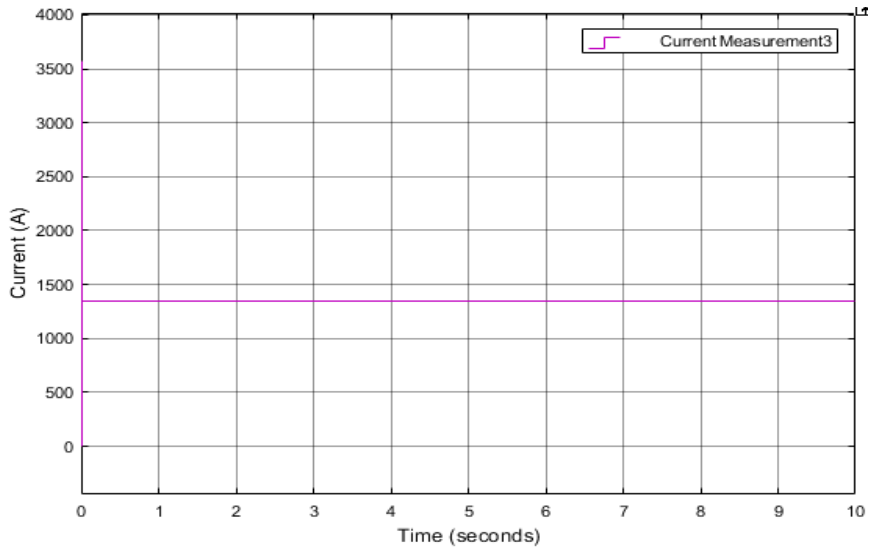

Figure 5.24: Load demands current for the DC micro-grid

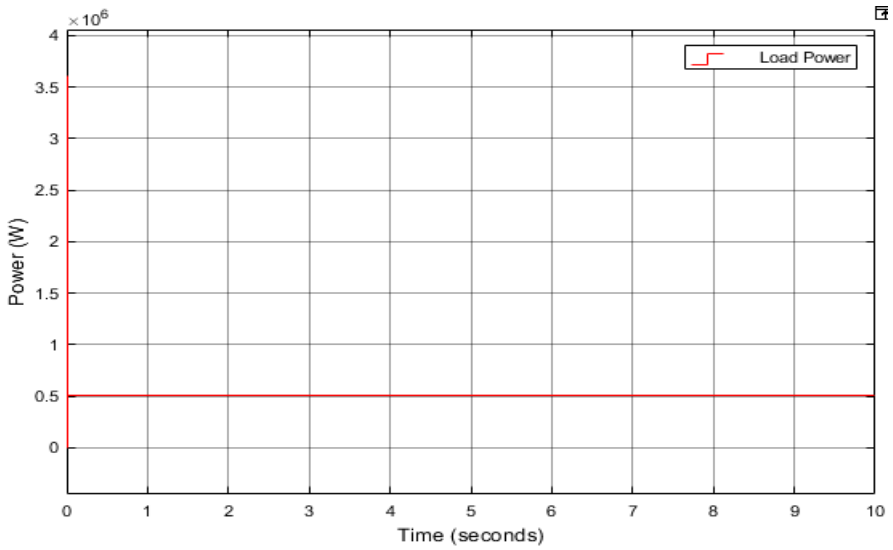

Figure 5.25: Power demand of Loads for the DC micro-grid

The above Figure 5.23, presents the load output voltage. This output voltage value is constant at 380 V_{dc}. The output current of the load is presented in Figure 5.24. According to the results, it is shown that the output current stays constant at 1346 A. The load output power is presented in Figure 5.25, and the power remains constant, which is 511,5 kW.

5.8. Description of the simulation of the Developed Energy Management System

The designed and developed DC micro-grid model and the energy management system was designed and built on MATLAB/SIMULINK environment by physical modelling. The energy management system model was designed on State-flow logical programming environment. All circuit elements are represented by their respective model blocks available in the software. A

completed model of the developed DC micro-grid and energy management system algorithm is shown on Figure 5.26.

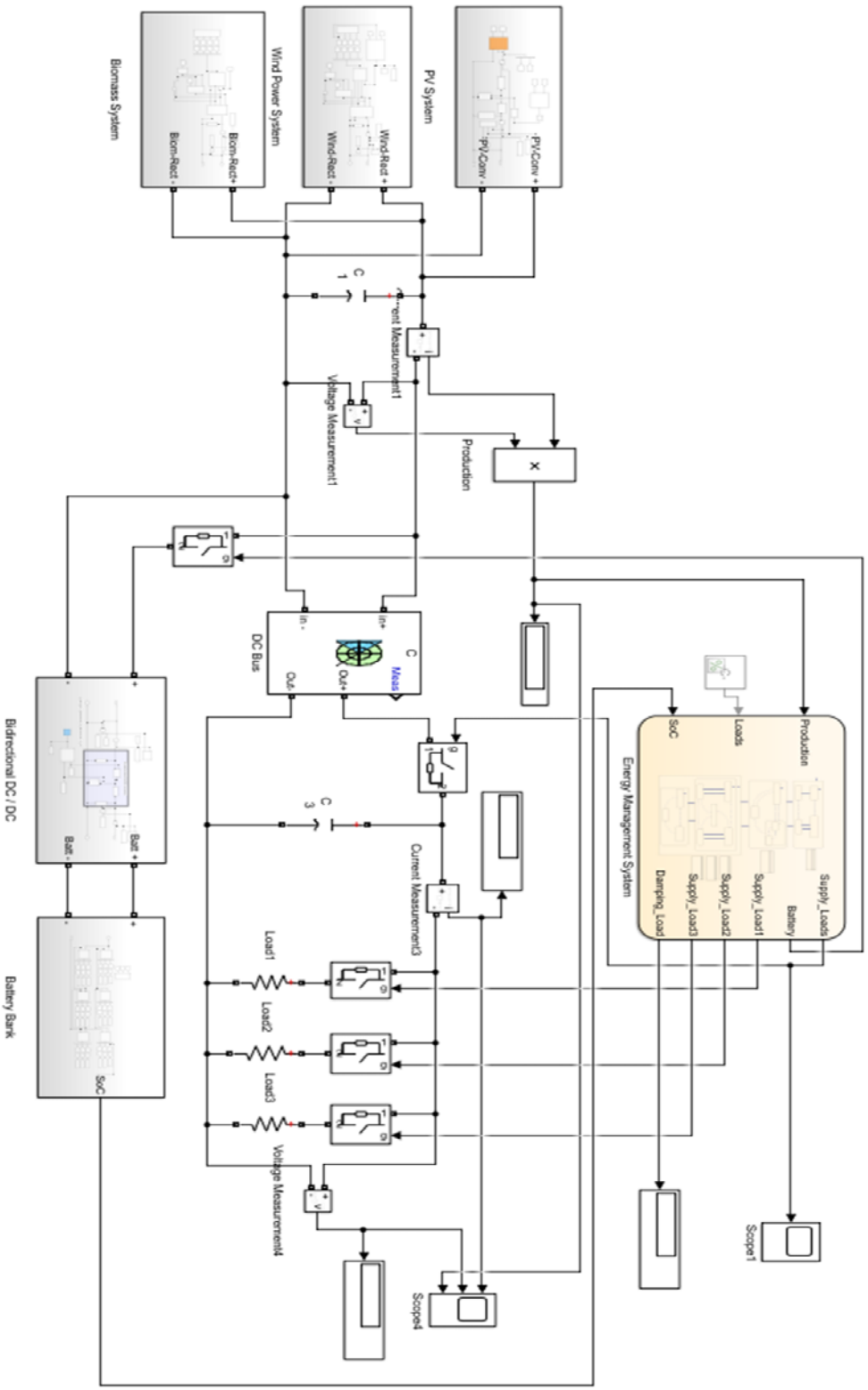

Figure 5.26: Developed DC micro-grid including the energy management system algorithm

Figure 5.26 describes the developed DC micro-grid including the energy management system algorithm, which controls the charge / discharge of the battery bank in BMS and the operation of the entire system. The system is designed so that there is no overcharging or under discharging of the battery. This implemented system control helps the battery bank to operate according to the consign from the EMS and allows to keep its SoC in the admissible limits to avoid the deep charging / discharging of the battery bank within the DC micro-grid operation. The developed model is implemented to allow the battery to charge at 100% and once the charge limit is reached, the battery is automatically disconnected from the system to wait for the discharge phase, when the power generation is not capable to provide power to the loads. When the battery is connected for the discharge phase, the system will continue to check the SoC of the battery. When the fixed discharge limit is reached (SoC < 20%), the battery will be automatically disconnected to the system because dropping below this threshold can cause deep discharges, which can drastically reduce battery endurance or destroy it completely. With this strategy, the battery will be able to maintain its qualities and capacities without having the problem of premature charging and discharging.

5.9. Simulation Results of the DC Micro-Grid Using the Developed Energy Management System Algorithm

This section focuses on the different simulation results of the developed EMS algorithm and diverse scenarios are considered. The adoption of scenarios allows to better understand the real environment and to position with a neutral and objective point of view. The use of scenarios is necessary because it allows to provide a concrete method and approach. Thus, using the scenarios chronologically provides a very useful guideline. Tables 5.2 and 5.3 summarize the different operating modes of these scenarios.

Table 5.2: Condition Table for the Energy Management System

Descriptions	Conditions	1	2	3	4	5	6	7	8	9	10	11
Scenario 1												
Supply Loads	$P_G = P_L$	**1**	0	0	0	0	0	0	0	0	0	0
Scenario 2												
Supply Loads & Charge Battery	$P_G > P_L$	0	**1**	0	0	0	0	0	0	0	0	0
Charge Battery	SoC < 100%	0	0	**1**	0	0	0	0	0	0	0	0
Disconnect Battery and Supply Auxiliary Load	SoC = 100%	0	0	0	**1**	0	0	0	0	0	0	0
Scenario 3												
Connect Battery	$P_G < P_L$	0	0	0	0	**1**	0	0	0	0	0	0
Discharge Battery	SoC > 20%	0	0	0	0	0	**1**	0	0	0	0	0

Disconnect Battery	$\mathrm{SoC} < 20\%$	0	0	0	0	0	0	**1**	0	0	0	0
Supply $Load_1$ + $Load_3$ and Charge Battery	$P_G \geq Load_1 + Load_3$	0	0	0	0	0	0	0	**1**	0	0	0
Supply $Load_1$ and Charge Battery	$P_G \geq Load_1$	0	0	0	0	0	0	0	0	**1**	0	0
Supply $Load_2$ and Charge Battery	$P_G < Load_1 \geq Load_2$	0	0	0	0	0	0	0	0	0	**1**	0
Shut down Loads and Charge Battery	$P_G < Load_2$	0	0	0	0	0	0	0	0	0	0	**1**

Where P_G is the power generation, P_L is the load demands power, $Load_1$ represents the industrial load, $Load_2$ is the residential load, $Load_3$ is the commercial load and SoC is the state of charge of the battery.

Table 5.3: Action Table for the Energy Management System

N*	**Descriptions**	**Actions**
1	Loads connected	**A1:** Loads = **ON**;
2	Load connected & Battery charging	**A2:** Loads & Battery = **ON**;
3	Battery charging	**A3:** Battery = **ON**;
4	Auxiliary Load connected	**A4:** Damp load = **ON**; Battery = **OFF**; Loads = **ON**;
5	Battery connected	**A5:** Battery = **ON**; Damp Load = **OFF**;
6	Battery discharging	**A6:** Battery = **ON**;
7	Battery disconnected	**A7:** Battery = **OFF**;
8	$Load_1$ & $Load_3$ connected	**A8:** $Load_1$ & $Load_3$ = **ON**; $Load_2$ = **OFF**; Battery = **ON**;
9	$Load_1$ & battery connected	**A9:** $Load_2$ & $Load_3$ = **OFF**; $Load_1$ = **ON**; Battery = **ON**;
10	$Load_2$ & battery connected	**A10:** $Load_1$ & $Load_3$ = **OFF**; $Load_2$ = **ON**; Battery = **ON**;
11	Loads disconnected & Battery connected	**A11:** Loads = **OFF**; Battery = **ON**;

The energy management system is implemented using the State-flow logical programming environment. The operating mode of the State-flow environment refers to a logical system either it is 0 or 1. When the output from the chart flow displays 1, it shows that the system operates (ON) and when the output indicates 0, that means the system is off.

Scenario 1: the power generation is equal to the loads demands in this first case. At this stage, the battery as well as the damp load are disconnected from the system. All production is

localized to the load and the battery SoC is assumed to be less than 100%. In this case, the battery SoC is estimated to be 50% as illustrated in Figure 5.27.

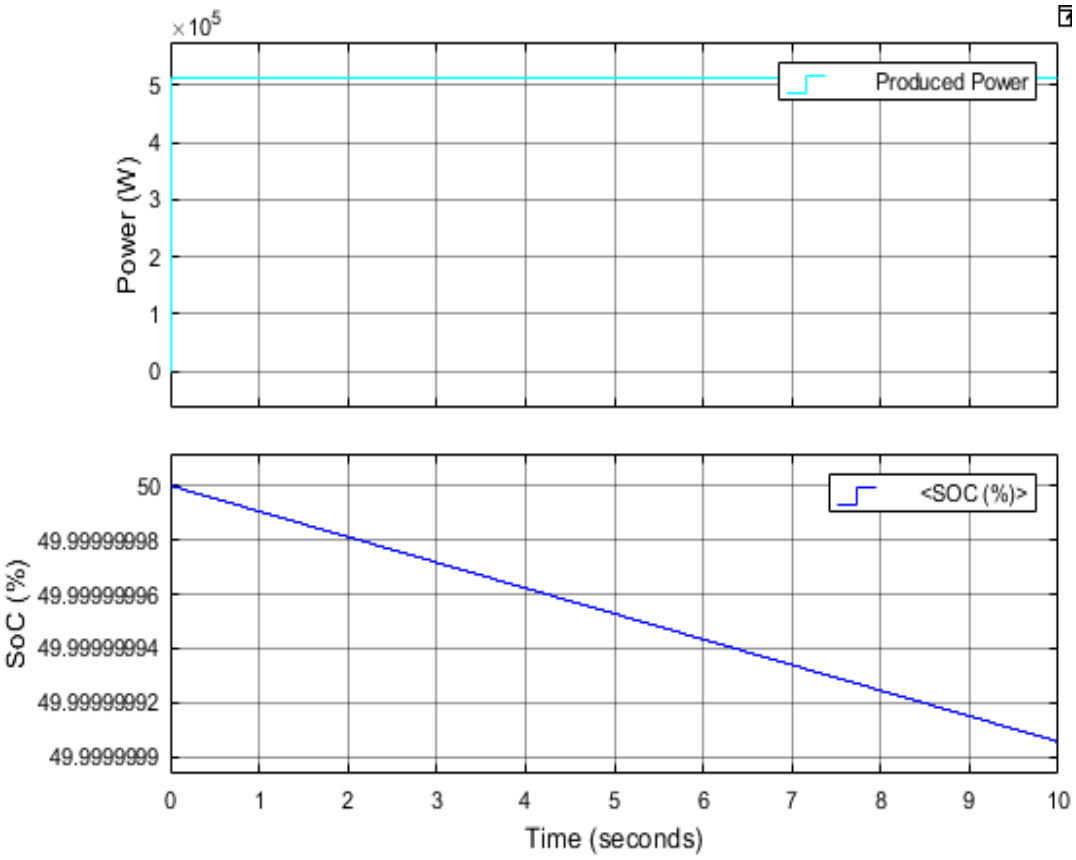

Figure 5.27: Power generation and battery SoC from the DC micro-grid

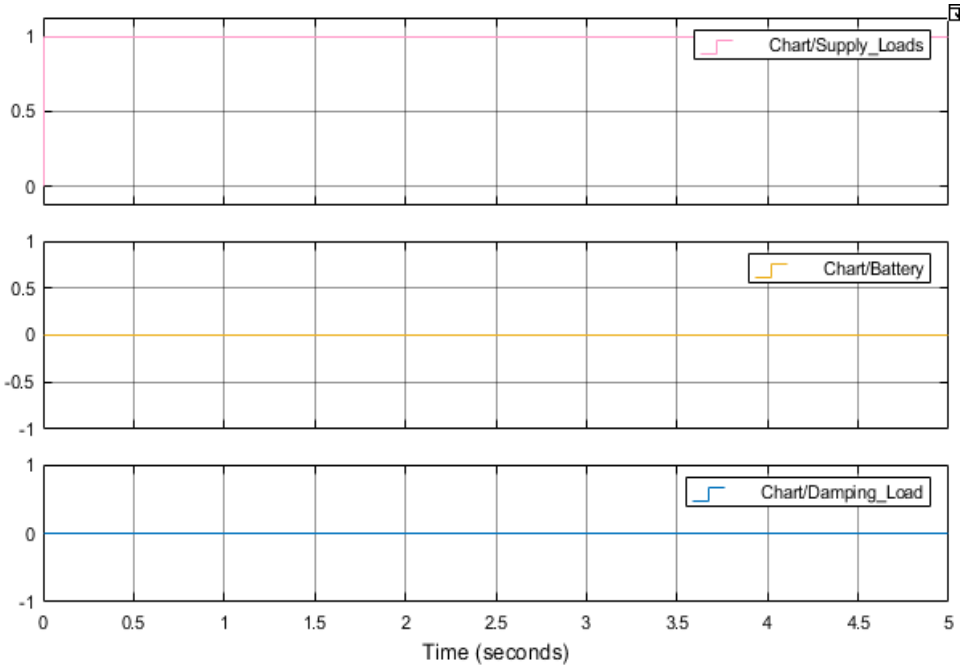

Figure 5.28: Output results from the energy management chart

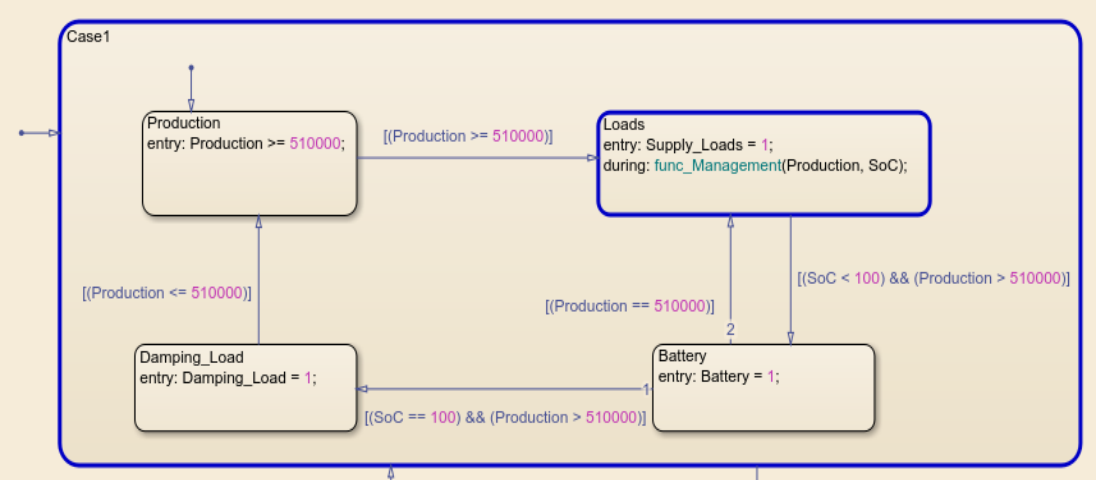

Figure 5.29: Transition State from the Stateflow Chart

Figure 5.27 illustrates the power generation from renewable generation and the percentage of the battery SoC. The power generation is approximately equal to the load demands so in Figure 5.28 the EMS displays 1 for the loads, 0 for the battery and the damp load to show that these two sources are not currently operational. And in Figure 5.29, it is shown that the flow chart transits from a state to another depending to the input and it can be seen, the flow chart displays the load dial in blue to show the operating mode, which explains that the condition is met.

Scenario 2: Here, the power generation exceeds the load demands. Thus, the EMS will check if the battery is fully charged or not as shown in Figure 5.30. If the SoC is less than 100%, the load demands will be provided by the power generation and at the same time, the battery is connected to be charged by the surplus of the power generation until it reaches its charge limit which is 100%. In this case, the SoC is assumed to be at 50%. When the battery reaches its maximum charge value (100%), it is isolated from the system to wait for the discharge phase. The surplus of the power generation will be transferred to the auxiliary load where it will dump until the power generation reaches the load demands or decreased.

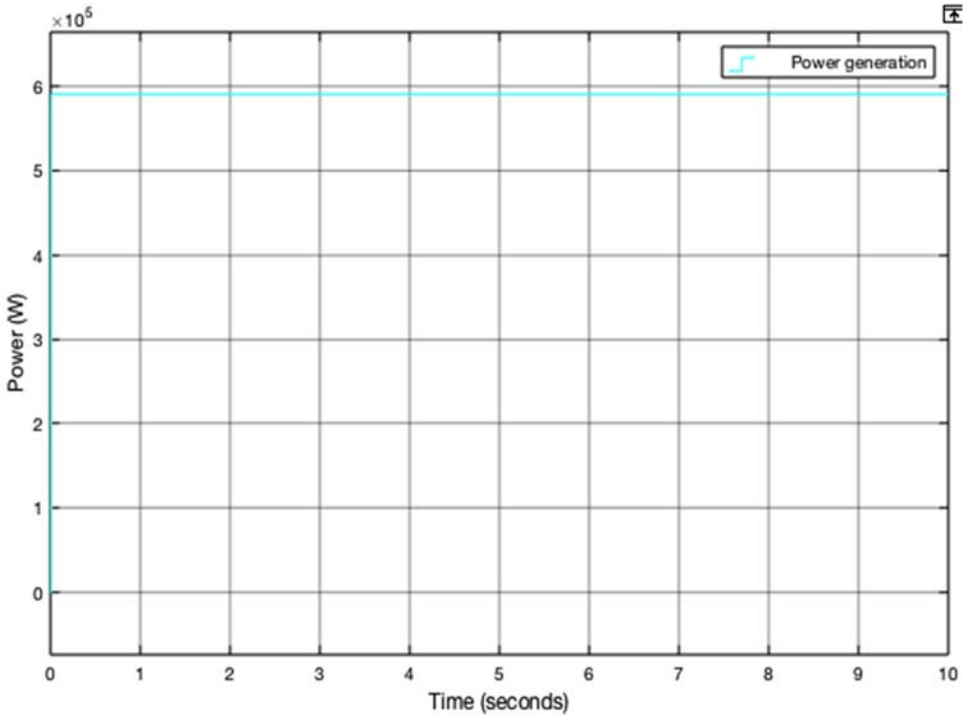

Figure 5.30a: Power generation from the DC micro-grid

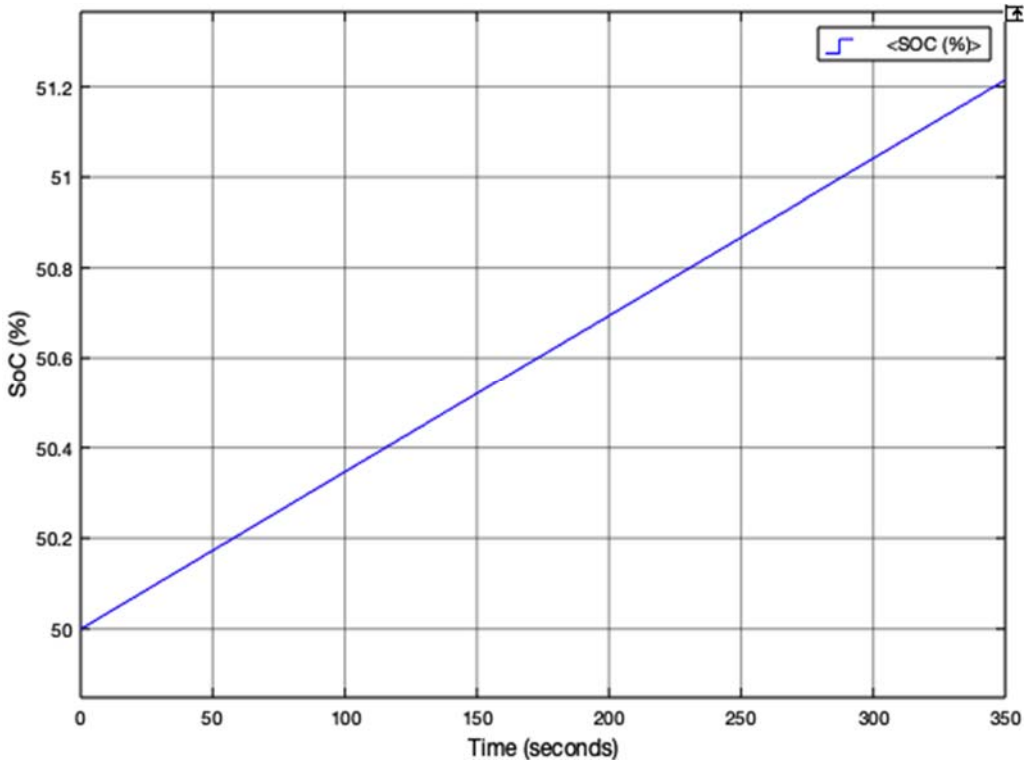

Figure 5.30b: Battery SoC from the DC micro-grid

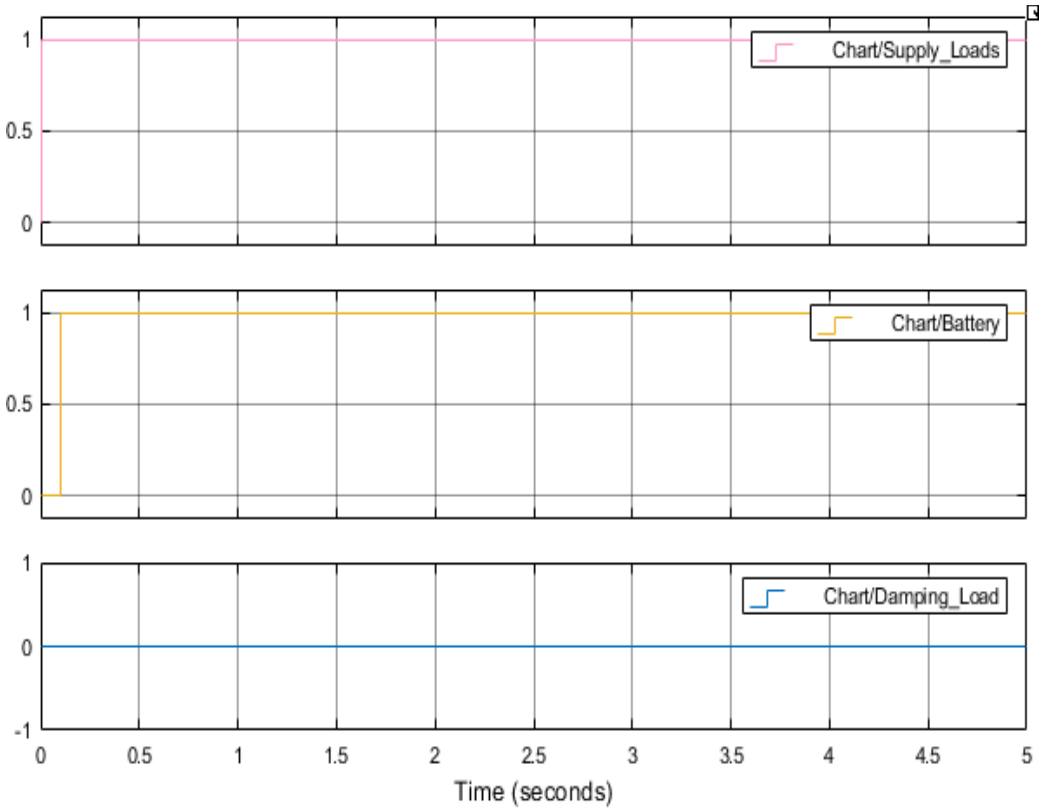

Figure 5.31: Output results from the energy management system chart showing that the battery is charging

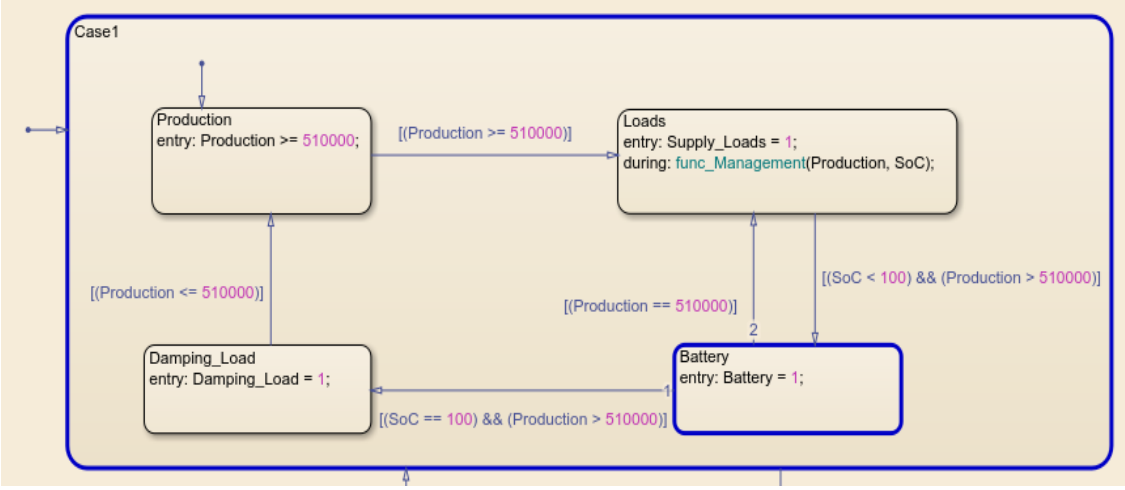

Figure 5.32: Transition state from the Stateflow chart

In Figure 5.31 the load and battery outputs are 1 while the damp load output is 0. This means that the loads are supplied and at the same time the battery is also charging. Thus, in Figure 5.32, the battery dial is displayed in blue to show its operating status. The two outputs cannot at the same time display in blue according to the design in Stateflow logical programming environment, hence it is the last output in operation which is displayed even if the others are running. But it will be noticed in the display as is the case in Figure 5.32.

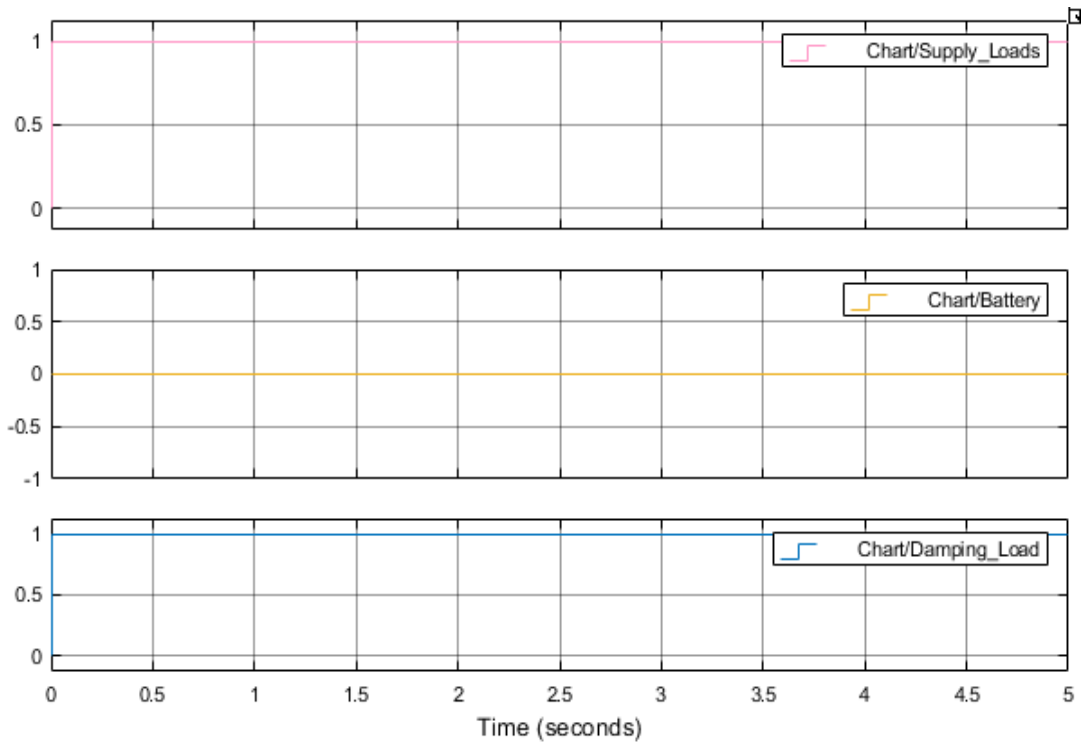

Figure 5.33: Output results from the energy management system chart showing that the auxiliary load is connected

Figure 5.33, shows that the load and auxiliary load outputs are at 1 while the battery output is 0. This means that the load is powered and the battery has reached its charge limit and it is isolated from the system. The auxiliary load is then connected and all the surplus of production from the renewable energy sources is supplied to the auxiliary load. Thus, the auxiliary load dial is displayed in blue to show its operating status. This confirms that the condition given from the EMS is met.

Scenario 3: The power generation is less than the load demands as illustrated in Figure 5.34. According to this scenario, the load will be supplied by the help of battery bank. Firstly, the SoC of the battery will be measured. If the SoC of the battery is higher than 20%, then the battery will be connected to the system where it will be discharged. The condition is that, when the SoC is less than 20%, automatically the battery bank must be disconnected to the system the avoid the deep discharge, which can damage the battery.

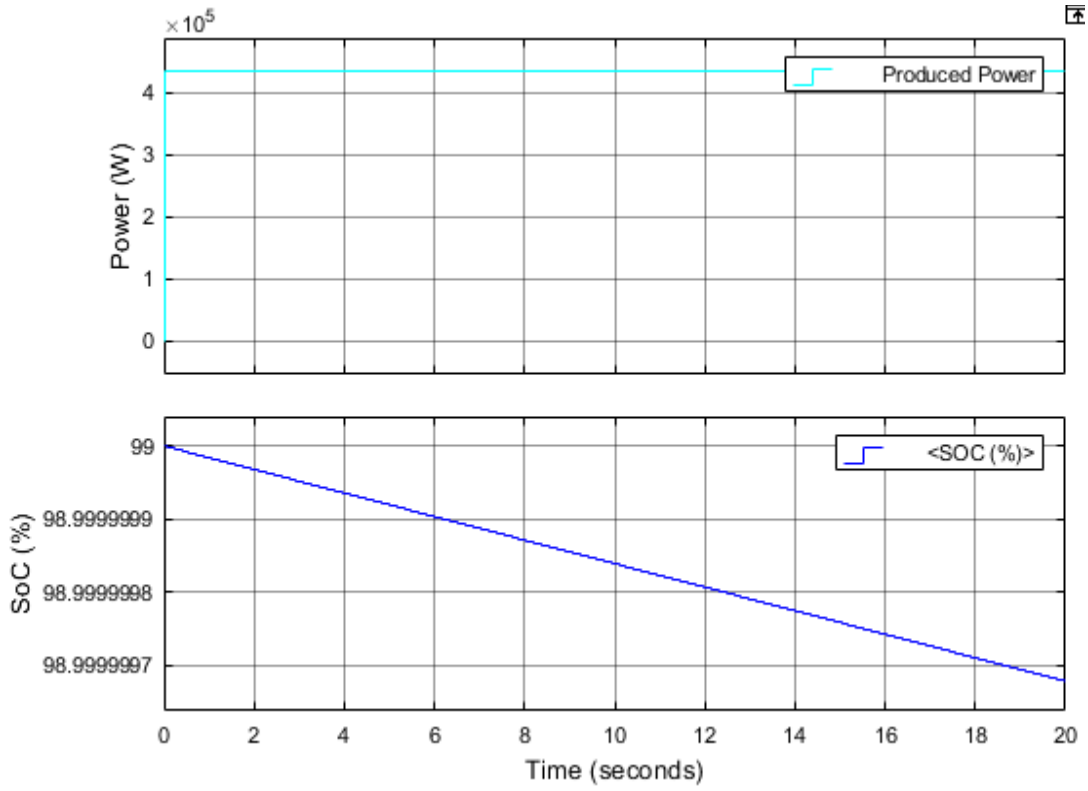

Figure 5.34: Power generation and battery SoC from the DC micro-grid

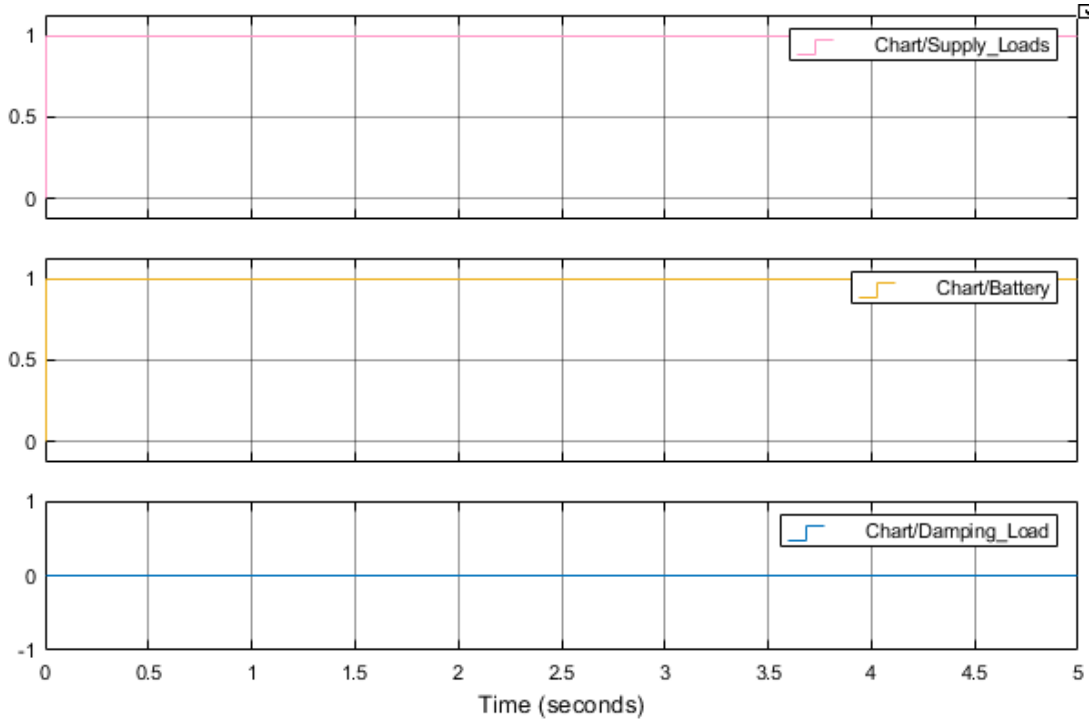

Figure 5.35: Output results from the energy management system chart showing that the battery is discharging

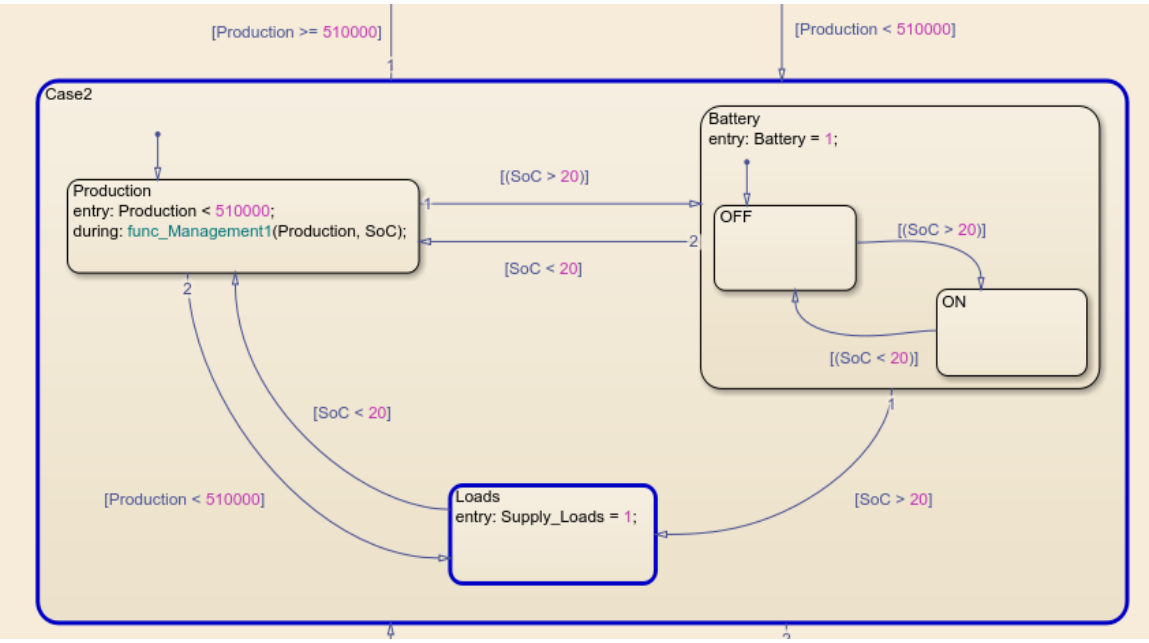

Figure 5.36: Transition state from the Stateflow chart

In Figure 5.35 above, the battery and the loads display 1 to indicate that the load demands is supplemented by the battery bank. Figure 5.36, presents the state of the battery in stateflow chart. It is remarkable that the battery is displayed in blue to show that it is operating. The battery bank is designed to first provide power to the entire load demands, but for an urgency case to supply the priority load within at least five hours. The battery bank is rated at 2400 Ah. If no generation power recharges the battery bank, then the battery should drain within more or less in five hours till it discharges. But in the case where the entire load demands is provided by the battery bank, thus, it should drain within more or less in two hours till it discharges, which means twice and half as fast than when the priority load is supplied.

Once the battery's SoC drops below 20% because dropping below this threshold can cause deep discharges, which can drastically reduce battery endurance or destroy it completely., the system disconnects the battery. The EMS allows the priority load, which is Industrial (Load1) or the combined loads (industrial and commercial loads (Load3)) to be supplied if the generated power is enough to provide power for these two load demands. Thus, the EMS will measure the power generation to check if the available power from the energy sources can handle the priority load demand (Load1) and at the same time the commercial load (Load3). If the condition meets, in this case the two loads will be supplied. If the EMS notices that the power generation can simultaneously supply both the priority and commercial load demands and charge the battery, if the condition is approved the excess of production will be stored in the battery bank. This is presented in Figure 5.37 and Figure 5.38. In Figure 5.37, it is shown that the two loads (Load1 and Load3) are supplied and the battery is charging.

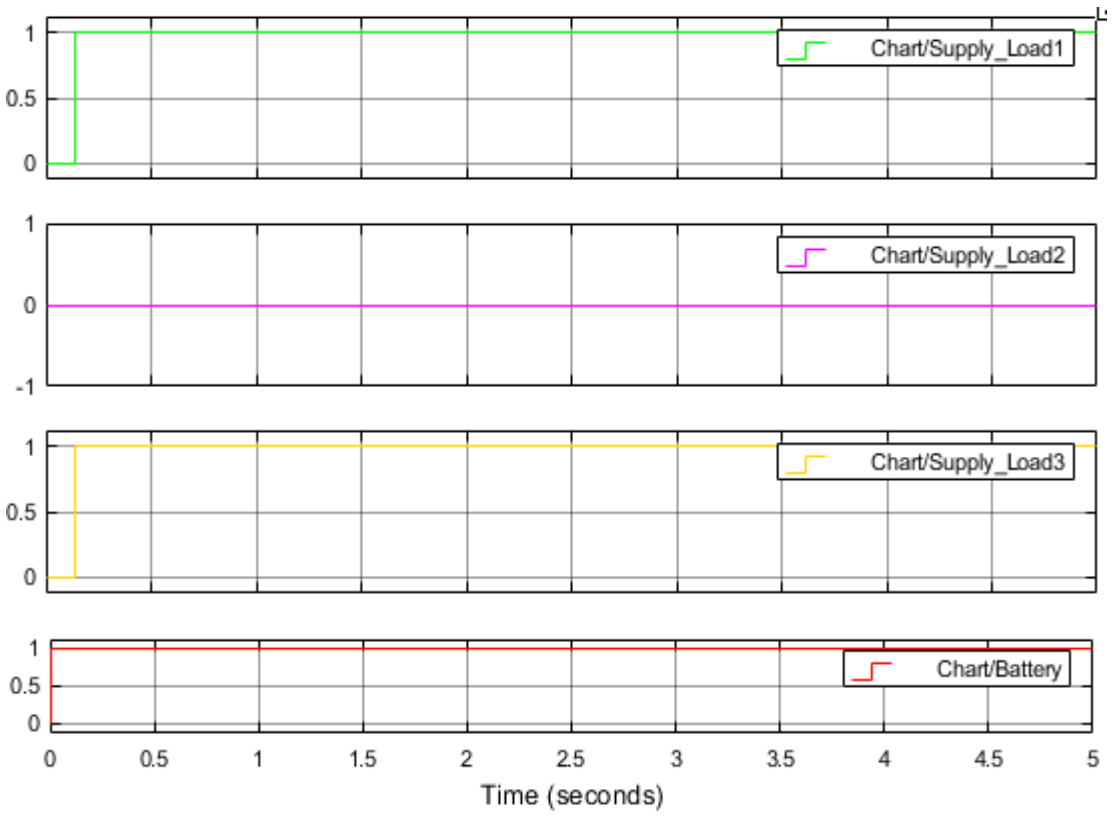

Figure 5.37: Output results from the energy management system chart

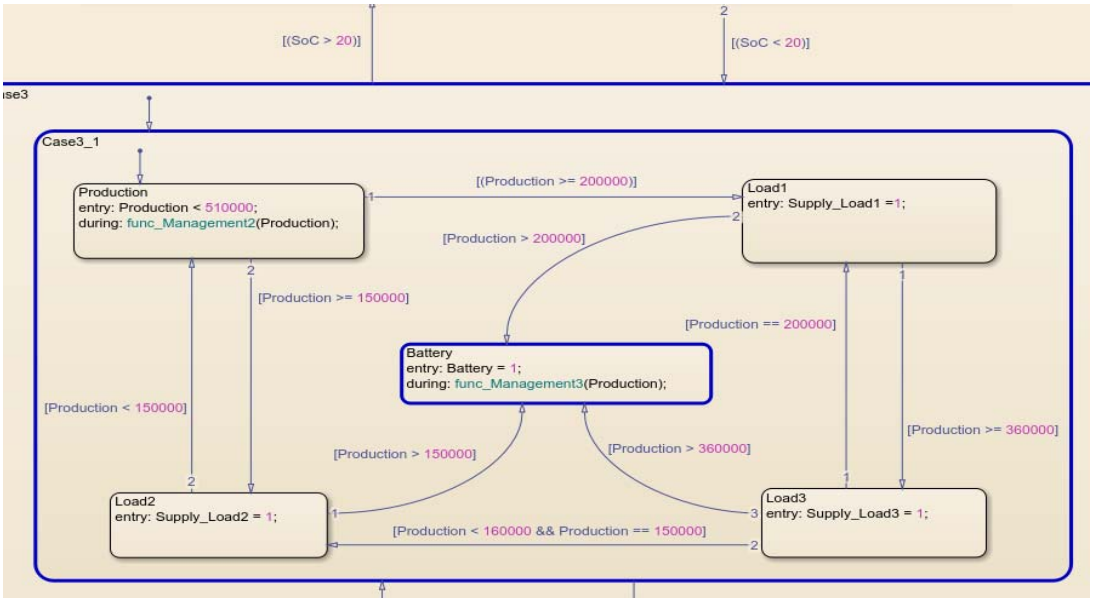

Figure 5.38: Transition state from the Stateflow chart

In the case where the power generation cannot supply the two load demands (priority and commercial loads), the EMS will check if the power generation can supply the priority load which is the Industrial load (Load1). If the condition is approved, then the priority load demand is supplied by the power generation. Before that, the EMS will measure the power generation to check if it will be able to provide power to priority load and charge the battery bank at the

same time, if the condition is approved, then the battery bank will also be connected to be charged. In this case, it is considered that the power generation can provide power to priority load and the excess of production is used to charge the battery as illustrated in Figure 5.39.

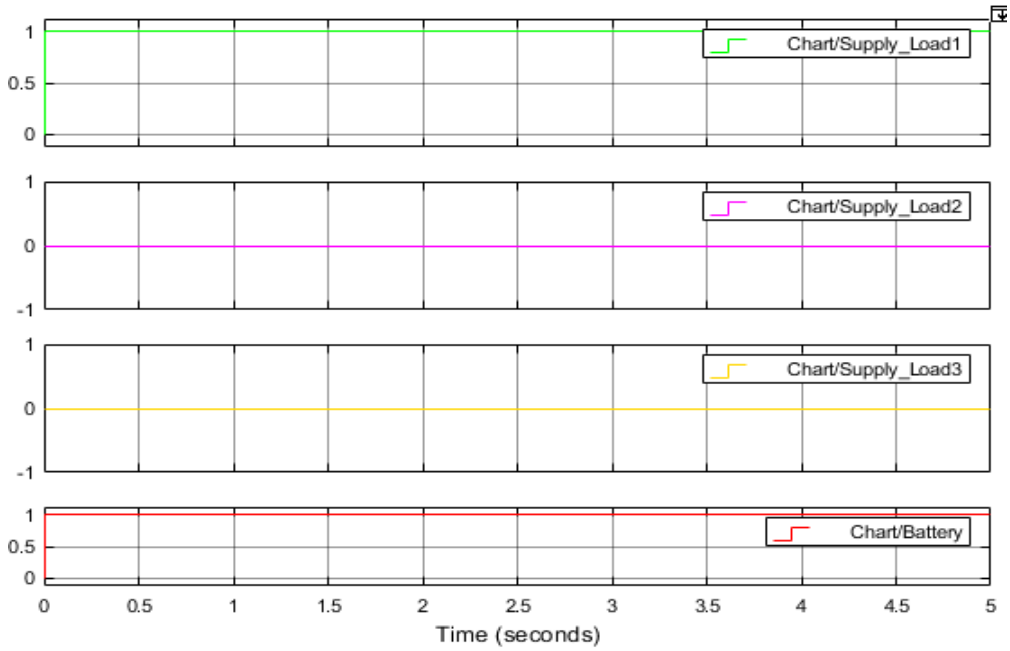

Figure 5.39: Output results from the energy management system chart

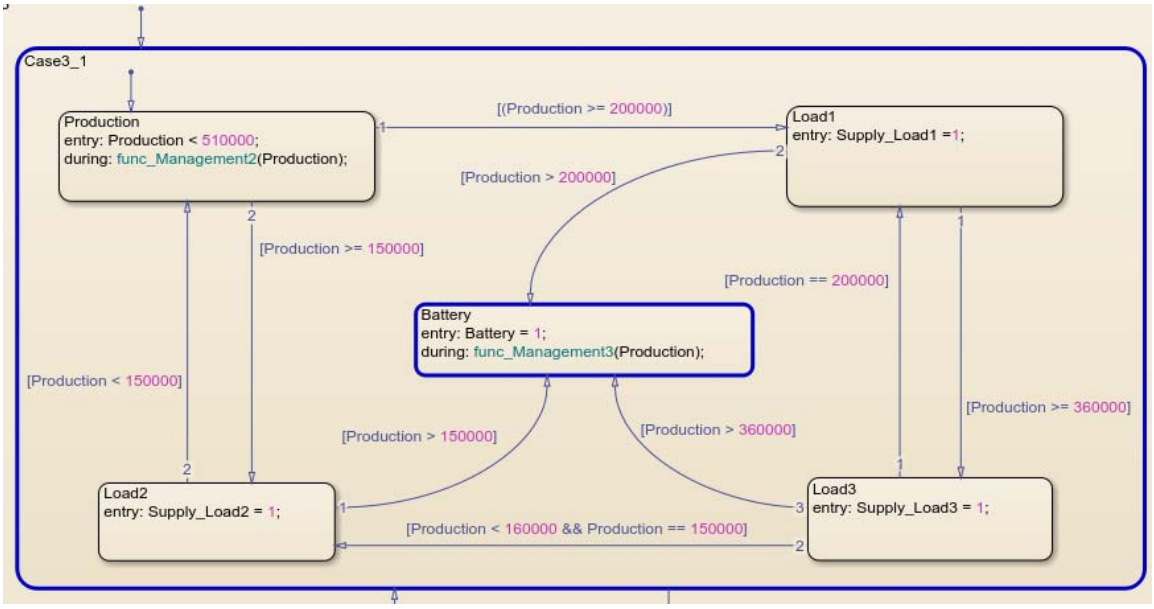

Figure 5.40: Transition state from the Stateflow chart showing that the Load1 and the battery are supplied

In Figure 5.40 shown above, it is considered that the available power from the renewable sources is enough to provide power to the priority load and charge the battery bank. The battery dial displays in blue to show that the battery is charging.

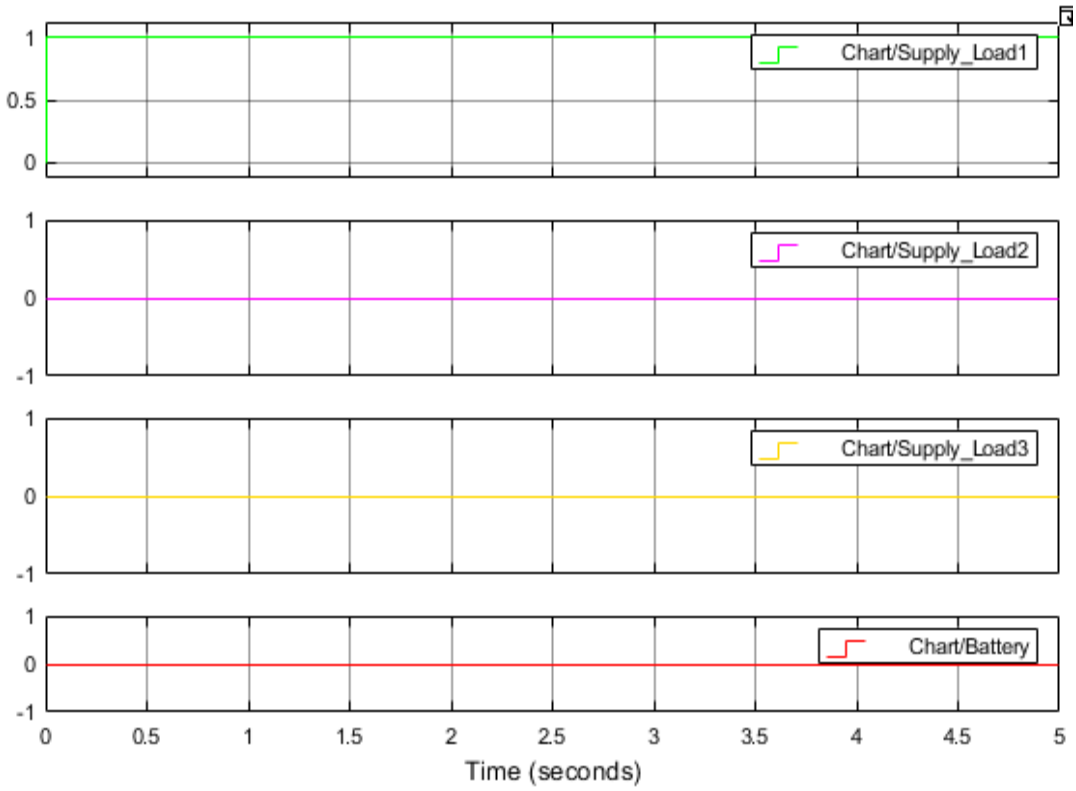

Figure 5.41: Output results from the energy management system chart

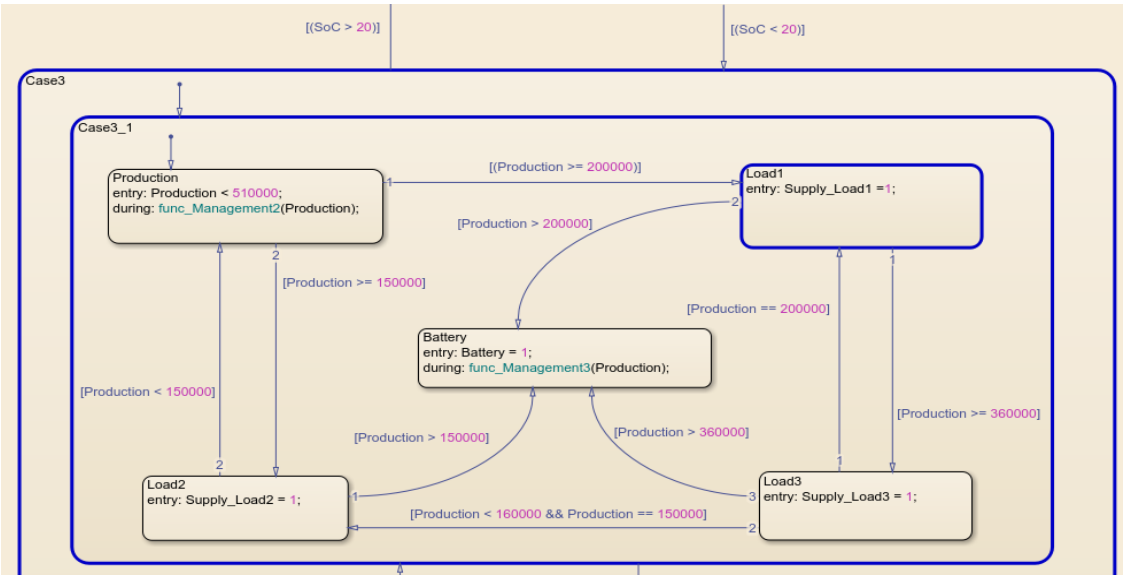

Figure 5.42: Transition state from the Stateflow chart showing that the Load1 is supplied

In the case of the Figure 5.42 shown above, it is considered that the power generation is only able to handle the priority load demand. The load1 dial is displayed in blue to show that the load1 is in the operating mode.

If the power generation is less than the priority load, it means that the production falls below 200 kW, then the EMS will check if the generated power is capable to supply power to

residential load (Load2) or supply power to both the residential load and battery bank. Two cases have been considered at this level, first when the residential load and the battery are supplied (see Figure 5.43 and Figure 5.44) and second when only the residential load is supplied (see Figure 5.45 and Figure 5.46).

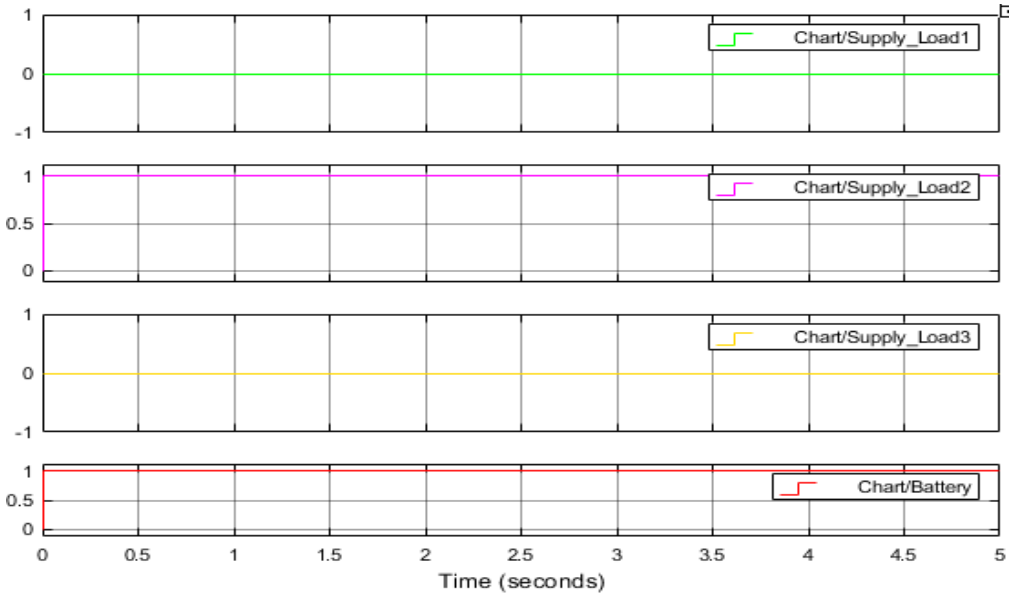

Figure 5.43: Output results from the energy management system chart

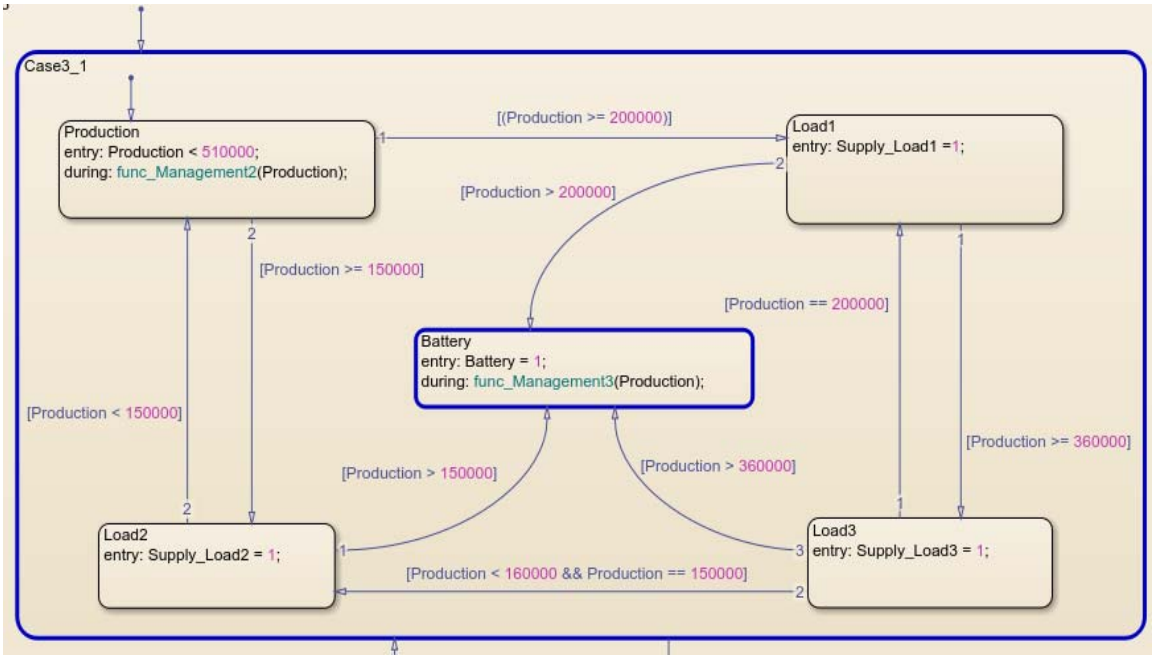

Figure 5.44: Transition state from the Stateflow chart showing that the Load2 and the battery are supplied

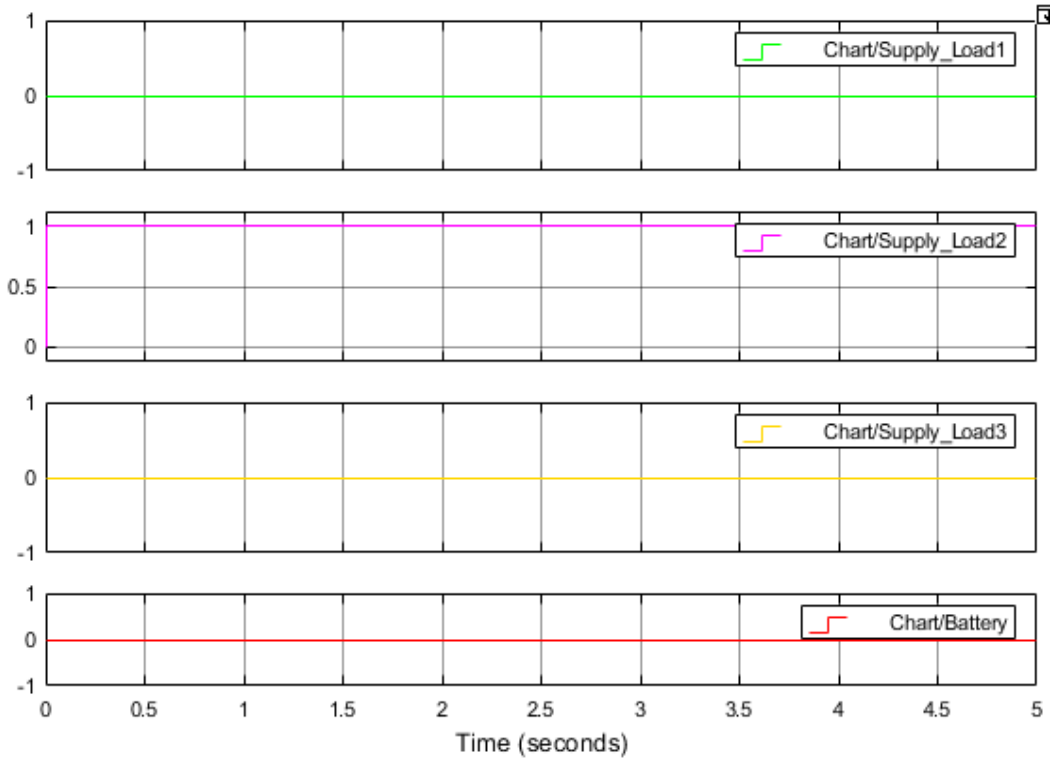

Figure 5.45: Output results from the energy management system chart

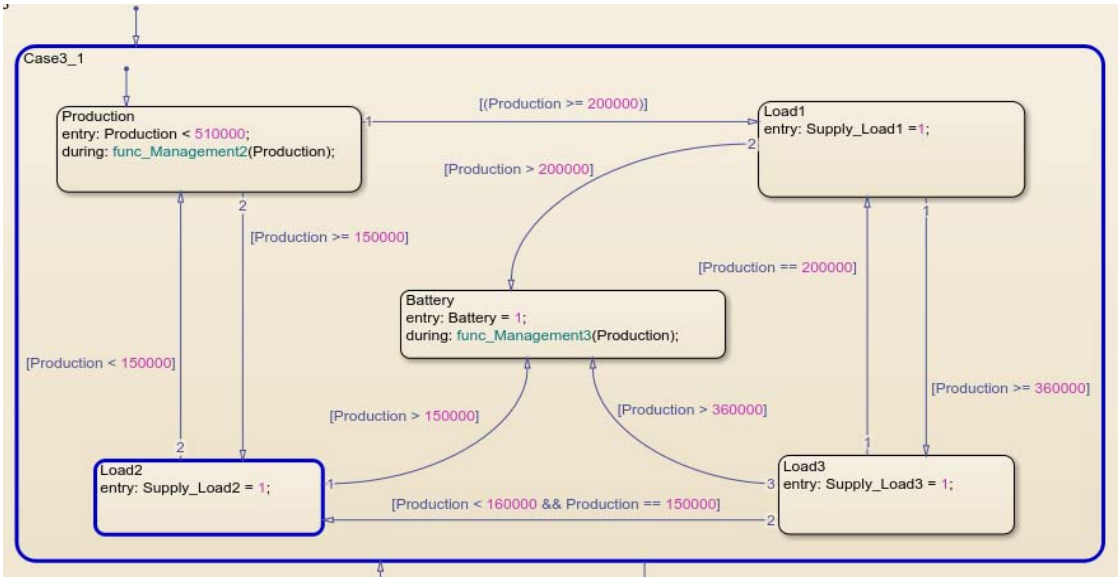

Figure 5.46: Transition state from the Stateflow chart showing that the Load2 is supplied

When the power generation falls below the residential load which is 150 kW, in this case the developed EMS algorithm will automatically disconnect all the loads (Shut-down the loads) momently and connect the battery to be charged as presented in Figure 5.47.

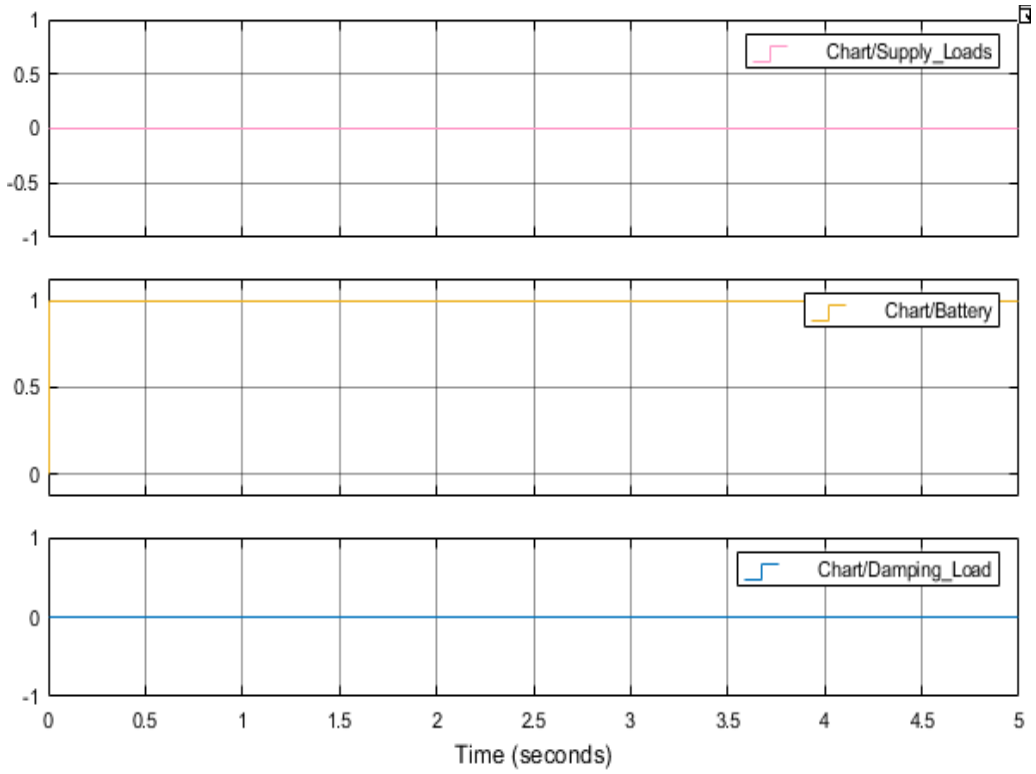

Figure 5.47: Output results from the energy management system chart

In Figure 5.48 below, it is shown that the battery dial is displayed in blue to show that only the battery are supplied by the power generation and the loads are isolated (shut-down). Based on the design specifications, the energy management system will continue to check the availability of the production from the renewable sources as well as the SoC of the battery storage until the power generation becomes active or the SoC reaches 20% as fixed in the design.

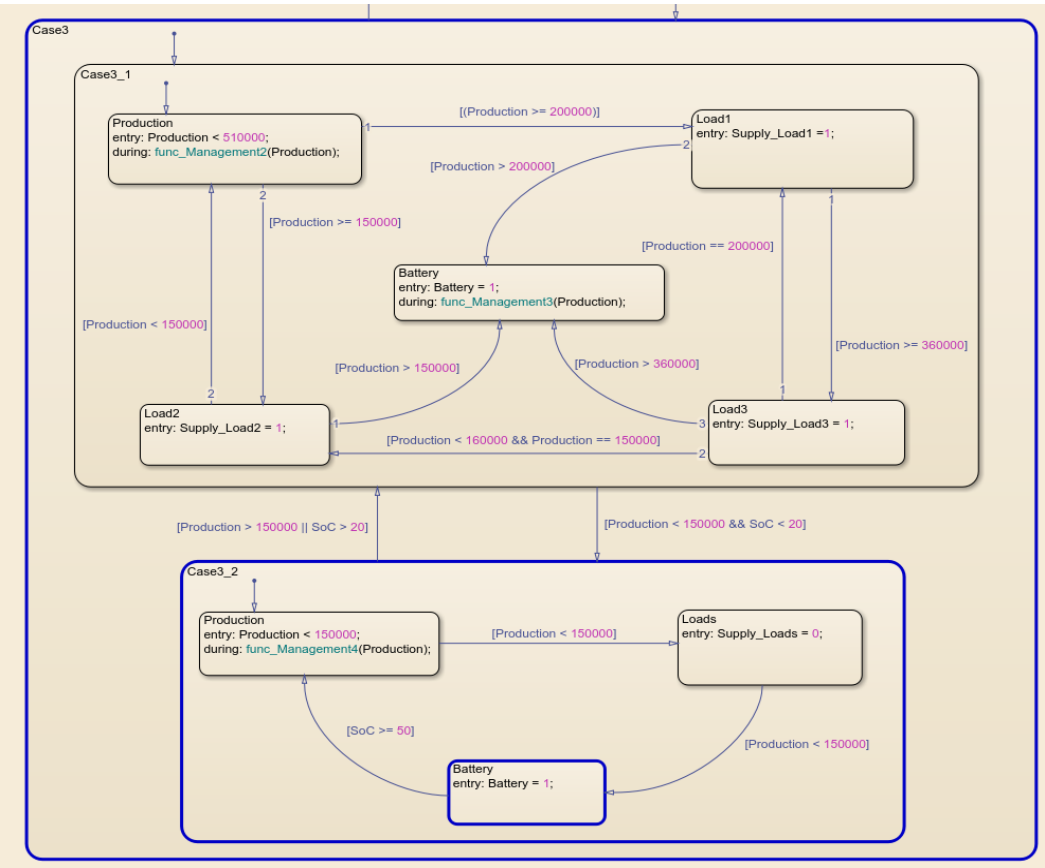

Figure 5.48: Transition state from the Stateflow chart showing that the load is shutdown

5.10. Conclusion

The simulation results of the developed DC micro-grid and energy management algorithm model were presented in this Chapter. The model was finally designed and developed to ensure the energy management of a battery bank in a DC micro-grid. The model was designed and developed using MATLAB/Simulink software and the presentation of the simulation results was realised into two ways. Firstly, the simulation model for the developed DC micro-grid, which includes PV system, Wind power, Biomass power, Battery and Load demands. Secondly, the simulation results of the developed DC micro-grid system and the energy management system algorithm. An effective management of the micro-grid and battery system is very essential to ensure a proper operation of the DC micro-grid, since this system depends on renewable energy, which is often variable sources. In this work, it was not only a question of focusing on the energy storage system; but also to ensure the energy management in all the system to finally maintain its proper operation and to avoid the damaging of the battery, which will often cause the problems of premature charge and rapid discharge of the battery bank. The following Table 5.4, presents the summary of the scenarios and the results, where P_G is the power generation, P_L is the load demands power, Ind_L is the industrial load, Res_L is the residential load and Com_L is the commercial load.

Table 5.4: Summary of Scenarios and Results

	Scenarios	Ind_L	Res_L	Cm_L	Battery	Analysis
1	$P_G = P_L$	1	1	1	0	In this first case, the load demands were 509 kW and the power generation was 510 kW. At this stage the loads were continuously supplied by the power generation without any interruption as shown in Figures 5.28 and 5.29 and the battery bank was in standby state. The SoC was settled at 50% in the simulation.
2	$P_G > P_L$	1	1	1	1	For this case, the produced power from the distributed generation was 590 kW and the load demands were 510 kW. The excess of the production (80 kW) was stored in the battery bank as illustrated in Figures 5.31 and 5.32.
3	$P_G < P_L$	1	1	1	1	In this case the demands exceeded the power generation and the battery bank was used to supplement the supply as presented in Figures 5.35 and 5.36.
4	So≤ 100%	1	1	1	1	During this stage, the battery was used to supply the entire loads until its SoC reached 50%.
5	So≤ 50%	1	0	0	1	When the SoC reached 50%, the commercial and residential loads were disconnected only the industrial load was supplied, which was the most consideration in the study.
6	SoC< 20%					In this case, the battery bank reached its limit of discharge, so it was disconnected. The demand was satisfied by the available power generated from energy sources based on the input power conditions from the EMS flow chart. When the available power generation from DG became low, the loads were shut down and the battery bank was charged from the available production until its SoC reaches 20% or the power generation becomes active. The results of these scenarios are shown from Figure 5.37 to Figure 5.48.
						In this scenario, the load demands exceeded the power generation, only the priority load and the commercial load were supplied, which needed

	P_G = 400 kW	1	0	1	1	350 kW to be supplied. The excess (50 kW) of the production was stored in the battery bank as illustrated in Figures 5.37 and 5.38.
	P_G = 200 kW	1	0	0	1	The power generation was less than the two loads priority loads and commercial load. The industrial load (priority) was supplied without any interruption by the available power generation and the excess of production (20 kW) was stored in the battery bank as it was shown in Figure 5.39 and 5.40.
	P_G = 180 kW	1	0	0	0	In this case, the power generation became equal to the priority load only, the battery bank was disconnected from the system and only the priority load was provided by the available power generation from the renewable sources as presented in Figure 5.41 and 5.42.
	P_G = 160 kW	0	1	0	1	The power generation was less than the priority load is this case and the SoC of the battery was still less than 20%. The residential load demand was 150 kW in this case. The residential load was supplied by the power generation and 10 kW of excess was stored in the battery bank as shown in Figure 5.43 and 5.44.
	P_G = 150 kW	0	1	0	0	The power generation became 150 kW, which was equal to the residential load. The battery bank was disconnected and the available power generation continuously supplied the residential load without interruption as presented in Figure 5.45 and 5.46.
	P_G=100 kW	0	0	0	1	In this scenario, no load was able to be supplied by the available power generation from the renewable energy sources. The loads were disconnected from the system momently and the available power generation charged the battery bank until its SoC reaches 20% or the power generation becomes active. The results of this scenario are shown in Figure 5.47 and 5.48.

According to the simulation results, the designed DC micro-grid model was perfectly found identical to the calculations and to the design. The method used to design and develop this energy management system algorithm was the State-flow logical programming environment in MATLAB/Simulink software. This method has helped to build the Flowchart diagram presented in Figure 4.7. Based on all these scenarios, the developed energy management system algorithm will ensure the reliability, the resiliency, the robustness and the proper operation of the battery systems in micro-grids. The principal advantage of this algorithm is that it will ensure the proper relation between the charge / discharge rate of battery energy storage systems on their operating conditions and keep its SoC in the admissible limits to avoid the deep charge / discharge of the battery bank, which in return will significantly impact on their lifespan and on the reliability in a DC micro-grid. Moreover, the developed software model is flexible to enable the users to access and to change any control parameter within the DC micro-grid.

Similarly, the operation costs of battery are also increased with significant battery degradation costs. Another important aspect that provide this algorithm is that the overall cost and degradation impact on battery will be lower. The SoC of this battery operation directly affects positively its achievable lifetime. Accordingly, the battery degradation costs increase due to premature charging and discharging cycles. Proper operation of battery results in reduced battery degradation and improve battery life. The results have shown that the initial investment cost is comparatively lower. The total cost minimisation objective over the battery system lifetime is expressed as follows:

$$Z = \sum_{n=1}^{N} (C_s + O_s + \emptyset)\omega^{(1-n)} \qquad (5-6)$$

Where, Z is the present value of the total lifecycle cost ($); ω = (1 / 1+r) is the discount factor and r is the discount rate; C_s is the capital cost ($); O_s is the annual operation and maintenance cost ($) over the lifetime of the equipment; $\emptyset$ is a cost component ($) and N is the number of years.

The detailed equation for the BESS levelized cost of energy (LCOE) ($ / kWh) is calculated as follows:

$$LCOE = \frac{Z}{\sum_{n\epsilon N}(\frac{Q_n}{(1+r)^n})} \qquad (5-7)$$

Where, Z is the total life-cost ($); Q_n (kWh) is the energy output in the year n; r is the discount rate.

Therefore, as the battery degradation decreases, LCOE value is expected to decrease. Based on this equation, the developed algorithm will decrease the economic analyse in terms of LCOE.

The developed system is considered for 20 years and the results were analysed on the basis of some assumptions and economic parameters. The LCOE of the developed system is:

$$LCOE = \frac{Z}{\sum_{n\epsilon N}(\frac{Q_n}{(1+r)^n})} = \frac{63.36}{576} = 0.11\ \$/kWh$$

Table 5.5 compares different results on Levelized cost of energy taken from previous studies, carried out by three different authors and the fourth case is for this study.

Table 5.5: Economic Parameters

Case	LCOE ($ / kWh)	Cycle ratio (%)	Lifetime (year)
1	0.35	0.09	8.26
2	0.19	0.05	15
3	0.15	0.03	18
4	0.11	0.02	20

Based on the analysis, the LCOE is 0.11 $/kWh, which is 20% lower than that of other similar studies. Extensive case studies and simulation results describes the energy and cost savings of the developed system operation, while significantly reducing CO_2 emissions and improving battery life.

CHAPTER 6: CONCLUSION AND RECOMMENDATIONS

6.1. Conclusion

A micro-grid can be defined as a reduced-size electrical network merged with renewable and non-renewable energy sources, also incorporating an energy storage system as well as local loads. They operate either independently or connected to the electrical utility grid. The use of energy storage systems is very necessary in renewable micro-grids as they can ensure the reliability of power supply. Battery energy storage systems are the types of energy storage widely used in renewable micro-grids. In case of battery bank, the deep discharge or the premature charge can lead to a reduced life of the storage system.

This research designed and developed an energy management of a battery energy storage system for DC micro-grid. The developed DC micro-grid model and energy management system algorithm was implemented using MATLAB/Simulink software, which used a physical modelling approach. The aim of this research was to develop a battery management system algorithm to control the charge and discharge of the battery and to keep its SoC in the admissible limits to avoid the deep charge / discharge of the battery in a DC micro-grid. Moreover, in a micro-grid, given that several power sources are connected, an energy management system needs to be implemented to ensure their proper operation. Thus, the objectives of this research were to design and develop a simulation model; to develop DC micro-grid component models to be used in the simulation model; to develop a simulation model of the DC micro-grid; to develop a control system schemes for the DC micro-grid; to develop an energy management system (EMS) algorithm for the DC micro-grid and to develop a battery management system (BMS) algorithm.

The developed DC micro-grid system was for a remote town. This developed DC micro-grid model considered different loads such as commercial, industrial and residential loads. The total load demands per day was assumed to be 507kW and the total power generation from the DG sources was 511 kW. To achieve the aim and objectives of the research, firstly a DC micro-grid model was designed and developed using MATLAB/Simulink software, secondly a control system schemes for the DC micro-grid was also developed using MATLAB/Simulink software and thirdly an algorithm for the battery management system and energy management system strategies were developed using Stateflow logical programming environment in MATLAB/Simulink software.

Finally, the simulation was conducted to show the interaction between different components of the system and to demonstrate the operation of the developed DC micro-grid and energy

management system algorithm. The different results of the scenarios of the developed energy management system algorithm have successfully shown that this developed algorithm will be able to ensure the reliability, the resiliency, the robustness and the proper operation of the battery systems in micro-grids. The main advantage of this developed algorithm is that it will ensure the proper relation between the charge / discharge rate of battery energy storage systems on their operating conditions and will allow to keep its SoC in the admissible limits (between 20% and 100%) according to the input power conditions from the EMS flow chart, to avoid the deep charge / discharge of the battery bank, which in return will significantly impact on their lifespan and on the reliability in a DC micro-grid. The results demonstrated that the battery is able to handle the load demands for different scenarios studied. Moreover, the developed software model presents another advantage, which enables the users to access and to change any control parameter within the DC micro-grid.

In addition, this developed algorithm provides a low overall cost, which is 20% lower than similar works and degradation impact on the battery. The SoC of the battery operation will directly affect positively its achievable lifetime and the battery degradation costs will significantly decrease. This algorithm offers a proper operation of the entire developed DC micro-grid system, which results in reduced battery degradation and improve battery life as well as the energy stored in the battery. The results have shown that the initial investment cost will comparatively be lower and will decrease the economic analyze in terms of LCOE.

6.2. Recommendations and Future Works

- In this research project, to ensure the proper operation of the developed DC micro-grid system and to ensure a proper use of battery system, an energy management system algorithm has been implemented using the State-flow logical programming method. Thereupon, other methods such as Fuzzy logic can also be used to compare the effectiveness of this method.

- A micro-grid can operate either independently or connected to the electrical utility grid. This research work, focused only on the operation of a DC micro-grid in autonomous mode. But, a connected micro-grid to the grid using the same method could be explored to verify the compatibility of the system.

6.3. Publication

The study outcome was produced in the following publication:

Ndeke and Adonis, 2020. “Energy Efficiency and Energy Management in South Africa –

Standards, Barriers and Policies". *AIUE Proceedings of the 18th Industrial and Commercial Use of Energy Conference 2020*, Cape Town, South Africa, 23 – 25 November 2020.

REFERENCES

Abdelhady, S., Abd-Elhady, M. S., & Fouad, M. M. (2017). An Understanding of the Operation of Silicon Photovoltaic Panels. *Energy Procedia*, *113*, 466–475. https://doi.org/10.1016/j.egypro.2017.04.041

Abdullah, Majid A., Yatim, A. H. M., & Tan, C. W. (2011). A study of maximum power point tracking algorithms for wind energy system. *2011 IEEE 1st Conference on Clean Energy and Technology, CET 2011*, 321–326. https://doi.org/10.1109/CET.2011.6041484

Abdullah, Md Abu, Muttaqi, K. M., Sutanto, D., & Agalgaonkar, A. P. (2015). An Effective Power Dispatch Control Strategy to Improve Generation Schedulability and Supply Reliability of a Wind Farm Using a Battery Energy Storage System. *IEEE Transactions on Sustainable Energy*, *6*(3), 1093–1102. https://doi.org/10.1109/TSTE.2014.2350980

Achkari, O., & Fadar, A. El. (2018). Renewable Energy Storage Technologies-A Review. *Conference Internationale En Automatique & Traitement de Signal*, *35*, 69–79.

Agrawal, M., & Mittal, A. (2011). Micro grid technological activities across the globe: A review. *Int. J. Res. Rev. Applied Sci*, *7*(May), 147–152. Retrieved from http://www.arpapress.com/Volumes/Vol7Issue2/IJRRAS_7_2_07.pdf

Akinyele, D., Belikov, J., & Levron, Y. (2017). Battery storage technologies for electrical applications: Impact in stand-alone photovoltaic systems. *Energies*, *10*(11), 1–39. https://doi.org/10.3390/en10111760

Ali, M. S., Kamarudin, S. K., Masdar, M. S., & Mohamed, A. (2014). An overview of power electronics applications in fuel cell systems: DC and AC converters. *Scientific World Journal*, *2014*. https://doi.org/10.1155/2014/103709

Amiryar, M. E., & Pullen, K. R. (2017). A review of flywheel energy storage system technologies and their applications. *Applied Sciences*, *7*(3). https://doi.org/10.3390/app7030286

Anderson, A., & Rezaie, B. (2019). Geothermal technology: Trends and potential role in a sustainable future. *Applied Energy*, *248*(April), 18–34. https://doi.org/10.1016/j.apenergy.2019.04.102

Arani, A. A. K., Karami, H., Gharehpetian, G. B., & Hejazi, M. S. A. (2017). Review of Flywheel Energy Storage Systems structures and applications in power systems and microgrids. *Renewable and Sustainable Energy Reviews*, *69*(November 2016), 9–18. https://doi.org/10.1016/j.rser.2016.11.166

Azzollini, I. A., Felice, V. Di, Fraboni, F., Cavallucci, L., Breschi, M., Rosa, A. D., & Zini, G. (2018). Lead-acid battery modeling over full state of charge and discharge range. *IEEE*

Transactions on Power Systems, *33*(6), 6422–6429. https://doi.org/10.1109/TPWRS.2018.2850049

Azzouzi, M., Popescu, D., & Bouchahdane, M. (2016). Modeling of Electrical Characteristics of Photovoltaic Cell Considering Single-Diode Model. *Journal of Clean Energy Technologies*, *4*(6), 414–420. https://doi.org/10.18178/jocet.2016.4.6.323

B. Subia, J. K. and S. C. K. *. (2010). *We are IntechOpen , the world ' s leading publisher of Open Access books Built by scientists , for scientists TOP 1 %*. *524*, 141–157.

Baharudin, N. H., Mansur, T. M. N. T., Hamid, F. A., Ali, R., & Misrun, M. I. (2018). Performance Analysis of DC-DC Buck Converter for Renewable Energy Application. *Journal of Physics: Conference Series*, *1019*(1). https://doi.org/10.1088/1742-6596/1019/1/012020

Bao, J., Bao, W., & Gong, J. (2012). Energy Procedia A PWM Multilevel Current-Source Inverter Used for Grid- Connected Wind Energy Conversion System. *ELSEVIER International Conference on Future Energy, Environment, and Materials*, *16*, 461–466. https://doi.org/10.1016/j.egypro.2012.01.075

Barambones, O., Cortajarena, J. A., Calvo, I., Durana, J. M. G. De, & Alkorta, P. (2019). Variable speed wind turbine control scheme using a robust wind torque estimation. *ELSEVIER Renewable Energy*, *133*, 354–366. https://doi.org/10.1016/j.renene.2018.10.009

Basar, M. F., Ahmad, A., Hasim, N., & Sopian, K. (2011). Introduction to the pico hydro power and the status of implementation in Malaysia. *Proceedings - 2011 IEEE Student Conference on Research and Development, SCOReD 2011*, 283–288. https://doi.org/10.1109/SCOReD.2011.6148751

Basics, T. (2011). *What is a fuel cell ? How do fuel cells work ?* (Dc), 1–6.

Bevrani, H., Daneshfar, F., & Daneshmand, R. P. (2010). *Intelligent Power System Frequency Regulations Concerning the Integration of Wind Power Units*. 407–437. https://doi.org/10.1007/978-3-642-13250-6_15

Bhayo, M. A., Aziz, M. J. A., Idris, N. R. N., & Yatim, A. H. M. (2017). Design and development of a wind turbine emulator for analyzing the performance of stand-alone wind energy conversion system. *International Journal of Power Electronics and Drive Systems*, *8*(1), 454–461. https://doi.org/10.11591/ijpeds.v8i1.pp454-461

Bidram, A., & Davoudi, A. (2012). Hierarchical structure of microgrids control system. *IEEE Transactions on Smart Grid*, *3*(4), 1963–1976. https://doi.org/10.1109/TSG.2012.2197425

Blaabjerg, F., Chen, Z., Teodorescu, R., & Iov, F. (2007). Power electronics in wind turbine systems. *Conference Proceedings - IPEMC 2006: CES/IEEE 5th International Power Electronics and Motion Control Conference*, *1*, 46–56. https://doi.org/10.1109/IPEMC.2006.297043

Blaabjerg, Frede, Liserre, M., & Ma, K. (2012). Power electronics converters for wind turbine systems. *IEEE Transactions on Industry Applications*, *48*(2), 708–719.

https://doi.org/10.1109/TIA.2011.2181290

Bolund, B., Bernhoff, H., & Leijon, M. (2007). Flywheel energy and power storage systems. *Renewable and Sustainable Energy Reviews*, *11*(2), 235–258. https://doi.org/10.1016/j.rser.2005.01.004

Bradbury, K. (2010). Energy Storage Technology Review. *A Brief Introduction to Batteries*, (September), 1–33.

Camacho, O. M. F., & Mihet-Popa, L. (2016). Tests de recharge rapide et intelligente de batteries pour voitures électriques utilisant des énergies renouvelables. *Oil and Gas Science and Technology*, *71*(1). https://doi.org/10.2516/ogst/2014001

Camblong, H., Sarr, J., Niang, A. T., Curea, O., Alzola, J. A., Sylla, E. H., & Santos, M. (2009). Micro-grids project, Part 1: Analysis of rural electrification with high content of renewable energy sources in Senegal. *Renewable Energy*, *34*(10), 2141–2150. https://doi.org/10.1016/j.renene.2009.01.015

Carpintero-Rentería, M., Santos-Martín, D., & Guerrero, J. M. (2019). Microgrids literature review through a layers structure. *Energies*, *12*(22), 1–22. https://doi.org/10.3390/en12224381

Casteleiro-Roca, J. L., Barragán, A. J., Segura, F., Calvo-Rolle, J. L., & Andújar, J. M. (2019). Fuel cell output current prediction with a hybrid intelligent system. *Complexity*, *2019*. https://doi.org/10.1155/2019/6317270

Chakraborty, S., & Simões, M. G. (2009). Experimental evaluation of active filtering in a single-phase high-frequency ac microgrid. *IEEE Transactions on Energy Conversion*, *24*(3), 673–682. https://doi.org/10.1109/TEC.2009.2015998

Chalamala, B. R., Soundappan, T., Fisher, G. R., Anstey, M. R., Viswanathan, V. V., & Perry, M. L. (2014). Redox flow batteries: An engineering perspective. *Proceedings of the IEEE*, *102*(6). https://doi.org/10.1109/JPROC.2014.2320317

Chandrasekaran, N., & Karthikeyan, A. (2019). Photovoltaic Pumping System Fed by DC-DC Push Pull Converter. *International Journal of Recent Technology and Engineering*, *8*(4), 1030–1034. https://doi.org/10.35940/ijrte.c6282.118419

Chen, F., Burgos, R., & Boroyevich, D. (2016). Output impedance comparison of different droop control realizations in DC systems. *2016 IEEE 17th Workshop on Control and Modeling for Power Electronics, COMPEL 2016*, 1–6. https://doi.org/10.1109/COMPEL.2016.7556761

Chen, H., Cong, T. N., Yang, W., Tan, C., Li, Y., & Ding, Y. (2009). Progress in electrical energy storage system: A critical review. *Progress in Natural Science*, *19*(3), 291–312. https://doi.org/10.1016/j.pnsc.2008.07.014

Chowdhury, S., Chowdhury, S. P., & Crossley, P. (2009). Microgrids and active distribution networks. In *Microgrids and Active Distribution Networks*. https://doi.org/10.1049/pbrn006e

Co., Minani-ku,. (1983). *4*(2), 70–74.

Cocco, D., Tola, V., & Petrollese, M. (2016). Application of Concentrating Solar Technologies in the Dairy Sector for the Combined Production of Heat and Power. *Energy Procedia*, *101*(December), 1159–1166. https://doi.org/10.1016/j.egypro.2016.11.157

Darrow, K., Tidball, R., Wang, J., & Hampson, A. (2015). Catalog of CHP Technologies: Section 5. Technology Characterization – Microturbines. *U.S. Environmental Protection Agency Combined Head and Power Partnership*, (March), 5.

Das, G., De, M., & Mandal, K. K. (2018). Design of Flyback Converter by Using an Ideal Switch and a MOSFET Switch. *Proceedings of International Conference on 2018 IEEE Electron Device Kolkata Conference, EDKCON 2018*, 110–114. https://doi.org/10.1109/EDKCON.2018.8770407

Das, M., & Das, N. (2009). BIOMASS: A sustainable source of energy. *Asia-Pacific Power and Energy Engineering Conference, APPEEC*, 1–4. https://doi.org/10.1109/APPEEC.2009.4918203

De Sousa, J. M., Bastos, G. H. A., Torrico-Bascope, R. P., & Cruz, C. M. T. (2015). High voltage gain Buck-Boost DC-DC converter based on Three-State Switching Cell. *2015 IEEE 13th Brazilian Power Electronics Conference and 1st Southern Power Electronics Conference, COBEP/SPEC 2016*. https://doi.org/10.1109/COBEP.2015.7420188

Developments, N. E. W., Batteries, I. N., & Secondary, A. S. (2018). *PROFESSOR ABUBAKAR SANI SAMBO ANNUAL LECTURE*. (2), 1–27.

Dragicevic, T., Guerrero, J. M., Vasquez, J. C., & Skrlec, D. (2014). Supervisory control of an adaptive-droop regulated DC microgrid with battery management capability. *IEEE Transactions on Power Electronics*, *29*(2), 695–706. https://doi.org/10.1109/TPEL.2013.2257857

Drewry, M. A., & Georgiou, G. A. (2007). A review of NDT techniques for wind turbines. *Insight: Non-Destructive Testing and Condition Monitoring*, *49*(3), 137–141. https://doi.org/10.1784/insi.2007.49.3.137

Du Plooy, H. (2016). *Comparative Strategies for Efficient Control and Storage of Renewable Energy in a Microgrid*. (September), 135.

Edenhofer, O., Pichs-Madruga, R., Sokona, Y., Seyboth, K., Eickemeier, P., Matschoss, P., … Stechow, C. Von. (2011). IPCC, 2011: Summary for Policymakers. In: IPCC Special Report on Renewable Energy Sources and Climate Change Mitigation. In *Cambridge University Press*. https://doi.org/10.5860/CHOICE.49-6309

electricaltechnology.org. (2017). *How to Make a Simple Solar Cell? Working of Photovoltaic Cells* (pp. 1–10). pp. 1–10. Retrieved from http://www.electricaltechnology.org/2015/06/how-to-make-a-solar-cell-photovoltaic-cell.html

Faisal, M., Hannan, M. A., Ker, P. J., Hussain, A., Mansor, M. Bin, & Blaabjerg, F. (2018). Review of energy storage system technologies in microgrid applications: Issues and challenges. *IEEE Access*, *6*, 35143–35164. https://doi.org/10.1109/ACCESS.2018.2841407

Feng, W., Jin, M., Liu, X., Bao, Y., Marnay, C., Yao, C., & Yu, J. (2018). A review of microgrid development in the United States – A decade of progress on policies, demonstrations, controls, and software tools. *Applied Energy*, *228*(July), 1656–1668. https://doi.org/10.1016/j.apenergy.2018.06.096

Generator, W. T., & Generator, W. T. (2020). *2018 Wind Turbine Generator Market by detail market analysis , huge demand , new opportunities , recent trends by - ABB , Gamesa , GE Renewable Energy , SANY , Suzlon , AVANTIS Energy , Bora Energy Press release from : Garner Insights*.

Ghanbari, M., & Hosseini, S. M. (2008). DC/DC boost converter design and development based on asynchronously paralleled switches. *Proceedings of the IEEE International Conference on Industrial Technology*. https://doi.org/10.1109/ICIT.2008.4608713

Ghosh, S., Satpathy, S., Das, S., Debbarma, S., & Bhattacharyya, B. K. (2018). Different controlling method of closed loop DC-DC buck converter: A review. *Proceedings of the International Conference on Smart Systems and Inventive Technology, ICSSIT 2018*, (July), 29–33. https://doi.org/10.1109/ICSSIT.2018.8748695

Guerrero, J. M., Chandorkar, M., Lee, T. L., & Loh, P. C. (2013). Advanced control architectures for intelligent microgridspart i: Decentralized and hierarchical control. *IEEE Transactions on Industrial Electronics*, *60*(4), 1254–1262. https://doi.org/10.1109/TIE.2012.2194969

Gunasekaran, M., Ismail, H. M., Chokkalingam, B., Mihet-Popa, L., & Padmanaban, S. (2018). Energy management strategy for rural communities' DC micro grid power system structure with maximum penetration of renewable energy sources. *Applied Sciences (Switzerland)*, *8*(4), 1–24. https://doi.org/10.3390/app8040585

Han, B., Kim, M., Lee, S., & Lee, J. S. (2015). Dynamic modeling and integral sliding mode controller design for Cuk converter under load variation. *9th International Conference on Power Electronics - ECCE Asia: "Green World with Power Electronics", ICPE 2015-ECCE Asia*, (July 2016), 449–455. https://doi.org/10.1109/ICPE.2015.7167824

Han, X., Li, X., White, J., Zhong, C., Deng, Y., Hu, W., & Ma, T. (2018). Metal–Air Batteries: From Static to Flow System. *Advanced Energy Materials*, *8*(27), 1–28. https://doi.org/10.1002/aenm.201801396

Hiksas, M. M., & Aninditio, M. L. (2017). Redox Flow Batteries for small scale energy storage. *2016 IEEE Conference on Technologies for Sustainability, SusTech 2016*, 134–139. https://doi.org/10.1109/SusTech.2016.7897155

Hirsch, A., Parag, Y., & Guerrero, J. (2018). Microgrids: A review of technologies, key drivers, and outstanding issues. *Renewable and Sustainable Energy Reviews*, *90*(September 2017), 402–411. https://doi.org/10.1016/j.rser.2018.03.040

Hong, P., Li, J., Xu, L., Ouyang, M., & Fang, C. (2016). Modeling and simulation of parallel DC/DC converters for online AC impedance estimation of PEM fuel cell stack. *International*

Journal of Hydrogen Energy, *41*(4), 3004–3014. https://doi.org/10.1016/j.ijhydene.2015.11.129

Hossain, E., Hossain, J., Sakib, N., & Bayindir, R. (2017). Modelling and simulation of permanent magnet synchronous generator wind turbine: A step to microgrid technology. *International Journal of Renewable Energy Research*, *7*(1), 1–8. https://doi.org/10.1234/ijrer.v7i1.5615.g7013

Hvljq, R., Ssolfdwlrqv, I. R. U., Eul, D. G. D. O., & Rxvhi, D. (2017). *'& '& %Rrvw &Rqyhuwhu &Rqwuroohu 'Hvljq Iru 39 $Ssolfdwlrqv*. 5–10.

I., B. (2013). ORC-Based Geothermal Power Generation and CO2-Based EGS for Combined Green Power Generation and CO2 Sequestration. *New Developments in Renewable Energy*. https://doi.org/10.5772/52063

Ibrahim, H., Ilinca, A., & Perron, J. (2008). Energy storage systems-Characteristics and comparisons. *Renewable and Sustainable Energy Reviews*, *12*(5), 1221–1250. https://doi.org/10.1016/j.rser.2007.01.023

Ilman, S. M., Dahono, A., Prihambodo, M. A. K., Putra, B. A. Y., Rizqiawan, A., & Dahono, P. A. (2019). Analysis and Control of Modified DC-DC Cuk Converter. *Proceedings of the 2nd International Conference on High Voltage Engineering and Power Systems: Towards Sustainable and Reliable Power Delivery, ICHVEPS 2019*, 2–7. https://doi.org/10.1109/ICHVEPS47643.2019.9011054

IRENA WORKING PAPER. (2012). Renewable Energy Techlogies: Cost Analysis Series, Hydropower. *International Renewable Energy Agency*, *1*(3/5), 44. Retrieved from http://www.irena.org/documentdownloads/publications/re_technologies_cost_analysis-hydropower.pdf

ISE, P. R. I. F. O. R. S. E. S. (2012). *Photovoltaics Report*. (November).

Islam, M. A., Hasanuzzaman, M., Rahim, N. A., Nahar, A., & Hosenuzzaman, M. (2014). Global renewable energy-based electricity generation and smart grid system for energy security. *Scientific World Journal*, *2014*(November). https://doi.org/10.1155/2014/197136

Islam, M. R., Guo, Y., & Zhu, J. (2013). Power converters for wind turbines: Current and future development. *Materials and Processes for Energy: Communicating Current Research and Technological Developments*, 559–571.

Jadav, K. A., Karkar, H. M., & Trivedi, I. N. (2017). A Review of Microgrid Architectures and Control Strategy. *Journal of The Institution of Engineers (India): Series B*, *98*(6), 591–598. https://doi.org/10.1007/s40031-017-0287-3

Jayaswal, K., & Palwalia, D. K. (2018). Performance Analysis of Non-Isolated DC-DC Buck Converter Using Resonant Approach. *Engineering, Technology & Applied Science Research*, *8*(5), 3350–3354. https://doi.org/10.48084/etasr.2242

Jones, G. W., & Chowdhury, B. H. (2008). Distribution system operation and planning in the

presence of distributed generation technology. *Transmission and Distribution Exposition Conference: 2008 IEEE PES Powering Toward the Future, PIMS 2008*, (June). https://doi.org/10.1109/TDC.2008.4517274

Justo, J. J., Mwasilu, F., Lee, J., & Jung, J. W. (2013). AC-microgrids versus DC-microgrids with distributed energy resources: A review. *Renewable and Sustainable Energy Reviews*, *24*, 387–405. https://doi.org/10.1016/j.rser.2013.03.067

Karfopoulos, E. L., Panourgias, K. A., & Hatziargyriou, N. D. (2016). Distributed Coordination of Electric Vehicles providing V2G Regulation Services. *IEEE Transactions on Power Systems*, *31*(4), 2834–2846. https://doi.org/10.1109/TPWRS.2015.2472957

Karshenas, H., & Daneshpajooh, H. (2011). Bidirectional DC-DC Converters for Energy Storage Systems. *Energy Storage in the Emerging ERA of Smart Grids*, 162–178. https://doi.org/10.5772/737

Kawasaki Heavy Industries. (2016). Battery Energy Storage System -GIGACELL-. *Kawasaki.Com*, (Cict), Characteristics, FAQs. Retrieved from http://global.kawasaki.com/en/energy/solutions/battery_energy/

Kinhekar, N., Padhy, N. P., Li, F., & Gupta, H. O. (2016). Utility Oriented Demand Side Management Using Smart AC and Micro DC Grid Cooperative. *IEEE Transactions on Power Systems*, *31*(2), 1151–1160. https://doi.org/10.1109/TPWRS.2015.2409894

Kishore, P. M., & Ravikumar, B. (2016). Refined Hybrid Microgrid Architecture for the Improvement of Voltage Profile. *Energy Procedia*, *90*(December 2015), 645–654. https://doi.org/10.1016/j.egypro.2016.11.233

Knopper, L. D., & Ollson, C. A. (2011). Health effects and wind turbines: A review of the literature. *Environmental Health: A Global Access Science Source*, *10*(1), 1–10. https://doi.org/10.1186/1476-069X-10-78

Krishnamurthy, S., Jahns, T. M., & Lasseter, R. H. (2008). The operation of diesel gensets in a CERTS microgrid. *IEEE Power and Energy Society 2008 General Meeting: Conversion and Delivery of Electrical Energy in the 21st Century, PES*, 1–8. https://doi.org/10.1109/PES.2008.4596500

Kuenzer, C., Campbell, I., Roch, M., Leinenkugel, P., Tuan, V. Q., & Dech, S. (2013). Understanding the impact of hydropower developments in the context of upstream-downstream relations in the Mekong river basin. *Sustainability Science*, *8*(4), 565–584. https://doi.org/10.1007/s11625-012-0195-z

Lago, J., & Heldwein, M. L. (2011). Operation and control-oriented modeling of a power converter for current balancing and stability improvement of DC active distribution networks. *IEEE Transactions on Power Electronics*, *26*(3), 877–885. https://doi.org/10.1109/TPEL.2011.2105284

Lalor, G., Mullane, A., & O'Malley, M. (2005). Frequency control and wind turbine technologies. *IEEE Transactions on Power Systems*, *20*(4), 1905–1913.

https://doi.org/10.1109/TPWRS.2005.857393

Lansburg, S., & Mcdowall, J. (2006). *A Solution for Niche Telecom Power Applications*.

Lasseter, R. H., & Paigi, P. (2004). Microgrid: A conceptual solution. *PESC Record - IEEE Annual Power Electronics Specialists Conference*, *6*, 4285–4290. https://doi.org/10.1109/PESC.2004.1354758

Lead-Acid Battery Technologies. (2015). In *Lead-Acid Battery Technologies*. Retrieved from https://www.taylorfrancis.com/books/9781466592230

Lotfi, H., & Khodaei, A. (2017). AC versus DC microgrid planning. *IEEE Transactions on Smart Grid*, *8*(1), 296–304. https://doi.org/10.1109/TSG.2015.2457910

Lu, X., Sun, K., Guerrero, J. M., Vasquez, J. C., Huang, L., & Teodorescu, R. (2012). SoC-based droop method for distributed energy storage in DC microgrid applications. *IEEE International Symposium on Industrial Electronics*, 1640–1645. https://doi.org/10.1109/ISIE.2012.6237336

Lumbreras, C., Guerrero, J. M., Garcia, P., Briz, F., & Reigosa, D. D. (2016). Control of a Small Wind Turbine in the High Wind Speed Region. *IEEE Transactions on Power Electronics*, *31*(10), 6980–6991. https://doi.org/10.1109/TPEL.2015.2508674

Luo, X., Wang, J., Dooner, M., & Clarke, J. (201AD). Original citation : The version presented in WRAP is the published version , or , version of record , and may technologies and the application potential in power system operation q. *Applied Energy*, *137*, 511–536.

Maghami, M. R., Hizam, H., Gomes, C., Radzi, M. A., Rezadad, M. I., & Hajighorbani, S. (2016). Power loss due to soiling on solar panel: A review. *Renewable and Sustainable Energy Reviews*, *59*, 1307–1316. https://doi.org/10.1016/j.rser.2016.01.044

Mandelli, S., Barbieri, J., Mereu, R., & Colombo, E. (2016). Off-grid systems for rural electrification in developing countries: Definitions, classification and a comprehensive literature review. *Renewable and Sustainable Energy Reviews*, *58*, 1621–1646. https://doi.org/10.1016/j.rser.2015.12.338

Maor, T. T. (2017). *Impacts of Power System-Tied Distributed Generation on the Performance of Protection*.

Mariam, L., Basu, M., & Conlon, M. F. (2016). Microgrid: Architecture, policy and future trends. *Renewable and Sustainable Energy Reviews*, *64*, 477–489. https://doi.org/10.1016/j.rser.2016.06.037

Mason, P E. et al. (2014). *Biomass fuel flexibility in future conventional power generation*. 1–5.

Mcfowland, N. A. (2012). *Forward Converter for Solar Power Applications*.

Meng, L., Shafiee, Q., Trecate, G. F., Karimi, H., Fulwani, D., Lu, X., & Guerrero, J. M. (2017).

Review on Control of DC Microgrids and Multiple Microgrid Clusters. *IEEE Journal of Emerging and Selected Topics in Power Electronics*, *5*(3), 928–948. https://doi.org/10.1109/JESTPE.2017.2690219

Miao, Y., Hynan, P., Von Jouanne, A., & Yokochi, A. (2019). Current li-ion battery technologies in electric vehicles and opportunities for advancements. *Energies*, *12*(6), 1–20. https://doi.org/10.3390/en12061074

Mo, C., Énergie, N. D. E. L., Kim, Y. D., & Frei, C. (2015). World Energy Resources: Charting the Upsurge in Hydropower Development. *World Energy Council*, 70.

Mohan, N., Undeland, T. M., & Robbins, W. P. (2003). *Power Electronics* (pp. 161–199). pp. 161–199.

Morstyn, T., Hredzak, B., & Agelidis, V. G. (2018). Control Strategies for Microgrids with Distributed Energy Storage Systems: An Overview. *IEEE Transactions on Smart Grid*, *9*(4), 3652–3666. https://doi.org/10.1109/TSG.2016.2637958

Mousavi G, S. M., Faraji, F., Majazi, A., & Al-Haddad, K. (2017). A comprehensive review of Flywheel Energy Storage System technology. *Renewable and Sustainable Energy Reviews*, *67*, 477–490. https://doi.org/10.1016/j.rser.2016.09.060

Mrcela, I., Sumina, D., Sacic, F., & Barisa, T. (2016). A wind turbine two level back-to-back converter power loss study. *Proceedings - 2016 IEEE International Power Electronics and Motion Control Conference, PEMC 2016*, 308–314. https://doi.org/10.1109/EPEPEMC.2016.7752016

Muthuvel, P., Arul Daniel, S., & Paul, S. K. (2017). Sizing of PV array in a DC nano-grid for isolated households after alteration in time of consumption. *Engineering Science and Technology, an International Journal*, *20*(6), 1632–1641. https://doi.org/10.1016/j.jestch.2017.12.006

Nadeem, F., Hussain, S. M. S., Tiwari, P. K., Goswami, A. K., & Ustun, T. S. (2019). Comparative review of energy storage systems, their roles, and impacts on future power systems. *IEEE Access*, *7*(January), 4555–4585. https://doi.org/10.1109/ACCESS.2018.2888497

Naeinian, B. (n.d.). *Seamless Operation of a Microgrid Using BESS During Transition Between Grid-connected and Stand-alone Modes*. Retrieved from http://repository.tudelft.nl/.

Nascimento, M. A. R. Do, Rodrigues, L. D. O., E. C. Dos Santos, E. E. B. G., Dias, F. L. G., Velásques, E. I. G., & Carrillo, R. a. M. (2013). Micro Gas Turbine Engine: A Review. *Progress in Gas Turbine Performance*, 108–142. https://doi.org/45114

Nrel, J. D., Nrel, P. M., Nrel, L. L., Nrel, J. B., & Group, D. J. (2015). *Photovoltaic-Thermal New Technology Demonstration*. (January).

Olivares, D. E., Mehrizi-Sani, A., Etemadi, A. H., Cañizares, C. A., Iravani, R., Kazerani, M., … Hatziargyriou, N. D. (2014). Trends in microgrid control. *IEEE Transactions on Smart Grid*,

5(4), 1905–1919. https://doi.org/10.1109/TSG.2013.2295514

Ortiz, L., Orizondo, R., Águila, A., González, J. W., López, G. J., & Isaac, I. (2019). Hybrid AC/DC microgrid test system simulation: grid-connected mode. *Heliyon*, *5*(12). https://doi.org/10.1016/j.heliyon.2019.e02862

Ould Amrouche, S., Rekioua, D., Rekioua, T., & Bacha, S. (2016). Overview of energy storage in renewable energy systems. *International Journal of Hydrogen Energy*, *41*, 20914–20927. https://doi.org/10.1016/j.ijhydene.2016.06.243

Padhi, M. K. (2010). *Micro-Turbine Generator System*. 28.

Pantelimon, R. F., Adam, M., Andrusca, M., & Pancu, C. (2013). Aspects regarding solar battery charge controllers. *2013 - 8th International Symposium on Advanced Topics in Electrical Engineering, ATEE 2013*. https://doi.org/10.1109/ATEE.2013.6563367

Parhizi, S., Lotfi, H., Khodaei, A., & Bahramirad, S. (2015). State of the art in research on microgrids: A review. *IEEE Access*, *3*, 890–925. https://doi.org/10.1109/ACCESS.2015.2443119

Parker, M. A., Soraghan, C., & Giles, A. (2016). Comparison of power electronics lifetime between vertical- and horizontal-axis wind turbines. *IET Renewable Power Generation*, *10*(5), 679–686. https://doi.org/10.1049/iet-rpg.2015.0352

Peres, Y., & Lissitsa, S. (2008). Criteria of integration: the case of “Russian immigration” to Israel in the 1990s. *Megamot*, *45*(4), 669–695. https://doi.org/10.13140/RG.2.1.4439.4328

Pérez, A., Santamaria, E. K., Operario, D., Tarkang, E. E., Zotor, F. B., Cardoso, S. R. de S. N., … Volk, J. E. (2017). No 主観的健康感を中心とした在宅高齢者における 健康関連指標に関する共分散構造分析 Title. *BMC Public Health*, *5*(1), 1–8. Retrieved from https://ejournal.poltektegal.ac.id/index.php/siklus/article/view/298%0Ahttp://repositorio.unan.edu.ni/2986/1/5624.pdf%0Ahttp://dx.doi.org/10.1016/j.jana.2015.10.005%0Ahttp://www.biomedcentral.com/1471-2458/12/58%0Ahttp://ovidsp.ovid.com/ovidweb.cgi?T=JS&P

Petrocelli, R. (2018). One-quadrant switched-mode power converters. *CERN Accelerator School: Power Converters, CAS 2014 - Proceedings*, 115–139. https://doi.org/10.5170/CERN-2015-003.115

Ponzo, G. M., Capponi, G., Scalia, P., & Boscaino, V. (2009). An improved flyback converter. *2009 6th International Conference on Electrical Engineering/Electronics, Computer, Telecommunications and Information Technology, ECTI-CON 2009*, *1*, 310–313. https://doi.org/10.1109/ECTICON.2009.5137015

Qxodeghhq, D. X., Nxodvhndud, K., Frp, J., Vollw, Y. V, Uhvrxufhv, U., Jhrwkhupdo, V., & Lv, H. (2019). *$ 5Hylhz Ri * Hrwkhupdo (Qhuj \ Iru) Xwxuh 3Rzhu * Hqhudwlrq*. 26–28.

Rahman, H., Sharif, M. R., Ahmed, R., Nijam, T., & Shoeb, M. A. (2015). Designing of biomass based power plant for residential building energy system. *2nd International Conference on*

Electrical Engineering and Information and Communication Technology, ICEEiCT 2015, (May), 1–6. https://doi.org/10.1109/ICEEICT.2015.7307366

Rai, B. K., Dhoorjati, V., Saini, L., & Jha, A. K. (2015). On adaptive distributed storage systems. *IEEE International Symposium on Information Theory - Proceedings*, *2015-June*, 1482–1486. https://doi.org/10.1109/ISIT.2015.7282702

Rajesh, K. S., Dash, S. S., Rajagopal, R., & Sridhar, R. (2017). A review on control of ac microgrid. *Renewable and Sustainable Energy Reviews*, *71*(December 2016), 814–819. https://doi.org/10.1016/j.rser.2016.12.106

Rajesh, R., & Carolin Mabel, M. (2015). A comprehensive review of photovoltaic systems. *Renewable and Sustainable Energy Reviews*, *51*, 231–248. https://doi.org/10.1016/j.rser.2015.06.006

Ravi, K., Sakthigokulrajan, C., Shilaja, C., Belwin Edward, J., & Sathish Kumar, K. (2014). Modeling of photovoltaic energy conversion system with integration to substation. *Global Journal of Pure and Applied Mathematics*, *10*(3), 451–464.

Raza, W., Ali, F., Raza, N., Luo, Y., Kim, K. H., Yang, J., … Kwon, E. E. (2018). Recent advancements in supercapacitor technology. *Nano Energy*, *52*, 441–473. https://doi.org/10.1016/j.nanoen.2018.08.013

Rgpv, U. I. T. (2014). *Discontinuous Mode of Operation*. (1), 77–83.

Richter, A., Van Der Laan, E., Ketter, W., & Valogianni, K. (2012). Transitioning from the traditional to the smart grid: Lessons learned from closed-loop supply chains. *2012 International Conference on Smart Grid Technology, Economics and Policies, SG-TEP 2012*. https://doi.org/10.1109/SG-TEP.2012.6642382

Sahoo, S. K., Sinha, A. K., & Kishore, N. K. (2018). Control Techniques in AC, DC, and Hybrid AC-DC Microgrid: A Review. *IEEE Journal of Emerging and Selected Topics in Power Electronics*, *6*(2), 738–759. https://doi.org/10.1109/JESTPE.2017.2786588

Salem, M. E. M. (2016). *Design of a pitch angle control system for a horizontal axis small wind turbine.* (November 2016).

Salmi, T., Bouzguenda, M., Gastli, A., & Masmoudi, A. (2012). MATLAB/simulink based modelling of solar photovoltaic cell. *International Journal of Renewable Energy Research*, *2*(2), 213–218. https://doi.org/10.20508/ijrer.42248

Salomonsson, D., Söder, L., & Sannino, A. (2009). Protection of low-voltage DC microgrids. *IEEE Transactions on Power Delivery*, *24*(3), 1045–1053. https://doi.org/10.1109/TPWRD.2009.2016622

Sánchez-Díez, E., Ventosa, E., Guarnieri, M., Trovò, A., Flox, C., Marcilla, R., … Ferret, R. (2021). Redox flow batteries: Status and perspective towards sustainable stationary energy storage. *Journal of Power Sources*, *481*. https://doi.org/10.1016/j.jpowsour.2020.228804

Sau-Bassols, J., Prieto-Araujo, E., Galceran-Arellano, S., & Gomis-Bellmunt, O. (2016). Operation and control of a Current Source Converter series tapping of an LCC-HVDC link for integration of Offshore Wind Power Plants. *ELSEVIER Electric Power Sysrems Research*, *141*, 510–521. https://doi.org/10.1016/j.epsr.2016.07.019

Schubel, P. J., & Crossley, R. J. (2012). Wind Turbine Blade Design. *MDPI Energies*, 3425–3449. https://doi.org/10.3390/en5093425

Science, C. (2005). Control and Topology Improvements in Half-Bridge Dc-Dc Converters. *Dissertation*, (2005), 2004–2019.

Shahariar, G. M. H., & Hasan, M. R. (2014). Design & construction of a vertical axis wind turbine. *IEEE 2014 9th International Forum on Strategic Technology, IFOST 20142014 9th*, 326–329. https://doi.org/10.1109/IFOST.2014.6991132

Shalini, R., Nagashree, A. N., & Anantha Murthy, B. G. (2017). Uninterruptable power supply design using float cum boost technology. *IEEE International Conference on Power Electronics, Drives and Energy Systems, PEDES 2016*, *2016-Janua*, 1–6. https://doi.org/10.1109/PEDES.2016.7914230

Sharma, D. K., & Purohit, G. (2015). Differential power algorithm based maximum power point tracking for a standalone solar PV system. *Journal of Energy in Southern Africa*, *26*(2), 103–109. https://doi.org/10.17159/2413-3051/2015/v26i2a2203

Sharma, R., & Goyal, V. (2015). A hybrid model of solar-wind - Biomass power generation system: A review. *2015 International Conference on Computing for Sustainable Global Development, INDIACom 2015*, 1201–1203.

Sheth, S., & Shahidehpour, M. (2004). Geothermal energy in power systems. *2004 IEEE Power Engineering Society General Meeting*, *2*, 1972–1977. https://doi.org/10.1109/PES.2004.1373222

Shi, F., Li, L., Wang, X. L., Gu, C. D., & Tu, J. P. (2014). Metal oxide/hydroxide-based materials for supercapacitors. *RSC Advances*, *4*(79), 41910–41921. https://doi.org/10.1039/c4ra06136e

Singh, O., & Rajput, S. K. (2016). Mathematical modelling and simulation of solar photovoltaic array system. *International Conference on Research Advances in Integrated Navigation Systems, RAINS 2016*, (September 2018). https://doi.org/10.1109/RAINS.2016.7764395

Strings, L. H., Strings, L. H., & Polysol, I. B. C. (2019). *Blog*.

Sumathi, S., Ashok Kumar, L., & Surekha, P. (2015). Solar PV and Wind Energy Conversion Systems: An Introduction to Theory, Modeling with MATLAB/SIMULINK, and the Role of Soft Computing Techniques. In *Green Energy and Technology*. https://doi.org/10.1007/978-3-319-14941-7

Tawfiq, K. B., Mansour, A. S., Ramadan, H. S., Becherif, M., Pina, A., Ferrão, P., … Corre, O. Le. (2019). Wind Energy Conversion System Topologies and Converters: Comparative Review. *ELSEVIER Energy Procedia*, *162*, 38–47.

https://doi.org/10.1016/j.egypro.2019.04.005

The Kathmandu Post. (2020). *Sugar mills in Nepal poised to generate electricity*. Retrieved from https://kathmandupost.com/money/2018/09/30/sugar-mills-in-nepal-poised-to-generate-electricity

Topić, D., Knežević, G., Perko, J., & Kosić, D. (2018). Simplified model for optimal sizing of the off-grid PV system regarding value of loss of load probability. *Tehnicki Vjesnik*, *25*(1), 420–426. https://doi.org/10.17559/TV-20171203150754

Totem, E. (2019). *Microgrids & First Nations*.

US Department of Energy. (2016). *Hydropower Vision. A New Chapter for America's Renewable Electricity Source. Chapter 2: State of Hydropower in the United States*. 1–228. Retrieved from http://energy.gov/eere/water/articles/hydropower-vision-new-chapter-america-s-1st-renewable-electricity-source

Ustun, T. S., Ozansoy, C., & Zayegh, A. (2011). Recent developments in microgrids and example cases around the world - A review. *Renewable and Sustainable Energy Reviews*, *15*(8), 4030–4041. https://doi.org/10.1016/j.rser.2011.07.033

Valishin, A. R., & Variamova, V. N. (2008). Geothermal energy and its applications. *2008 International Conference Modern Technique and Technologies, MTT 2008*, 127–130. https://doi.org/10.1109/SPCMTT.2008.4897519

Vazquez, S., Lukic, S. M., Galvan, E., Franquelo, L. G., & Carrasco, J. M. (2010). Energy storage systems for transport and grid applications. *IEEE Transactions on Industrial Electronics*, *57*(12), 3881–3895. https://doi.org/10.1109/TIE.2010.2076414

Wang, C., Yu, Y., Niu, J., Liu, Y., Bridges, D., Liu, X., … Hu, A. (2019). *applied sciences Recent Progress of Metal – Air Batteries — A Mini Review*. 1–22.

Wang, X., Guerrero, J. M., Blaabjerg, F., & Chen, Z. (2012). A review of power electronics based microgrids. *Journal of Power Electronics*, *12*(1), 181–192. https://doi.org/10.6113/JPE.2012.12.1.181

Wrobel, K., Tomczewski, K., Sliwinski, A., & Tomczewski, A. (2018). The Impact of a Wind Turbine Characteristics on the Annual Energy Performance at Given Wind Speed Distribution. *2018 Applications of Electromagnetics in Modern Techniques and Medicine, PTZE 2018*, 281–284. https://doi.org/10.1109/PTZE.2018.8503230

Yadav, A. K., Ray, A., & Lokhande, M. M. (2017). Low-voltage DC microgrid network: A case study for Standalone system. *International Journal of Renewable Energy Research*, *7*(3), 1186–1194.

Yahyaoui, I., Fardin, J. F., & Tadeo, F. (2018). *technologies*. (Irec).

Yu, S. Y., Kim, H. J., Kim, J. H., & Han, B. M. (2016). SoC-based output voltage control for BESS with a lithium-ion battery in a stand-alone DC microgrid. *Energies*, *9*(11).

https://doi.org/10.3390/en9110924

Zhao, L., Li, F., Zhuang, Z., Li, Z., & Luo, Z. (2020). A Dual Half-Bridge Converter with Current Doubler Rectifier. *IEEE Transactions on Industrial Electronics*, *67*(8), 6398–6406. https://doi.org/10.1109/TIE.2019.2935986

Zhou, N., Liu, N., Zhang, J., & Lei, J. (2016). Multi-objective optimal sizing for battery storage of PV-based microgrid with demand response. *Energies*, *9*(8). https://doi.org/10.3390/en9080591

APPENDIX

The Developed Model of the Energy Management System